

UNIVERSITY OF OKLAHOMA

GRADUATE COLLEGE

BINDING AND TRANSPORT THROUGH FERRIC SIDEROPHORE
RECEPTORS, FEPA AND FHUA

A Dissertation

SUBMITTED TO THE GRADUATE FACULTY

in partial fulfillment of the requirements for the

degree of

Doctor of Philosophy

By

RAJASEKARAN ANNAMALAI

Norman, Oklahoma

2006

UMI Number: 3213384



UMI Microform 3213384

Copyright 2006 by ProQuest Information and Learning Company.
All rights reserved. This microform edition is protected against
unauthorized copying under Title 17, United States Code.

ProQuest Information and Learning Company
300 North Zeeb Road
P.O. Box 1346
Ann Arbor, MI 48106-1346

BINDING AND TRANSPORT THROUGH FERRISIDEROPHORE RECEPTORS,
FEPA AND FHUA

A Dissertation APPROVED FOR THE
DEPARTMENT OF CHEMISTRY AND BIOCHEMISTRY

BY

Phillip Klebba

Bruce Roe

Ann West

George Richter-Addo

Randall Hewes

© Copyright by RAJASEKARAN ANNAMALAI 2006

All Rights Reserved

Acknowledgements

Every step in a man's life is the harvest of his past and a seed for his future. In this journey, great is my debt to my professors, my colleagues and my family. From each I carry a precious piece, which helps to define me everyday.

It has been my privilege to work with Dr. Klebba, my major professor. At every turn, this exemplary scientist instilled in me the confidence that any problem can be addressed with a systematic approach. Dr. Klebba always treated every idea on its merit, which encouraged us more than anything to be independent thinkers. I thank our associate professor, Dr. Newton whose dedication is an inspiration to all of us. I shall miss her encouraging nods every time I address an audience.

I would like to take this opportunity to thank Dr. Lalitha Venkatramani, who was instrumental in my entering this wonderful group and who has been a constant source of encouragement through the years.

I appreciate the direction and guidance given me by the members of my committee throughout the years.

The trip so far has been hard and I have my wife, Anu and my son, Arjun to thank for making everyday worthwhile. My gratitude goes out to our families who stood with us through the thick and crucially the thin. Finally it would be remiss of me, to not pay homage to the spirit of inquiry that drives the pursuit of knowledge since the dawn of history.

Table of contents

Chapter 1	1
Introduction	1
Iron and bacteria	1
Siderophores	3
Ligand-gated porins	7
Structure of ligand-gated porins – FepA and FhuA.....	12
Binding of FeEnt by FepA.....	16
Ligand specificity.....	18
Transport of FeEnt by FepA	22
Surface loops in FepA transport	23
The N domain in FepA transport	24
TonB and ferric siderophore transporters	27
The N domain– where art thou?.....	29
Chapter 2	36
Materials and methods	36
Bacterial strains, plasmids and culture conditions:.....	36
Site-directed mutagenesis	39
Protein detection	39
Siderophore nutrition assay.....	40
Siderophore binding.....	41
Siderophore transport.....	41
Colicin killing assay.....	42
Competition between ferric catecholates	43
Periplasmic incorporation of TEV protease.....	43
Periplasmic expression of TEV protease	44
Proteolysis by incorporated TEV-protease	44
Proteolysis by co-expressed TEV protease.....	45
Cloning of FepA-TEV site- PhoA	45
Expression of FepA-TEV site-PhoA	46
FM labeling of bacterial proteins in vivo.....	46
Fluorescence spectrophotometry	46
Labeling in the presence of FeEnt	47
Detection of labeling.....	47
Chapter 3	49
Results.....	49
Aromatic residues in the binding and transport of FeEnt	49
Identification of candidate residues for mutagenesis.....	49
Protein expression and localization	49
Colicin sensitivity	50
Aromatic residues in the binding interaction:.....	54
Aromatic residues in the transport of FeEnt	54
Chapter 4.....	62
Loops of the N-domain	62
Site directed mutagenesis.....	62
Protein expression and localization	62
Colicin sensitivity	65
Binding and transport by N domain loop deletion mutants	65

Chapter 5	67
Recognition of ferric catecholates by FepA.....	67
Binding of ferric catecholates	67
Transport of ferric catecholates	67
Competition of FeEnt with other siderophores.....	68
Chapter 6	70
Complementation between isolated barrel and N domains.....	70
Expression of FepA and FhuA protein constructs	70
Colicin susceptibility	70
Siderophore nutrition analysis	73
Protein expression.....	76
Chapter 7	78
Disposition of the N domain during transport	78
Protease accessibility of the N domain	78
Introduction of TEV protease into the periplasm	78
Proteolysis of control substrate by introduced TEV protease:.....	79
Proteolysis of control substrate by expressed TEV protease	82
Control substrate in the OM.....	84
Expression of FepA-TEV site-PhoA	84
Proteolysis of OM substrate.....	85
Expression of FepA-TEV site-PhoA in protease deficient strains.....	87
Proteolysis of Fhu targets by introduced TEV protease	87
Experiments in FhuA target proteolysis	92
Fluorophore labeling of residues in the N domain.....	95
Selection of fluorophores.....	95
Entry of fluorophores into the periplasm.....	95
Location of the introduced cysteines	98
Siderophore nutrition assay.....	100
Colicin killing	100
Protein expression.....	100
Labeling with FM	100
Labeling with AM.....	114
Labeling and TonB	114
Labeling and FeEnt.....	115
Chapter 8	118
Discussion	118
Recognition of ferric catecholates	118
Aromatic amino acids in FepA function.....	120
Loops of the N domain in FepA function	123
N domain of ligand gated porins.....	124
Disposition of the N domain of FhuA during transport.....	127
Disposition of the N domain of FepA during transport	129
References	133

List of tables

Table 1. Properties of siderophores.	6
Table 2. Ligands of LGPs, FepA and FhuA.	19
Table 3. List of strains used in this study.....	37
Table 4. List of plasmids, their relevant genotypes and their sources/references.....	38
Table 5. Binding and transport by FepA and its derivatives.....	61
Table 6. Binding and transport by FepA N domain loop deletion.....	66
Table 7. Colicin B and D sensitivity of FepA derivatives.	71
Table 8. Colicin M sensitivity of FhuA derivatives.....	72
Table 9. FeEnt nutrition of FepA derivatives.	74
Table 10. Fc nutrition of FhuA derivatives.....	74
Table 11. Comparison between FM and AM.....	97
Table 12. Siderophore nutrition assay of cysteine substitution mutants.....	99
Table 13. Colicin sensitivity of cysteine substitution mutants.	101
Table 14. Duration of FeEnt transport at different concentrations of FeEnt.	117

List of illustrations

Figure 1. Catecholate and hydroxamate siderophores.	5
Figure 2. Schematic representation of the gram-negative bacterial envelope.	9
Figure 3. The crystal structure of FepA and FhuA.	13
Figure 4. Space-filled representations of the crystal structures of FepA and FhuA. ...	14
Figure 5. Location of FhuA TEV site mutations.	35
Figure 6. Target residues for alanine mutagenesis.....	51
Figure 6a. Expression of FepA and its derivatives.	51
Figure 7. Localization of FepA and its derivatives.....	52
Figure 8. Sensitivity to colicins B and D.	52
Figure 9. Siderophore nutrition assay of FepA and its derivatives.....	53
Figure 10a. Binding and transport by class I substitution mutants.	56
Figure 10b. Binding and transport by class I substitution mutants.....	56
Figure 10c. Binding and transport by class I substitution mutants.	57
Figure 11a. Binding and transport by class II substitution mutants.....	57
Figure 11b. Binding and transport by class II substitution mutants.	59
Figure 11c. Binding and transport by class II substitution mutants.....	59
Figure 12. Binding and transport by class III substitution mutant.....	60
Figure 13. Loops of the N domain of FepA.....	63
Figure 14. Expression of FepA and its derivatives.	63
Figure 15. Localization of FepA and its derivatives.....	63
Figure 16. Sensitivity to colicins B and D of N domain loop deletion mutants.	64
Figure 17. Siderophore nutrition assay of FepA and its derivatives.....	64
Figure 18. Binding and transport by N-loop deletion mutants.	66
Figure 19. Binding and transport of ferric catecholates.....	69
Figure 20. Competition of ⁵⁹ FeEnt binding to FepA by ferric siderophores.	69
Figure 21. ¹²⁵ I-Protein A immunoblot profiling the expression of FepA derivatives..	75
Figure 22. Western blot profiling the expression of FepA derivatives.....	77
Figure 22a. Expression of FepNFhuβ.	77
Figure 23. Western blot showing the retention of TEV protease by permeablized cells.	81
Figure 24. Western blot showing the proteolysis of periplasmic substrate, MBP-TEV site-PhoA by introduced TEV protease.	81
Figure 25. Western blots showing the degradation of periplasmic substrate by coexpressed TEV protease.....	83
Figure 26. Expression of FepA-TEV site-PhoA fusion protein.....	86
Figure 26a. Proteolysis of OM substrate by periplasmic TEV protease.....	86
Figure 27. Proteolysis of Fhu targets by introduced TEV protease.....	90
Figure 28. Protease accessibility assay with FhuA and its TEV site derivatives.	90
Figure 29. Western blot showing the coexpression of FhuA derivatives and the MBP- TEV protease fusion by E. coli KDF541.	91
Figure 30. Labeling of AcrA by FM and AM.....	97
Figure 31. Target residues for cysteine mutagenesis.	99
Figure 32. ¹²⁵ I- Protein A immunoblot profiling the expression of FepA derivatives.	101
Figure 33. Detection of FM labeled FepAG54C.	102
Figure 34. Labeling of wild type FepA by FM.....	102
Figure 35. Labeling of FepAW101C by FM.	106

Figure 36. Detection of FM-FepAW101C in the presence and absence of sulfhydryl reagents.	106
Figure 37. Distance between W101 and C494 in the crystal structure.	107
Figure 38. Labeling of FepAI14C by FM.	107
Figure 39. Labeling of FepAT51CC by FM.	108
Figure 40. Labeling of FepAG54C by FM.	108
Figure 41. Labeling of FepAG300C by FM.	109
Figure 42. Labeling of FepAG565C by FM.	109
Figure 43. Labeling of wild type FepA by AM.	110
Figure 44. Labeling of FepAW101C by AM.	110
Figure 45. Labeling of FepAI14C by AM.	111
Figure 46. Labeling of FepAG54C by AM.	111
Figure 47. Labeling of FepAT51C by AM.	112
Figure 48. Labeling of FepAG300C by AM.	112
Figure 49. Labeling of FepAG565C by AM.	113
Figure 50. Distance between isoleucine 14 and glycine 300 in the barrel wall.	113
Figure 51. Labeling of FepAG54C by FM in the presence of increasing concentrations of FeEnt.	117
Figure 52. Model of FeEnt transport through FepA.	132

Abstract

Under iron deficient conditions, gram-negative bacteria like *E. coli* secrete siderophores to chelate iron in the extracellular medium. Ligand-gated porins (LGPs) transport the ferric siderophore complexes across the outer membrane (OM) of the bacterium. The C-terminal domains of LGPs form channels across the OM, which are occluded by their N domains. The LGPs, FepA and FhuA transport ferric enterobactin (FeEnt) and ferrichrome (Fc) respectively into the periplasm of *E. coli*.

The FeEnt-FepA binding interaction binding reaction is biphasic with two binding stages, B1 and B2 which may reflect two anatomical locations or two kinetic stages. The interaction is also specific and is characterized by high affinity. Binding competition experiments between FeEnt and other ferric siderophores show that the initial adsorption of the ligand happens with bonafide specificity. The interaction is unaffected by unrecognized ferric siderophores like ferrichrome and ferric Agrobactin. The triscatecholate and cognate siderophore, ferric TRENCAM competes with FeEnt. Despite being triscatecholate, ferric corynebactin only partially inhibits the binding of FeEnt. When compared to FeEnt, the iron center in ferric corynebactin has the opposite configuration of the chelating groups around the iron. Further more, the ferric siderophore is larger in size than FeEnt. The partial inhibition presumably reflects the fact that the molecule participates in the initial stage of binding, B1 but does not progress to B2 in the biphasic binding.

The surface loops of FepA bind and enclose FeEnt at the top of the barrel. Site-directed mutagenesis studies show that aromatic residues like tyrosine 481 and 638 make a major contribution to the high affinity of the interaction. Intriguingly, some of the aromatic residues like tyrosines 478, 495 and tryptophan 101 although

located in the outer reaches of the protein are crucial to the uptake reaction despite making only modest contributions to the binding reaction.

Upon binding and closure of the loops, the N domain of FepA undergoes a conformational change to allow FeEnt to pass through the barrel. Labeling experiments with fluorophores and cysteine mutants of FepA show that this process involves the extrusion of the N domain from its location within the beta barrel. This is evidenced by the fact that G54C in the N domain is labelled during the transport, but G565C in the interior of the barrel is not labelled. The model of transport envisages the specific adsorption of the ferric siderophore followed by the closure of the loops over the bound ligand. Subsequently the N domain extrudes out of the barrel and FeEnt is transported into the periplasm.

Chapter 1

Introduction

Iron and bacteria

The biological utility of iron stems from its ability to form a multitude of complexes with O, S, and N ligands. These complexes readily undergo acid-base and electron transfer reactions. In biological systems, iron undergoes changes between Fe^{2+} and Fe^{3+} states in response to the redox status of the environment.

Iron containing proteins participate in a variety of essential metabolic processes that sustain life. For example, proteins containing heme perform crucial roles in the electron transport system. Several cytochromes serve as members of the electron transport chain. The iron centers of these proteins are central to the oxidoreductive functions of these proteins. Cytochrome oxidase is involved in the activation of oxygen (Vernon 1960, Blaylock 1963). Peroxidase and catalase work in the reduction of hydrogen peroxide. Proteins containing iron-sulfur clusters play several important roles. The enzymes, aconitase (Martius 1937, Breusch 1937, Dickman 1950, Dickman 1951) and succinate dehydrogenase (Singer 1955) function in the citric acid cycle. Ferredoxin is involved in the electron transport chain (Mortenson 1963). Other processes involve proteins carrying non-heme and non-iron-sulfur cluster forms of iron. Examples include proteins involved in nucleic acid synthesis like ribonucleotide reductase (Brown 1968). Superoxide dismutase is crucial for protection from free radicals (Yost 1973). Therefore, it is not surprising that iron is a premium nutrient for microorganisms including bacteria and fungi. Several studies have reported the correlation between the growth and virulence of several pathogenic bacteria and the supply of iron. These include gram-positive (*Staphylococcus* (Szabo

1971, Trivier 1996)), gram-negative (like *Neisseria* (Kellog 1968)) and acid-fast (like *Mycobacterium*) pathogens (Kochan 1963, Golden 1974).

Besides its role in bacterial metabolism, iron also directly affects the pathogenicity of bacteria. In diphtheria, an infection caused by *Corynebacterium diphtheriae*, the production of diphtheria toxin is regulated by iron availability (Pappenheimer 1936). Diphtheria toxin ADP-ribosylates elongation factor, EF-2. The levels of expression of diphtheria toxin increase in proportion to the degree of iron deficiency. Iron repletion decreases toxin production.

Bacteria require iron only in micromolar concentrations. However, several factors impede iron acquisition forcing the bacteria to evolve several different strategies. Under anaerobic conditions, iron exists in the Fe^{2+} oxidation state. Fe^{2+} iron is soluble and bio-available. Therefore, anaerobes directly accumulate Fe^{2+} iron. Aerobes are not so fortunate. Under aerobic conditions, iron exists predominantly as Fe^{3+} iron. At neutral pH, Fe^{3+} forms insoluble oxy hydroxy polymers, which are not available for bacterial assimilation. Bacterial species inhabiting the human colon face additional constraints in their iron acquisition. Numerous host proteins like lactoferrin and transferrin sequester iron, further depleting the sources of the element. In the human colon, the concentration of free iron is of the order of 10^{-18} M (Bullen 1978, Neilands 1980). This concentration is too low to support the iron requirements of microorganisms (Klebbba 1982).

Several gram-negative bacteria inhabit the human colon. This includes pathogenic and non-pathogenic species of *Escherichia*. Pathogenic *E. coli* cause several infectious diseases. Enterotoxigenic *E. coli* are an important cause of traveler's diarrhea (Dupont 1971). Enteroinvasive, enteropathogenic and enterohemorrhagic *E. coli* are implicated in a variety of disorders including dysentery,

bacterial gastroenteritis and the hemolytic-uremic syndrome. Despite the advent of several antibiotics, *E. coli* continues to be an important causal factor of human morbidity.

Siderophores

Commensal and pathogenic gram-negative bacteria share several strategies to acquire iron in free iron-deficient environments. Bacteria employ certain proteins in their outer membrane (OM) to capture heme from hemoglobin or directly acquire iron from host proteins. Another prominent strategy involves the expression of iron-chelators called siderophores (Lankford 1973, Neilands 1981). Bacteria and fungi export these molecules into the extracellular medium. More than 100 different siderophores have been reported (Neilands 1981, Neilands 1991). In general, siderophores are organic molecules weighing less than 1000 Da. They are secreted under iron-deficient conditions. They possess phenolate and carboxylate oxygen ligands. These ligands bind iron in the Fe^{3+} state with high affinity. They have much lower affinity for Fe^{2+} iron. Based on their chemistry, siderophores are broadly classified into catecholates and hydroxamates (table 1). This traditional classification has been extended to recognize carboxylate, heterocyclic and mixed siderophores.

Enterobactin, a tricatecholate siderophore is a native siderophore of *E. coli* (Pollack 1970, O'Brien 1970). Enterobactin contains three dihydroxybenzoyl serine (DHBS) moieties. The 3 serines form the lactone ring backbone of the siderophore. The iron center of the siderophore is provided by the three catechol groups. The molecule possesses trivalent symmetry around the axis connecting the iron center and the center of the lactone ring. Enterobactin possesses extremely high affinity for Fe^{3+} . The association constant has been reported to be as high as 10^{52} . Enterobactin binds Fe^{3+} forming the ferric siderophore, ferric enterobactin (FeEnt). FeEnt is negatively

charged (-3). Its molecular weight is 729. Enterobactin also binds Vanadium and Gallium with high affinity. The crystal structure of FeEnt is not available. However, the crystal structure of Vanadium enterobactin (VEnt) has been solved (Karpishin 1992). FeEnt is expected to resemble VEnt. In VEnt, vanadium is coordinated by six deprotonated hydroxyl groups (Figure 1).

Corynebactin (also called bacillibactin) is a catecholate siderophore produced by the gram-positive bacilli, *Corynebacterium* and *Bacillus* (Budzikiewicz 1997, May 2001). The siderophore is formed by three dihydroxybenzoyl threonylglycine moieties. The threonyl moieties form the trilactone backbone. Similar to enterobactin, the three catecholates form the iron center. However, the substitution of threonyl glycines for the smaller serines renders the conformation of ferric corynebactin to be opposite of FeEnt. While enterobactin forms a π -complex with Fe^{3+} , corynebactin forms a σ -complex. Corynebactin has a molecular weight of 882.

Ferric TRENCAM (Rodgers 1987) and Ferric MECAM (Venuti 1979, Harris 1979) are synthetic ferric siderophores belonging to the catecholate group. In TRENCAM, a tertiary amine substitutes for the lactone ring in enterobactin and corynebactin. The iron centers of ferric TRENCAM (FeTRENCAM) and ferric MECAM (FeMECAM) are similar to that of FeEnt.

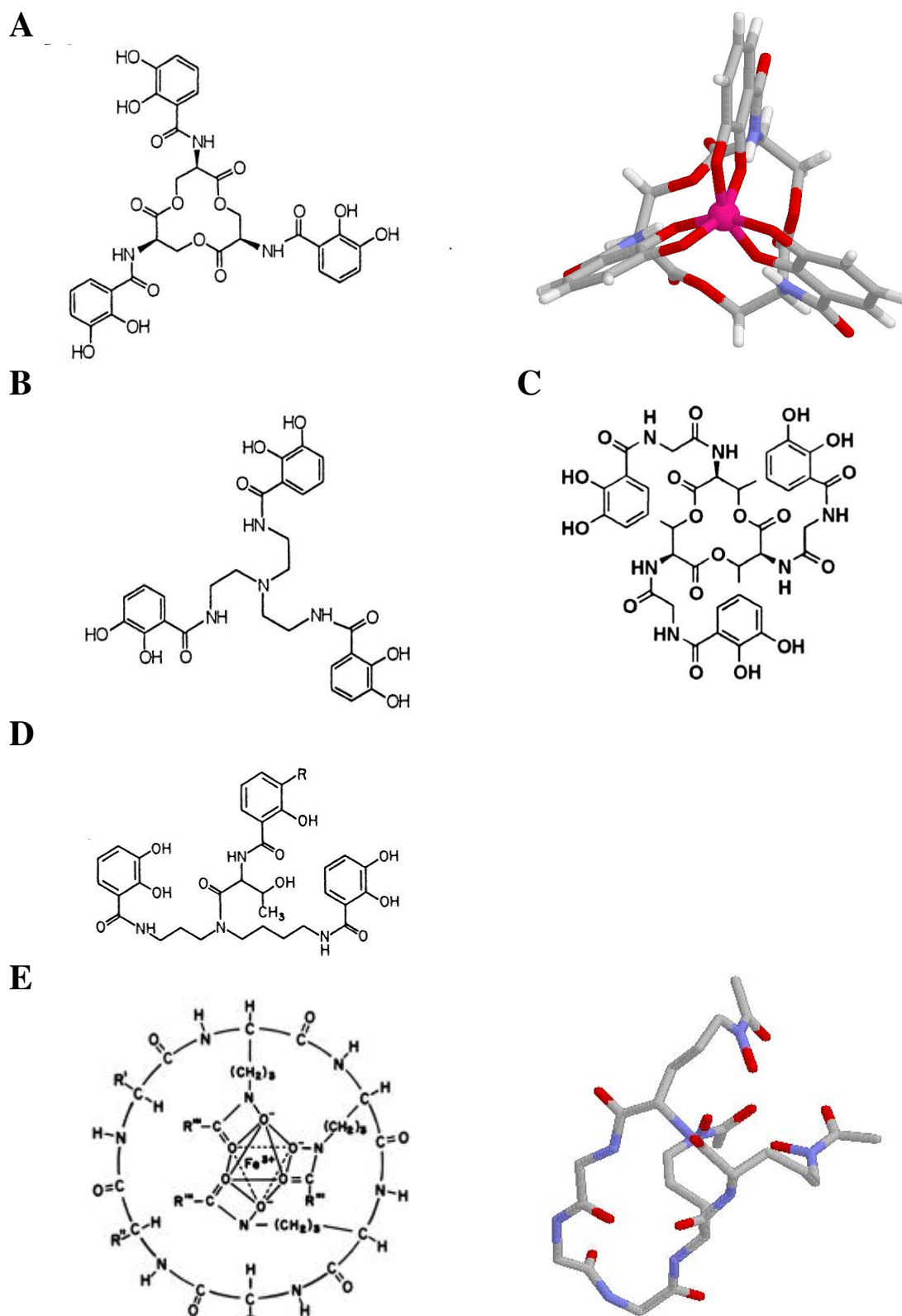


Figure 1. Catecholate and hydroxamate siderophores. A. Enterobactin, B. TRENCAm, C. Corynebactin, D. Agrobactin, E. Ferrichrome (Neilands 1952, Pollack 1970, O'Brien 1970, Ong 1979, van der Helm 1980, Rodgers 1987, Karpishin 1992, Budzikiewicz 1997). The crystal structures of vanadium enterobactin and apoferrichrome are shown to the right of the enterobactin and ferrichrome respectively.

Siderophore	Source	Structure	Iron complex	Charge
Enterobactin	<i>Escherichia coli</i> native siderophore	Triscatecholate. Dihydroxybenzoyl serine (DHB) moieties. Backbone: Cyclic triserine lactone.	Hexadentate coordination by deprotonated hydroxyl groups Trivalent symmetry Δ – configuration $K_a = 10^{52}$	-3
Agrobactin	<i>Agrobacterium tumefaciens</i>	Triscatecholate. Bulk of the III aromatic ring displaced away from the iron center. Threonine forms an oxazoline ring, attached to the central nitrogen. Backbone: Triamine, spermidine.	Hexadentate coordination of iron by Hydroxyls of 2 catechol groups, Proximal hydroxyl of the III catechol group. Nitrogen of the oxazoline ring, Assymmetrical.	-2.5
Corynebactin	<i>Corynebacterium diphtheriae</i>	Triscatecholate Glycine spacer Backbone: Trithreonine lactone	Hexadentate coordination by deprotonated hydroxyl groups Λ -configuration	-3
TRENCAM	Synthetic siderophore	Triscatecholate Backbone: Tertiary amine	Similar to enterobactin	-3
Apoferriochrome	<i>Ustilago sphaerogena</i>	Hydroxamate. 3 modified ornithine residues 3 glycines	Octahedral coordination by hydroxamate groups	Neutral

Table 1. Properties of siderophores. In the column on the right, charge refers to the net charge of the ferric siderophore complex (Neilands 1952, Pollack 1970, O'Brien 1970, Ong 1979, van der Helm 1980, Rodgers 1987, Karpishin 1992, Budzikiewicz 1997).

Agrobactin is another catecholate siderophore, secreted by the plant pathogen, *Agrobacterium tumefaciens* (Ong 1979). Agrobactin is characterized by a threonyl peptide of the triamine, spermidine acylated with 3 residues of 2, 3-dihydroxybenzoate (DHB). The carbonyl group of one of the DHB residues participates in an oxazoline ring with the β -hydroxyl of the threonine moiety. In contrast to enterobactin, the bulk of the third aromatic ring is displaced away from the iron center. Therefore, only two of the catechol groups participate in chelating iron. The fifth and sixth ligands derive from the nitrogen of the oxazoline ring and from the proximal hydroxyl of the third catechol group. The net charge of ferric agrobactin is -2.5. Several other natural and synthetic catecholate siderophores have been reported.

The hydroxamate siderophore, apoferrichrome is secreted by the smut fungus, *Ustilago sphaerogena* (Neilands 1952). Apoferrichrome is a cyclic hexapeptide of triglycyl-tri (N5 hydroxy-N5 acetyl- ornithine). Apoferrichrome binds Fe^{3+} forming neutral ferrichrome (Fc). In Fc, iron is coordinated by 3 deprotonated hydroxyl groups and 3 carbonyl oxygens of the hydroxamate moieties. The molecular weight of Fc is 660. Other members of the hydroxamate group include aerobactin produced by *Aerobacter* (Gibson 1969) and some plasmid-bearing strains of *E. coli* (Neilands 1981).

Ligand-gated porins

Bacteria secrete the siderophores into the extracellular fluid. The chelators capture Fe^{3+} iron from its insoluble polymers. These molecules also strip iron from host proteins (Tidmarsh 1983). The next step in iron acquisition is the internalization of these ferric siderophores. In gram-negative bacteria, the envelope includes the cytoplasmic membrane, a multilamellar sheet of peptidoglycan, linked to a lipid bilayer, the OM. The OM is in turn is surrounded by the polar lipopolysaccharide (O-

antigen). The cell wall restricts the entry of extraneous substances. However, the OM of *E. coli* houses proteins that form water-filled channels. These pore forming proteins are called porins.

Several different classes of porins are recognized. These include the general porins, specific porins and ligand-gated porins (LGPs). General porins allow the free incursion of molecules smaller than 600 Da (Nikaido 1985). However, the siderophore complexes are typically larger than this limit. Therefore, bacteria have evolved specific mechanisms to internalize the ferric siderophores. Specific receptors belonging to the class of porins called ligand-gated porins, transport ferric siderophores. LGPs transporting other substrates like vitamin B12 (BtuB) and nucleosides (TsX) have also been described. These porins are ligand-gated in the sense that they are not open channels like the general porins. Upon ligand binding, these proteins achieve the requisite conformation to enable its transport (Rutz 1992, Jiang 1997, Killmann 1993).

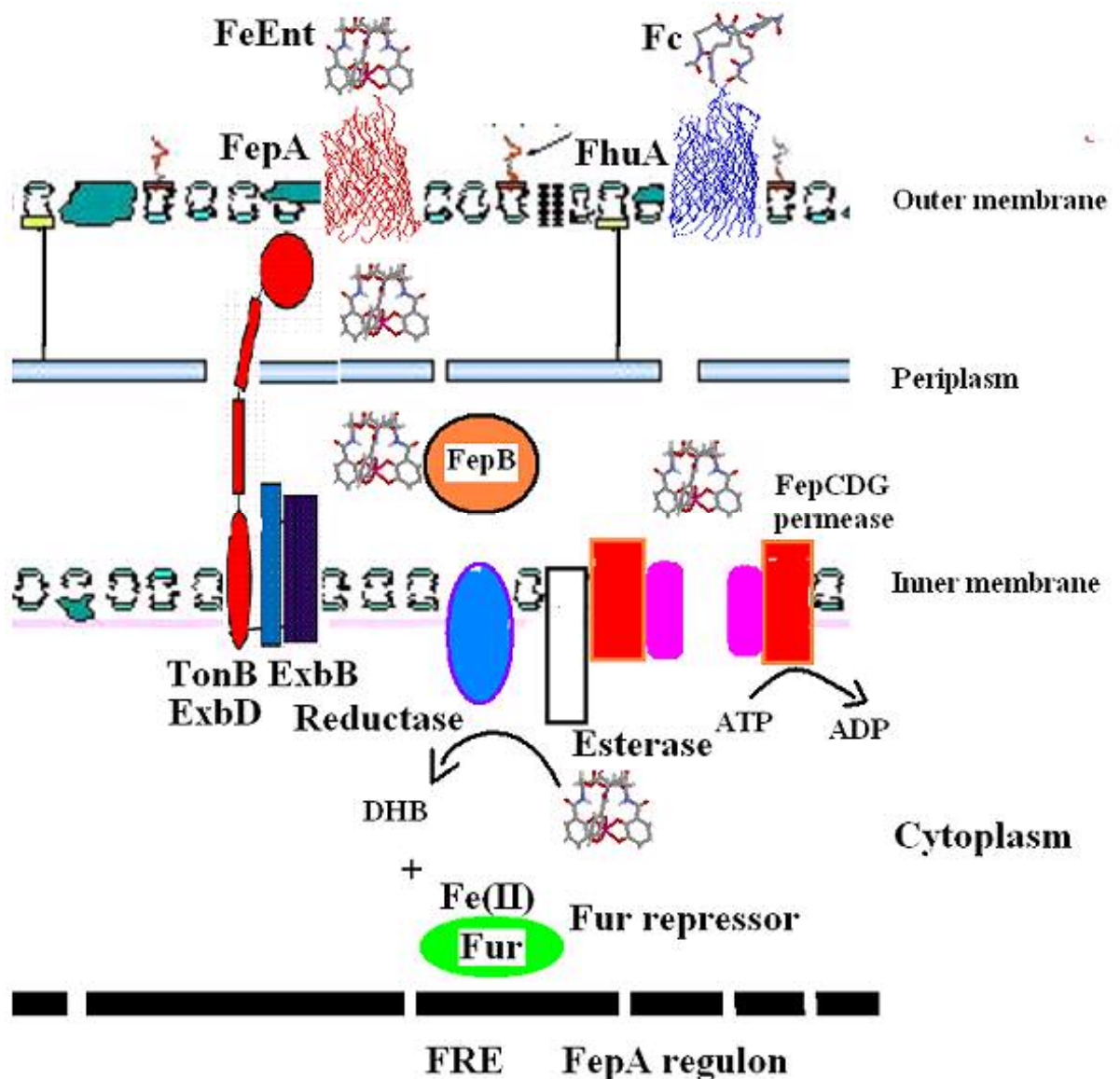


Figure 2. Schematic representation of the gram-negative bacterial envelope. The figure represents the known components of the pathway of FeEnt transport. Questions remain about the role of TonB in this scheme (see text for details). The ferric siderophores FeEnt and Fc bind to the LGPs, FepA and FhuA. FeEnt is transported by FepA across the outer membrane and enters the periplasm. This process requires the function of the inner membrane protein, TonB. FeEnt is then bound by the periplasmic binding protein, FepB, which delivers it to the inner membrane permease, FepCDG. The ferric siderophore is transported across the inner membrane. Iron is released from enterobactin by the activity of reductase and Fes esterase. The reductase reduces iron to its ferrous form and the esterase cleaves enterobactin to give dihydroxybenzoyl serines (DHBS). The ferrous iron binds to the Fur (Ferric uptake regulator) repressor and the complex binds to the fur regulation element (FRE) and negatively regulates the transcription of the genes coding for the proteins involved in FeEnt transport (FepA regulon).

The ferric siderophore transporters share several structural and functional similarities. They are usually named after the ligands that they transport. FepA (originally named FeEnt permease A, later renamed as FeEnt porin A) transports FeEnt (Pugsley 1976, Wayne 1976). FepA also transports the ferric siderophores, Femyxochelin C (Trowitzsch-Kienast 1996, Rabsch 1999), FeMECAM and FeTRENCAM (Heidinger 1983, Thulasiraman 1998). FhuA (Ferric hydroxamate uptake) receives Fc (Wayne 1975). FecA (Ferric citrate) acts on ferric citrate (Wagegg 1981). These proteins are generally larger than 70 kDa. Their occurrence in the OM of gram-negative bacteria is a reliable indicator of iron deficiency (Klebba 1981).

A specific protein binding sequence, usually a 19-bp inverted repeat called the fur box, flanks the genes encoding these proteins. Fur stands for ferric uptake regulator proteins. Under iron rich conditions, the concentration of Fe^{2+} iron inside the cell rises and is taken up by the Fur protein. Upon Fe^{2+} binding, the affinity of fur for fur box rises dramatically. Fur proteins bind with high affinity to the fur box (De Lorenzo 1988). Fe^{2+} -fur binding to fur recognition element (fur box) down-regulates transcription from genes encoding these LGPs. Under iron deficient conditions, fur releases the fur-box. The genes encoding the LGPs and their downstream partners in the iron acquisition are clustered together in the *E. coli* genome. The *fepA* (Lundrigan 1986) gene cluster also houses the genes encoding the biosynthetic components for enterobactin.

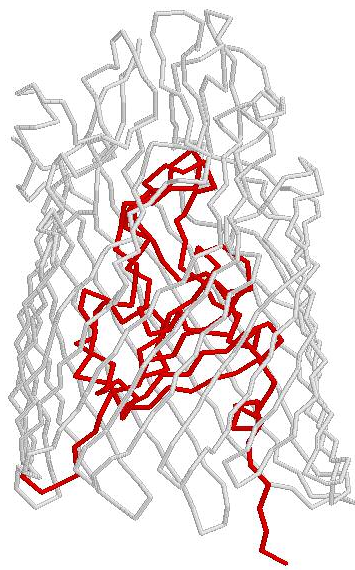
Upon entry into the periplasm, the ferric siderophore is taken up by the periplasmic binding protein. For FeEnt, FepB fulfills this role. FepB delivers the FeEnt to the inner membrane permeases (Pierce 1983, Elkins 1989, Stephens 1995, Sprencel 2000).

The inner membrane permeases belong to the ATP-binding cassette (ABC) family of transporters. The multimeric complex of proteins includes a dimer of FepC (Pierce 1986), which contains the ATP binding domain. FepD (Ozenberger 1987, Chenault 1991) FepC and FepG (Chenault 1991, Chenault 1992) form hydrophobic membrane spanning segments. For Fc, similar functions are performed by FhuD (the periplasmic binding protein) and FhuB (hydrophobic membrane spanning components) and FhuC (ATP binding unit) (Fecker 1983, Rohrbach 1995, Mademidis 1997). While it has not been reported that FepB binds ferric siderophores other than FeEnt, FhuD has been shown to carry several hydroxamate ferric siderophores (Koster 1990) including ferric aerobactin and coprogen. Similarly, the inner membrane permeases FhuB and FhuC act on these additional ferric siderophores.

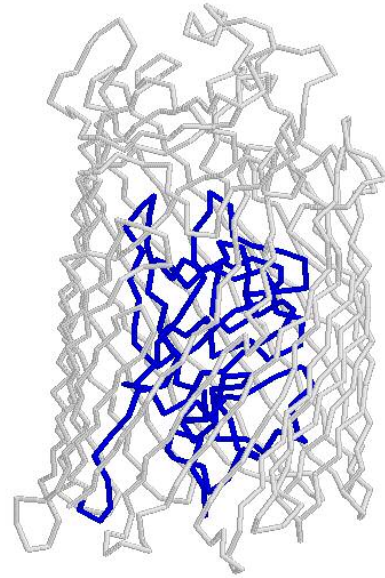
The consortium of FepA, FepB and FepCDG deliver FeEnt into the *E. coli* cytoplasm. The release of iron from FeEnt requires the presence of the product of the *fes* gene. Fes is FeEnt esterase (Porra 1972, Langman 1972). The release of iron from FeEnt faces the difficulty of overcoming the high affinity between enterobactin and Fe^{3+} . Instead, a reduction mechanism is proposed where in the Fe^{3+} is reduced to Fe^{2+} . Fe^{2+} iron binds enterobactin with much lower affinity. The *fes* protein cleaves the ester bonds of the enterobactin moiety releasing oligomers of DHBS. Some evidence exists that the DHBS is recycled for the synthesis of Enterobactin. However, the exact process of iron release has not been resolved. The reduction potential of FeEnt is so low that it is beyond the scope of known physiological reducing agents (O'Brien 1971, Cooper 1978). Fes may be involved in this process in addition to its esterase functions (Brickman 1992).

Structure of ligand-gated porins – FepA and FhuA

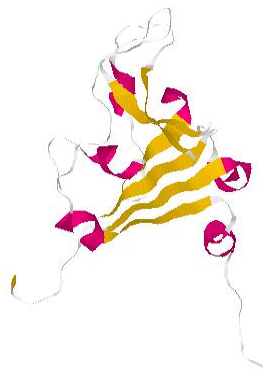
The tertiary structures of ferric siderophore transporters show several common features (Figure 3 and 4). To date, the crystal structures of FepA, FhuA and FecA have been solved (Buchanan 1999, Locher 1998, Ferguson 1998, Ferguson 2002). The C domain of these LGPS forms a β barrel bridging the exterior with the periplasm of the bacterium. The barrel consists of 22 antiparallel strands. With 22 strands, the barrel is larger than those found in general and specific porins. FepA's C domain forms an elliptical cylinder. The molecule is about 70 Å high, with an elliptical cross section of 40 Å x 30 Å. The β strands are anchored in the lipid bilayer by a girdle formed by aromatic amino acids. The aromatic amino acids interact with the hydrophobic interiors of the bilayer. On the surface, the strands of the barrel are linked by eleven long surface loops. Unlike in specific porins like LamB (Schirmer 1995), no gating loop is observed in the LGPs. Rather, the loops extend out into the extracellular space. They lean towards each other forming a conical vestibule that extends about 30 Å above the lipid bilayer interface. Although there is no gating loop obstructing the intrusion of the ligand, several lines of evidence indicate that the loops exhibit considerable dynamics.



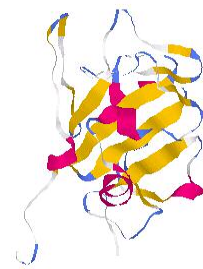
FepA backbone



FhuA backbone

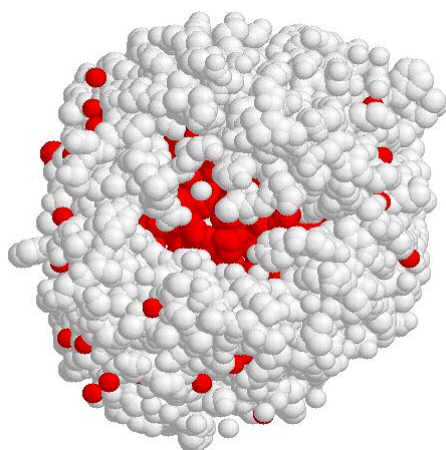


FepA N domain

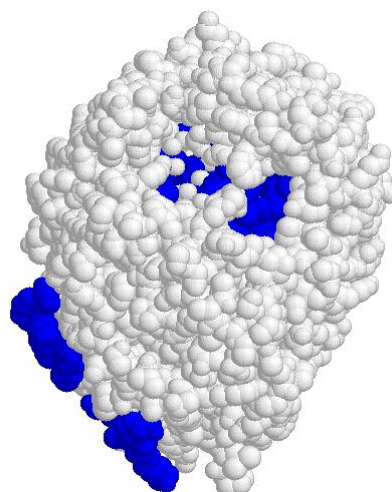


FhuA N domain

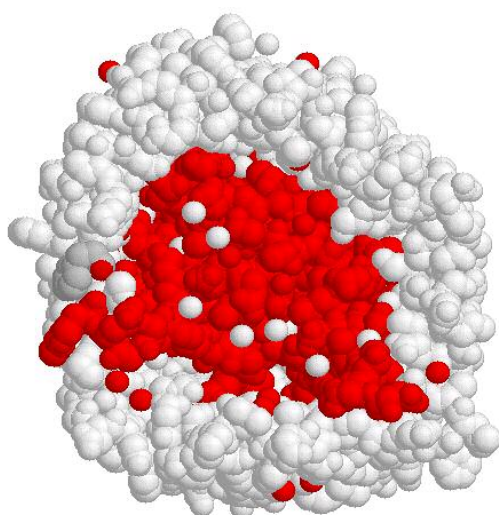
Figure 3. The crystal structure of FepA and FhuA. FhuA's N domain is more compact within the barrel in both the vertical and the horizontal dimensions. In the first row, the C-domain of the LGPs is represented in grayscale while the N domain of FepA is represented in red and that of FhuA in blue (Buchanan 1999, Locher 1998, Ferguson, 1998).



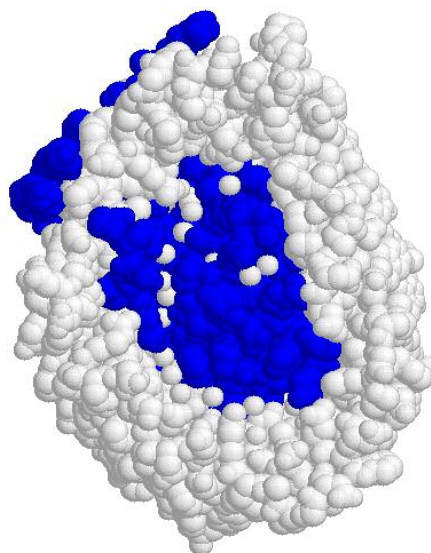
FepA surface view



FhuA surface view



FepA periplasmic face



FhuA periplasmic face

Figure 4. Space-filled representations of the crystal structures of FepA and FhuA. In all the figures, the C-domain of the LGPs is represented in grayscale while the N domain of FepA is represented in red and that of FhuA in blue (Buchanan 1999, Locher 1998, Ferguson, 1998).

Scott et al. (2002) demonstrated in-vivo cross-linking of residues in loop 7 of FepA to other OM porins like OmpA (Chen 1980). The authors employed the homobifunctional, crosslinker sulfo-EGS (Pierce). Sulfo-EGS acts on secondary amines, like in the side chain of lysine. The study also revealed that the binding of FeEnt abolished such crosslinking. Upon ligand binding, the extracellular loops moved towards each other and enclosed the ferric siderophore. From the length of the crosslinker, the authors estimated that loop 7 moved almost 15 Å, in response to ligand binding.

A subsequent study by Ferguson et al. (2002) showed similar translational motion in an equivalent loop in FecA. Portions of loop 7 traverses nearly 11 Å, while that of loop 8 moves nearly 15 Å. On the periplasmic side, short β turns connect the β strands of the barrel. The lumen of the barrel is plugged by the N-domain. This globular structure is located inside the barrel (Buchanan 1999, Locher 1998, Ferguson 1998). The N domain contains two loops NL1 and NL2. These loops extend out along side the surface loops. Several interactions anchor the N domain inside the C domain (see below). Apart from the structural similarities, LGPs share exhibit several functional similarities. Their transport mechanism requires the presence of an inner membrane protein complex, TonB-ExbB-ExbD (Bassford 1976, Hantke 1978). TonB (Wang 1969, Wang 1971, Frost 1975) is a 230-residue protein residing in the cytoplasmic membrane of *E. coli* (Postle 1978, Wookey 1978, Postle 1983, Evans 1986). Its N terminus is located in the cytoplasm (Postle 1988, Schoffler 1989, Roof 1991). ExbB and ExbD are considered necessary to stabilize TonB in the inner membrane (Fischer 1989).

Binding of FeEnt by FepA

Several studies have examined the binding interaction of FepA and FeEnt in detail. Early studies with purified protein demonstrated a very high affinity of interaction ($K_d \sim 20$ nM, Newton 1997). In vivo, the K_d of FeEnt binding has been determined to be as low as 0.2 nM (Newton 1999). When proteins are removed from their natural habitat, small differences occur in their binding affinity. However, a 100-fold difference is rather unusual. This difference emphasizes the fact that in the membrane, FepA occurs in quite a different conformation from that in the crystal structure. The cross-linking studies and the crystal structures of FecA underscore this point. The loops are not static in three-dimensional space. Rather they change conformations over time. This process may optimize the binding process.

An important aspect of the interaction is the biphasic nature of binding. Payne et al. (1997) demonstrated this aspect employing fluorescence spectroscopy. The authors monitored the adsorption of FeEnt to FepA dissolved in the detergents dodecyl maltoside and Triton X-100. Analysis of the binding kinetics revealed a rapid initial phase (with rate constant $k_1 = 1.8 \times 10^{-2} \pm 8 \times 10^{-4} \text{ s}^{-1}$) followed by a slower second phase of adsorption (rate constant $k_3 = 2.1 \times 10^{-3} \pm 2 \times 10^{-4} \text{ s}^{-1}$). These two stages may reflect the presence of two binding sites for FeEnt, B1 and B2.

Alternatively, they may reflect two different events in the binding interaction. The orientation of the loops in the bacterium is probably very different from where the crystal structure located them. Rather than sloping towards each other, the loops may exist in an open conformation like the spread petals of a flower. In this light, it is possible that there is a preliminary weak association with the loops in the open conformation. Subsequently, the loops may undergo a conformational change and move to enclose the ferric siderophore. The difference in the rates of reverse reactions

of these two events may be the reason for the biphasic release of the ferric siderophore.

Some evidence exists to support the former two-site model. The crystal structure of FepA showed two closely spaced iron peaks (Buchanan 1999). These two peaks are located too closely to each other to represent two ferric siderophores. Rather, they presumably represent the twin binding sites predicted by the kinetic model. Using a site-directed mutagenesis approach, Cao et al. identified residues in both sites, whose change affected the binding interaction (Cao 2000). The authors identified residues Y272, F329 and Y260 as contributors to the binding interaction. The former two map to the putative binding site B1 and the latter to B2. The substitution of alanine for tyrosine 260 produces a 100-fold decrease in binding affinity, the largest reported effect of a single amino acid substitution in FepA.

In vivo analysis of the dissociation of FeEnt from FepA further supports the biphasic nature of the reaction (Annamalai and Jin 2004). A rapid initial phase and a slow secondary phase characterized the dissociation reaction. Upon FeEnt binding, the fluorescence intensity of fluorescein 5-maleimide (FM) labeled FepA S271C decreases. Release of the bound siderophore restores the fluorescence. This enables the direct observation of the dissociation process. FepA-S271C was expressed from a *tonB*-strain of *E. coli*, which renders it incapable of transport. The authors saturated FepA-S271C-FM with FeEnt. Subsequently, they monitored the release of FeEnt from the labeled protein. *E. coli* expressing wild type FepA acted as a 'sink' for the released FeEnt. The release reaction followed a biphasic pattern. The rate constant k_{off1} for the rapid initial release was 0.03/s and the k_{off2} for the slower second phase was 0.003/s. In vivo experiments with radioisotopic FeEnt also reproduced the two phases of its release reaction. The loops of FepA and FecA undergo rather large

translations during the binding reaction. The energy required for this motion may be provided by the binding of the siderophore. Motion in vivo and in vitro suggests that the process is independent of the cellular energy sources.

Ligand specificity

The search for a structural explanation for the binding affinity originated from the chemistry of the ferric siderophore. FepA recognizes the iron center of the ferric siderophore (Ecker 1986, Matzanke 1986, Thulasiraman 1998). By comparing the binding of a panel of natural and synthetic siderophores, the authors identified several facets of the process. The interaction is not stereospecific. The change in the chirality of the catechol groups around the iron center did not affect the binding. The catechol groups of FeEnt as mentioned earlier, adopts a Δ configuration around the iron center. Ferric enantioenterobactin (FeEnEnt) contains the opposite Λ chirality. Nevertheless, FeEnt and FeEnEnt bound with similar affinity to bacteria expressing genomically encoded FepA. However, the protein required the presence of an intact iron center. Changes to the backbone of the molecule like substitution of a tertiary amine for the lactone ring in FeTRENCAM did not affect the binding. Nor did substitution with a benzene ring in FeMECAM affect binding. However, any alteration to the catechol moieties as occurs in either natural siderophores like agrobactin or in synthetic siderophores like TRENCAM derivatives abolished binding. Ferric agrobactin also contains a different net negative charge (see above). The change in the iron center with or without the change in the net charge renders ferric agrobactin unrecognized.

FepA	FhuA
Ferric siderophores	Ferric siderophores
– Ferric enterobactin	– Ferrichrome
– Ferric myxochelin C	– Ferricrocin
– Ferric enantioenterobactin	– Ferric coprogen
– Ferric TRENCAM	
– Ferric MECAM	
Toxins	Toxins
– Colicin B	– Colicin M
– Colicin D	– Microcin J25
Phage	Phage
– H8	– T5, T1, UC-1, Φ80
	Antibiotics
	– Albomycin
	– Rifamycin CGP 4832

Table 2. Ligands of LGPs, FepA and FhuA.

In addition to recognizing FeEnt, FepA also serves as the receptor for the bacteriocins, colicin B and D (Pugsley 1976). Colicins are toxins secreted by coliform bacteria to eliminate other coliforms. The genes encoding colicins are usually carried on plasmids called col factors. The colicin operon carries the *activity* gene named cXa, X indicating the particular colicin. The operon also includes the *immunity* gene, cXi. The presence of the latter's gene product protects the colicin secreting bacterium from the toxin. Colicins function in a variety of ways to kill bacteria. Colicin B belongs to a class of colicins called pore forming colicins. The C terminal domain of the colicin kills bacterium by forming pores in the cytoplasmic membrane of the target cell. The resultant loss of proton motive force presumably kills the cell. The interaction of FepA with these large proteins presumably involves larger surface areas of contact than with the siderophores. However, common determinants have been found in FepA for these two processes. Payne et al. (1997) demonstrated the in vivo competition for binding between the colicin B and FeEnt. Further, colicin B shares the biphasic binding kinetics of FeEnt. In addition to binding, for their transport, colicins B and D also share components of FepA with FeEnt (see below).

The elucidation of the proteinic basis of the binding started from a study of the ferric siderophore chemistry. The two prominent features of the complex are its negative charge and its aromaticity. This led to the postulate that the binding site must complement the chemistry of the ligand. The negative charge prompted the search for basic residues in experiments that preceded the crystal structure of FepA (Newton 1997). At neutral pH, the positive charge of the basic amino acids lysine, arginine and histidine will complement the siderophores negative charge.

A comparison of the sequence of FepA receptors from different gram-negative bacteria showed conserved arginines between amino acids 255 and 336. Double mutagenesis of Arg 286 and Arg316 to alanine increased the K_d of binding 80-fold. Single mutagenesis caused little change in binding affinity. This underscores the importance of the chemical nature of the amino acids rather than their contribution to local secondary structure. Their location in the interior of the barrel, just below the extracellular loops favors their assignment as residues participating in the B2 binding site.

Fluorescence spectroscopy with FepA carrying two mutations in its B2 amino acids (Y260A and R316A) supported this notion. The authors monitored the kinetics of binding of FeEnt to FepA Y260A E280C-FI R316 by recording the change in fluorescence intensity. In contrast to FeEnt-FepAE280C-FI interaction, the second phase of the biphasic binding was abolished (Cao 2000). The simplest explanation for this observation is that mutation of these two residues changed the binding properties of B2. R316A also caused more than a 10-fold reduction in the sensitivity to colicin B and D.

Newton et al. (1999) also adopted a different line of approach to the problem. The authors used site-directed mutagenesis to investigate the participation of

individual surface loops in the process. These experiments preceded the determination of the crystal structure of FepA. The authors deleted segments of the FepA polypeptide corresponding to the putative loops postulated in a previously proposed model of FepA (Murphy 1990). The deletions had differing effects on the binding and transport process. However, many of the constructs retained some if not complete functionality towards FepA's ligands, FeEnt, colicins B and D. The deletion of loops 7 and 8 abolished FepA's function. However, the constructs remained accessible to binding by surface epitope specific antibodies. This suggested that loop 7 and loop 8 are essential for FepA's binding function.

In general, the deletion of long segments from a polypeptide is expected to cause global disruption of its tertiary structure. So an argument can be made that the deletion of the loops altered the global protein configuration and it is this disfigurement that caused the observed effects. The accessibility to the monoclonal antibodies argues against this supposition. Furthermore, the crystal structure of the FecA protein (Ferguson 2002) and the experiments with cross-linking (Scott 2002) and justified the prediction that these loops are important in the binding process. Upon ligand binding, the corresponding loop 7 and 8 in FecA exhibit large translations and enclose the siderophore after the initial binding. The cross-linking studies predict a similar translation for loop 7 of FepA. The deletion of loops 7 and 8 of FepA also abolished sensitivity to colicin B.

Three catecholate rings surround the iron center of FeEnt forming a zone of aromaticity around the cognate face of the siderophore. This led to the proposition that aromatic stacking interactions with FepA may contribute to the binding interaction. The search for aromatic amino acids in the central region of FepA revealed seven conserved residues. Tyrosine 260 is conserved among FeEnt

transporters in gram- negative bacteria. Other residues identified include tyrosine 272 and phenylalanine 329. Genetic replacement of residues 260 (see above), 272 and 329 with alanine produced significant drops in the adsorption affinity. FepA F329A bound FeEnt with 2-fold less affinity. Double and triple mutagenesis of these residues caused synergistic defects in binding. Mutagenesis of these residues also affected the transport capabilities of the FepA protein. Y260A and Y272A caused commensurate reductions in transport and binding, while F329A caused more than a 20-fold impairment of transport, ten times the effect on binding. These results suggest that the former 2 tyrosine residues act primarily in ligand binding. The effect of their mutation on transport derives from the effect on binding. The latter phenylalanine participates in the transport process.

The above studies identified some of the aromatic and basic determinants of binding. It is noteworthy that some of the residues like F329, although located at the extremities of the surface loops affected transport more than binding. The crystal structure of FepA also shows additional aromatic residues, mainly tyrosines in the outer reaches of the surface loops. Several of these tyrosines are conserved among FeEnt and other ferric siderophore transporters (see below). Based upon sequence comparison and exposure in the crystal structure, we selected nine tyrosines and one tryptophan in the polypeptide for further investigation (see below).

Transport of FeEnt by FepA

Despite intense scrutiny, the transport mechanism of FepA has not yet been fully resolved. Several experiments have addressed this problem with varying results. Some of these experiments focused on the identification of segments or even domains important for the transport function. Armstrong et al. (1990) generated segmental deletions in frame in the FepA polypeptide using restriction enzymes. They also

inserted linker sequences encoding the peptide Leu-Glu, after specific residues in the polypeptide sequence. The authors analyzed the phenotypes of these mutant constructs. The authors used susceptibility to proteinase K to check localization of the proteins. Several of the constructs localized to the OM despite lacking large portions of their polypeptides. A derivative of FepA lacking 87 internal residues close to the N terminus was unable to transport FeEnt. The deletion named H261 stretched from residue 55 to residue 142. The mature protein lacked the latter two-thirds of the N domain. The construct also conferred less than 5% sensitivity to Colicins B and D compared to the wild-type protein. The insertion of Leu-Glu peptides after residue 204 or 635 affected only colicin sensitivity. The mature proteins transported FeEnt at almost wild-type levels. These studies preceded the elucidation of the crystal structure of the LGPs.

Surface loops in FepA transport

The surface loops of FepA also play important roles in the transport process in addition to their role in binding. The fact that the effects of their deletion on transport did not always derive from the effects on binding supports this conclusion (Newton 1999). Newton et al. (1999) identified these ‘class i and ii mutants’ by comparing the change in the K_d of binding and the K_m of transport. These mutants had greater effects on transport than on binding. Class ii mutants had such large effects on the K_m that the authors had to extend uptake times up to an hour to measure the slow rates of transport. Class i includes loops 3, 4, 5 and 9. Loops 2, 10 and 11 showed class ii effects. As mentioned earlier, alanine mutagenesis identified F329 as one of the residues important for the transport process (Cao 2000). F329 lies in a segment of the polypeptide that was not mapped in the crystal structure (from residues 324 to 334). However, its probable location is in the outer reaches of surface loop 5. Despite this

location, the amino acid plays a greater role in transport than in binding. This underscores the point that the transport of the ferric siderophore employs components from all parts of FepA including the surface loops.

The N domain in FepA transport

Scott et al. (2001) utilized site directed mutagenesis to excise the N domain of FepA. The resultant construct, Fep β bound and transported FeEnt (Scott 2001). The K_d of binding and K_m of transport were similar to wild type FepA. However, the capacity of binding and the maximum velocity of the transport were severely reduced. The latter two parameters reflect the fraction of functional protein molecules on the surface of the bacterium. The mutations also affected colicin B and D sensitivity. FepB required the presence of TonB in order to accomplish these functions. A similar result was obtained with FhuA (Braun 1999, Scott 2001). In addition to the deletion of the N domain, the authors also constructed chimerical proteins, wherein they genetically exchanged the N domains of FepA and FhuA to generate FhuNFep β and FepNFhu β . The chimeras behaved similar to the deletions. The results implied that the N domains of LGPs serve secondary roles in their binding and transport functions. The surface loops discriminate between the siderophores FeEnt and Fc. They are able to transport without their own N domain or even with a different N domain. They are also able to interact directly with TonB. The N domains of the LGPs have no specificity for their cognate siderophores. The chief role of the N domain is to interact with the surface loops to enable them to adopt functional conformations. This could explain the low fraction of competent proteins in the deletions and the chimeras.

A subsequent investigation (Vakharia 2002) contradicted these findings. The deletion of the N domain of FepA rendered it nonfunctional in their host strain, *E. coli* KP1411. The mutation abolished colicin B sensitivity. However, their constructs

rendered colicin B susceptibility to *E. coli* RWB18-60 (*F⁺ leu proC trp thi rpsL recA entA fepA*). The strain of *E. coli* used by Scott et al. (2001) was KDF541 (*F⁺ leu proC trp thi rpsL recA entA fepA fhuA cir*). KDF541 is derived from RWB18-60. They contain the same mutation in the FepA gene. The mutation is so located that the gene could still express 363 residues of the protein. The resultant fragment, if expressed contains the complete N domain, which may in turn complement Fep β . The low efficiency of this complementation may explain the lower capacity of binding and the lower V_{max} of transport. A similar explanation may hold true for FhuA. Braun et al. (2003) cloned the isolated N domain and the C domain in tandem and expressed these fragments in the *fhuA* strain of *E. coli*, BL21. They employed formaldehyde crosslinking to conclude that the separately expressed N domain incorporated itself into the C domain in the OM. They also used cysteine substitutions on each domain to obtain similar evidence for incorporation by observing inter-domain disulfide bond formation. Although these results suggest that close proximity between the isolated domains happens, they do not prove that the domain interaction results in native protein-like conformation. The interactions observed may take place during protein folding or assembly into the OM. The requirement for signal sequences on both the individual gene fragments suggests that this process happens outside the cytoplasm. Nevertheless, the role of the fragment containing the N domain in Fep β expressing clones needs to be resolved.

The possibility of complementation between the chromosomal fragment and Fep β or Fhu β necessitated the development of *E. coli* strains with precise deletions of FepA and FhuA structural genes (see below). To clarify the functionality of the different FepA and FhuA constructs (Scott 2001), I examined the phenotype they

conferred on *fepA*- and *fhuA*- bacteria. I also repeated some of the experiments reported earlier (Vakharia 2002, Braun 2003).

The role of the N domain in toto needs further investigation. However, evidence attributing important functions to parts of the N domain has been obtained. A random mutagenesis approach identified residues in the N domain that affected both FeEnt transport and colicin binding and sensitivity (Barnard 2001). The study identified three regions in the N domain. These include the tonB box (see below), the loops and a cluster near the barrel wall. The three regions house one or more residues that affect the protein function. The tonB box residues are Ile14 and Val16. Gly64 is located in loop NL1 and Arg105 belongs to NL2 (see above). The cluster near the barrel wall included residues Arginines 75 and 126 and glycines 127, 139 and 140. Although the random mutagenesis identified these amino acids, the replacement of amino acids with residues other than alanine poses a potential problem. For example, the substitution of a proline for arginine105 may cause large-scale differences in the conformation of the protein. Similar effects need to be demonstrated with site-directed mutagenesis of the said residues to alanine. Further more, the authors subjected a part of the *fepA* gene coding for the N domain to random mutagenesis. They exchanged the segment with that of the wild-type *fepA* gene on a plasmid, transformed a *fepA*-strain of *E. coli* and selected the resultant clones for resistance to colicin B. The authors then sequenced the N domain portion of the gene and identified these mutations. Although it is a small possibility with the short sequence of the plasmid encoded genes, the colicin B screening may have selected for other mutations located in the rest of the *fepA* gene. Sequencing the entire *fepA* gene would have excluded this confounding possibility. Using site-directed mutagenesis, Chakraborty et al. (2003) changed arginines in the N domain that formed part of a lock-box with glutamates of

the C domain. These changes had little effect on binding but had moderate to severe effects on the transport functions.

The N domain of FepA contains two loops NL1 and NL2. The loops connect the strand N β 1 with N β 4 (loop NL1) and the strand N β 4 with N β 5 (loop NL2). Loop NL1 contains an additional antiparallel β -hairpin (N β 2, N β 3). Both loops extend from the center of the pore toward the extracellular loops of the barrel, at heights of ~ 17 Å (NL1) and ~ 19 Å (NL2) above the bilayer interface. The loops are well placed to interact with the ligand, FeEnt during its binding and transport. In the crystal structure, the loops exist in close proximity to the electron density considered to be the iron atom of FeEnt. Therefore, these loops were dubbed as the sensor loops. In order to determine their role in the protein's function, portions of these loops were deleted and the binding and transport properties of the resultant constructs were examined (see below).

TonB and ferric siderophore transporters

One of the intriguing aspects of LGP function is their dependence on TonB and energy. Almost all functions of LGPs require TonB. The interaction of the phage T5 with FhuA is a known exception (Hantke 1978). The binding of ligand happens independently of TonB. FepA expressed in functionally *tonB*⁻ strains binds FeEnt just like *tonB*⁺ strains. However, the absence of the protein abrogates transport. Questions remain about the mechanism of tonB action. Does TonB bind LGPs? If it does, what are the binding sites? How does this intermembrane communication happen?

Numerous studies have suggested the direct interaction of TonB with LGPs (Heller 1988, Gunter 1990). One of the models proposed for the interaction involves the cycling of TonB between the outer and inner membrane of *E. coli* (Letain 1997). The authors of this model observed that TonB fractionated with both the outer and

inner membranes of *E. coli* in sucrose density gradient separations. Another methodology assessed the accessibility of the TonB N terminus to labeling with dyes (Larsen 2003). The authors labeled a cysteine mutant of TonB with the dye, Oregon green. Oregon green freely enters the periplasm (Yan 1993), but does not penetrate the cytoplasmic membrane. By making the cysteine substitution close to the N terminus of the protein, the authors concluded that this labeling reflected exposure of the target cysteine and thereby the N terminus to the periplasm. The N terminus of TonB is normally located in the cytoplasm. The authors postulate that the protein cycles between membranes and delivers the transport signal to ligand-gated porins. However, it remains doubtful whether this cycling can occur fast enough for the 10-fold fewer tonB molecules to enable transport by FepA proteins. It is unclear whether TonB or FepA or both have sufficient lateral mobility in their membranes to sustain the process as the model envisages. The exterior surface of the outer leaflet of the OM bilayer is covered by the contiguous lipopolysaccharide (LPS). Since the LGPs project 30 to 40 Å above the lipid bilayer, they would have to negotiate their way laterally through not only the lipid bilayer but also the LPS. In other words, both the LPS and the membrane bilayer would need to be fluid structures. It is also noteworthy that no membrane rafts serving as protein-protein interfaces have been reported for bacterial inner and OMs. The relative localization of tonB and FepA molecules on the bacterial membrane structure is as yet unresolved. Questions remain whether these molecules are spread diffusely throughout the bacterial membrane or localized to specific loci like Bayer's zones of adhesion (Bayer 1991). The latter location can conceivably provide a ready interface for interaction between the LGPs and TonB.

Other investigators have employed different approaches to study the interaction between the LGPs and TonB. Skare et al. (1993) used formaldehyde

crosslinking to observe complexes between FepA and TonB. Ogierman et al. (2003) observed disulfide formation in vivo between introduced cysteines in TonB and FecA. The cysteines were substituted for residues in the tonB box of FecA (D80C, A81C, L82C, T83C and V84C) and the C domain of TonB (Q160C, Q162C and Y163C). Paired combinations of these mutations, one on each protein, showed in vivo disulfide formation between the cysteine mutants of TonB and FecA. The authors also performed formaldehyde cross-linking between the two proteins. The cross-linking studies suggest that the C domain of TonB comes in close proximity with the LGPs. The proteins may therefore interact with one another and the LGPs transport their ligands across the OM. At what stage of the uptake after binding, this interaction happens and how it helps transport, remains unsolved. TonB has also been suggested as the energy transducer for transport. However, it has not yet been discovered as to how this supposed energy transduction takes place.

The N domain– where art thou?

The crystal structures of LGPs like FepA and FhuA show their N domain completely filling the β barrel formed by the C domains. This location of the N domain within the C domain necessitates a change in its own conformation in order to allow transport of the cognate ligands. We can construe at least three different models to explain the transport process (Klebba 2004). The entire N domain may efflux out of the channel into the periplasm (the concerted transport model). Alternatively, a variation of the concerted model is that the N domain may incur a compaction inside the barrel. Both these possibilities predict the creation of a tunnel in the protein linking the surface with the periplasm. A third possibility is that the siderophore may slide along successive portions of the barrel and the N domain (sequential). This model envisages the creation of serial binding pockets for the siderophore along the

length of the protein. The latter two models also involve conformational changes within the N domain.

Each postulate has its own merits and demerits. There are 46 direct or water mediated hydrogen bonds tethering the N domain to the β strands of the C domain. Moreover, there are 17 interactions between the N domain and the extracellular loops (Buchanan 1999). These hydrogen bonds may seem to be an energetic barrier for the efflux of the N domain. However, the extruded N domain will enter the aqueous periplasm. This should enable the reformation of these hydrogen bonds with water. Therefore, the hydrogen bonds by themselves do not exclude the efflux model.

Usher et al. (2001) reported that the isolated N domain of FepA is expressed in the periplasm of the host strain in a partially denatured form. They found that the isolated N domain can bind FeEnt in vitro with 1000-fold less affinity than the whole protein. The authors postulated that the denaturation of the N domain in the periplasm may help to release the bound ferric siderophore. However, the return of the N domain into the barrel would then involve its refolding as seen in the crystal structure. TonB may be involved in this process. The physiological function of the LGPs is the internalization of small ligands like ferric siderophores. Additionally, they support the transport of much larger entities like domains of proteins and phages. The transport of ferric siderophores does not require the entire diameter of the barrel.

The concerted efflux model is also the most suitable for the transport of domains of the macromolecules such as colicins. The concerted compaction model would also involve a similar rearrangement of some of the hydrogen bonds. A relevant consideration here is the volume available in the barrel. β -barrels are stable structures and they are not expected to undergo large scale distortions in their configurations. The calculated exterior volume of the elliptical cylinder formed by the

C domain is around 15,000 Å³ (ABE Volume Calculator Page, S.D. Filip To, <http://www.abe.msstate.edu/~fto/tools/vol/index.html>). If a bridging tunnel arises in the interior of the barrel, it would need to be sufficiently large to accommodate FeEnt, the radius of whose iron center is about 4.5 Å. Therefore, a cylinder of about 9 Å cross-sectional diameter and around 70 Å high is required. The volume of the space will be around 4450 Å³. It is not clear if the N domain can compact itself to less than two-thirds of the available volume. This consideration favors the next model.

The sequential model is perhaps the least attractive model. The transport process may happen in one of two ways. As the ferric siderophore slides along the channel, successive binding pockets are formed with increasing affinity for the ligand. The lowermost pocket may equilibrate with the periplasmic aqueous medium. However, this would imply that this pocket is in some way destabilized in order to release the ferric siderophore. TonB and/or energy may drive this process. Alternatively, the creation of each high affinity site may be succeeded by its own destabilization and the simultaneous creation of the successor site. At the lowermost site, this would enable the siderophore to enter the periplasm.

The concerted efflux of the N domain is relatively more amenable to experimental investigation. If the N domain exits out of the barrel and enters the periplasmic space, it implies that it will be physically accessible in the periplasm. I adopted two different strategies that could potentially detect the N domain in the periplasm. The first strategy involved the use of the Tobacco Etch Virus protease (TEV protease). The analytical utility of TEV protease (Dougherty 1988) in protein chemistry stems from its having a relatively unique target amino acid sequence, ENLYFQ*G. The introduction of this sequence into surface exposed loci of cellular proteins renders these molecules susceptible to proteolysis by the cysteine protease

(Target directed proteolysis, coined by Micheal Ehrmann, School of Biosciences, Cardiff University, Cardiff, UK). The experimental design involved the introduction of the protease recognition site in the N domain of the receptor protein by site-directed mutagenesis. The protease was introduced into the periplasm of the bacteria. Transport through the receptor was induced by adding the cognate ferric siderophore. If the N domain travels outside the periplasm, then the protease will gain access to the target sequence and cleave the receptor into two fragments, which can be observed with standard protein detection techniques. Accordingly, I engineered protease recognition sites in the N domain of FhuA.

The rationale behind my choice of FhuA and not FepA stemmed from two observations. One of them, which still holds true is the nature of the domain in FhuA and FepA. In FhuA, the globular N domain is more compact inside the barrel. On the other hand, FepA's N domain fills out its barrel (Buchanan 1999, Locher 1998, Ferguson 1998). I felt that this difference might cause changes to FepA's N domain to be more disruptive than FhuA's domain. The other observation was that when the N domains of the proteins were exchanged between FepA and FhuA, the FhuA β barrel – FepA N domain (HPEB) chimera functioned better than the reverse combination (Scott 2001). This suggested that changes in the N domain of FhuA and even its complete replacement leaves a more functional Fc transporter than similar manipulations of FepA does a FeEnt transporter. This conclusion has since been questioned by subsequent investigations (Vakharia 2002, Braun 2003) (see also below).

I selected sites based on their surface inaccessibility in the crystal structure and on the local amino acid sequence (Coulton 1986) to minimize structural and chemical perturbations to the protein. They are located at three levels in the FhuA N

domain; near the periplasmic opening, FhuA136-142, and one each on the two N domain loops, FhuA71-77 and FhuA113-119, the former on the loop away from the hinge and the latter at the highest point on the side of the hinge between the N- and the C- domains (Figure 5). Using biochemical and microbiological techniques, I attempted to characterize the orientation of the N domain during the FhuA's transport cycle.

For my experiments, I used both purified as well as coexpressed TEV protease. We obtained purified recombinant TEV protease (rTEV protease) from Invitrogen. 1 unit of rTEV protease cleaves >95% of 3 µg control substrate in 1 hr at 30°C. In the past, proteolytic specificity has been harnessed to map the topology of a protein, particularly membrane proteins (protease accessibility assay, Murphy 1992). The capability has been also been expanded to the analysis of proteins by coexpression *in vivo* (Mondigler 1996). Here I attempt to extend the technique further to analyze the chronological disposition of a dynamic domain of a transport protein.

The second strategy that I employed to investigate the disposition of the N domain involved fluorophore labeling. Cao et al. described the protocols for specifically labeling FepA with fluorophores *in vivo* (2003). The authors introduced cysteines in the polypeptide by site-directed substitution mutagenesis. The cysteines were then labeled with sulfhydryl reactive fluorochemicals including FM and Alexa Fluor® 680 C5-maleimide. The maleimidyl moiety specifically targets cysteines on proteins. In the oxidative environments in the periplasm and the cell exterior, the cysteines on proteins usually form cystines with each other. As a result, unbonded cysteines are rare in secreted proteins. The paucity of reduced cysteines enables the specific labeling of introduced cysteines *in vivo*.

The experimental design in this case involved the introduction of cysteines by site-directed substitution mutagenesis in different parts of the N domain. Some of these loci are surrounded by the barrel in the crystal structure, while others are expected to be exposed either to the cell surface or to the periplasm. I then assessed the accessibility of these cysteines to labeling by fluorophores. By comparing their susceptibility to labeling with their location in the crystal structure, I hoped to map the location of these regions of the protein during the transport cycle. If residues that are hidden in the crystal structure can be made susceptible to labeling by inducing transport, then it follows that these regions undergo conformational changes to expose the cysteines. In this manner, I hoped to characterize the chronological disposition of the N domain during protein function.

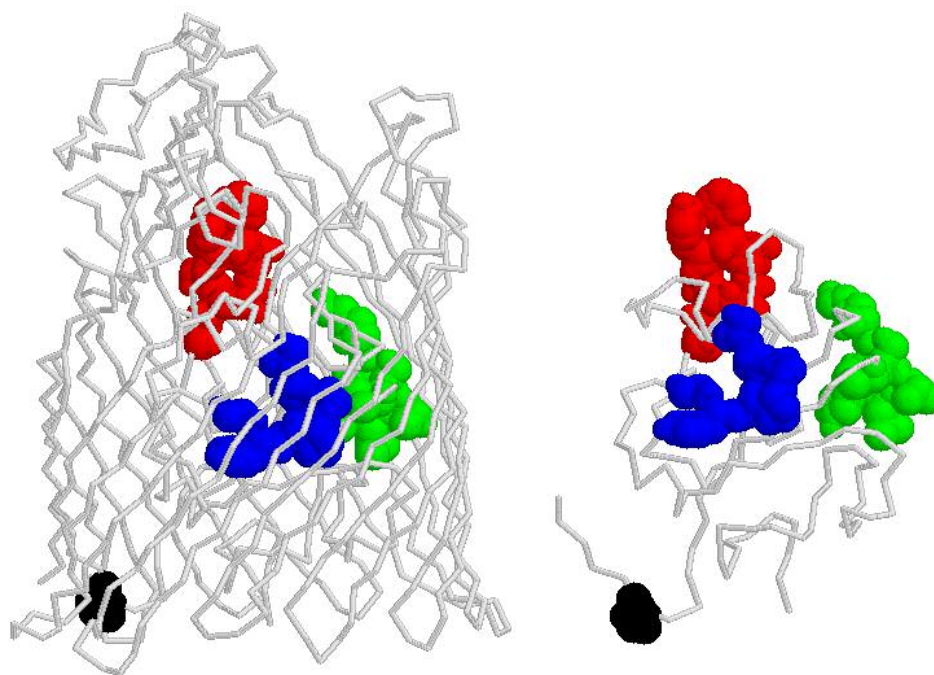


Figure 5. Location of FhuA TEV site mutations. The crystal structure of the FhuA backbone is depicted in grayscale. On the left is the whole protein and on the right is the N-domain. The amino acids substituted for the TEV sites are depicted in space-filled fashion, amino acids 71-77 (blue), 113-119 (red) and 136-142 (green). The hinge residue 160 is featured in black.

Chapter 2

Materials and methods

Bacterial strains, plasmids and culture conditions:

Bacteria and plasmids used in this study are listed in the tables below (tables 3 and 4). Unless otherwise mentioned, all the bacterial strains are derivatives of *E. coli* K12. Unless otherwise stated, bacteria were grown in Luria Bertani (LB) medium (Miller 1972) at 37°C. Bacteria expressing the pUC18, pCC1 or pMER1 plasmids grew poorly in plain LB medium (LB is frequently rich in lactose and induces debilitating protein expression): therefore, I added 1% glucose (catabolite repressor) to the culture. Where required, I used terrific broth, tryptone and nutrient broth.

For subculture, I used a variety of defined media including MOPS medium (Neidhardt 1974) with or without zinc and copper, T medium, minimal medium A and minimal medium 9. Unless otherwise stated, the antibiotics ampicillin (100 µg/ml), streptomycin (100 µg/ml) and chloramphenicol (20 µg/ml) were added as required. All antibiotics were purchased from Sigma. Glucose (0.4%) or acetate (0.25%) was used as carbon sources, as dictated by the nature of the plasmid promoters. To induce protein expression from specific promoters, I added inducers including 0.2% arabinose (for *ara* promoter) and 10 µM IPTG (for *lacZ* or *lacIq*) respectively to exponentially growing cultures. When required, I used the sulfhydryl reducing agents 1 mM of cysteine, 2-mercaptoethanol, dithiothreitol (DTT) or dimercaprol (BAL) (SIGMA).

Strain	Relevant genotype	Reference or source
AB2847	<i>aroB tsx malT thi</i>	Braun 1978
BN1071	<i>F- thi entA pro trp rpsL</i>	Klebba 1982
CC118	<i>F- Δ(ara-leu)7697 araD 139 ΔlacX74 galE galK ΔphoA20 thi rpsE rpoB argE (Am) recA1appR1</i>	Manoil 1985
KDF541	<i>F- leu pro trp thi rpsL recA entA fepA fhuA cir</i>	Rutz 1992
KDF571	KDF541 <i>tonB</i>	Rutz 1992
KDL118	CC118 <i>fepA</i>	Murphy 1989
KS272	<i>F- ΔlacX74 galE galK thi rpsL(strA)ΔPhoA(PvuII)</i>	Strauch 1998
MB 97	AB2847 <i>fhuA</i>	Braun 2003
OKN3	BN1071 <i>fepA</i>	Salete Newton
OKN73	MB97 <i>fepA</i>	This study
SF120	KS272 <i>ptr-32::ΩCmrdegP41(ΔPstI-Kanr)ΔompT</i>	Meerman 1994
SF130	SF120 <i>rpoH 15 (minitet)</i>	Meerman 1994

Table 3. List of strains used in this study.

Plasmid name	Relevant genotype/phenotype	Reference
pCC1	<i>Ptac male::TEV protease lacIq Cmr</i>	Ehrmann, M
<i>pfepNfhuβ</i>	pHSG575 <i>fepA 1-152::fhuA160-723</i>	Scott 2001
<i>pfepβ</i>	pHSG575 <i>fepA (Δ17-150)</i>	„
<i>pfhuNfepβ</i>	pHSG575 <i>fhuA1-155::fepA149-724</i>	„
<i>pfhuβ</i>	pHSG575 <i>fhuA (Δ5-160)</i>	„
pFP100	pUC18 <i>fepA1-100::phoA</i>	Murphy 1995
pFP227	pUC18 <i>fepA1-227::phoA</i>	„

pFP258	<i>pUC18fepA1-258::phoA</i>	„
pFP290	<i>pUC18fepA1-290::phoA</i>	„
pFP352	<i>pUC18fepA1-352::phoA</i>	„
pFTPc	<i>pHSG575 fepA-TEV site-PhoA fusion</i> <i>Cmr full fepA promoter</i>	This study
pHP751	<i>pT7-5 cma cmi</i>	Pilsl 1993
pITS11TEV site 113-119	<i>fhuA113-119ENLYFQG</i>	This study
pITS11TEV site 136-142	<i>fhuA136-142ENLYFQG</i>	„
pITS11TEV site 71-77	<i>fhuA71-77ENLYFQG</i>	„
pITS11	<i>full promoter-fhuA</i>	Scott 2001
pITS23	<i>pHSG575 fepA (full fepA promoter)</i>	Scott 2001
pITS449	<i>pUC18fepA (No -35 region of</i> <i>fepA's promoter)</i>	Armstrong 1990
pMER1	<i>pBAD22 malE-TEVsite-phoA Apr</i>	Ehrmann, M
pUC18fepN	<i>pUC18fepA (1-150)</i>	Scott, DC
pUC18fhuA	<i>fhuA</i>	Scott, DC
pUC18fhuATEV site 113-119	<i>fhuA113-119ENLYFQG</i>	„
pUC18fhuATEV site 136-142	<i>fhuA136-142ENLYFQG</i>	„
pUC18fhuATEV site 71-77	<i>fhuA71-77ENLYFQG</i>	This study

Table 4. List of plasmids, their relevant genotypes and their sources/references.

Site-directed mutagenesis

The mutations were engineered either by Kunkel's M13 mutagenesis (Kunkel 1985) or by Quikchange[®] site directed mutagenesis method (Stratagene, San Diego, CA). Kunkel's mutagenesis was used to generate the alanine substitutions of surface residues in pITS 449 (Rutz 1992). Plasmid pITS449 (*Plasmid iron transporter system*) is a derivative of pUC 18 (a high copy plasmid vector, Yanisch-perron 1985) with the *fepA* gene cloned into the SmaI site of the vector (Armstrong 1990). The gene is under the control of its natural fur regulated promoter. However, only one (-10) of the two promoter regions, located upstream of the structural gene, is cloned into the plasmid. The mutation was then transferred to pITS23 by restriction fragment exchange with the endonucleases KpnI and SstI (Invitrogen). Mutations W101A, Y217A and Y540A were directly engineered on pITS23 using the Quikchange kit. All the mutations were confirmed by double stranded sequencing using the Alf Express sequencer (Amersham Pharmacia), and appropriate CY-5 labeled oligonucleotide primers.

I introduced the TEV-protease target sites in FhuA (Table) by site-directed mutagenesis (Quikchange, Stratagene). I substituted 7 amino acid segments of the polypeptide with the TEV recognition sequence, ENLYFQ*G. The mutant FhuA proteins were cloned into the plasmid vectors, either the high copy pUC18 or the low copy pHSG575. FhuA-TEV site constructs were expressed in either KDF541 (FepA-FhuA-) or MB97 (*fhuA*) or OKN73 (*fhuA**fepA*).

Protein detection

Bacteria were grown overnight in LB broth, and subcultured into iron deficient MOPS minimal medium (containing glucose and other nutritional supplements, Neidhardt 1974) for 5.5 to 6.5 hours at 37°C with vigorous aeration. For strains that failed to grow in MOPS medium, I used T medium or iron poor nutrient broth. For

non-iron regulated proteins, bacteria were grown in LB broth or other rich media. Volumes corresponding to 5×10^8 bacteria were centrifuged at $17,000 \times g$ and resuspended in 100 μ l of sample buffer (60 mM Tris, pH 6.8, 10% glycerol, 2% sodium dodecyl sulfate (SDS), 3% 2-mercaptoethanol), and boiled for 3 min to achieve complete cell lysis. 2-mercaptoethanol was omitted for nonreducing electrophoresis. After centrifugation at $10,000 \times g$ for 3 min to pellet cell debris, 20 μ l samples of the whole cell lysates were loaded onto a 10% SDS polyacrylamide gel (SDS-PAGE, Laemmli 1970). The sample was electrophoresed at room temperature for about 1.5 hours and electro-eluted on to nitrocellulose membranes.

For nondenaturing electrophoresis, the samples were not boiled and electrophoresed at room temperature or at 4°C . Western immuno blots were performed using specific antibody solutions and developed with ^{125}I -Protein A. The nitrocellulose was exposed to a phosphor imaging screen overnight. The radioactivity was quantitated by phosphor imaging (Molecular Dynamics). Alternatively, the blots were developed colorimetrically with Nitroblue tetrazolium and bromochloroindolyl phosphate (NBT/BCIP). In some experiments, the gel was also stained with coomassie blue (Fairbanks 1971) for observing the protein bands.

Siderophore nutrition assay

Bacteria were grown in LB medium until they reached an $\text{Abs}_{600} \sim 0.5\text{-}1.0$ (exponential phase of growth). Alternatively, I grew bacteria in iron-poor nutrient broth or iron-free MOPS medium. A 100 μ l sample of the bacterial culture was plated with 3 ml of soft nutrient top agar (low iron medium) containing 100 μM of the iron chelator, apoferrichrome A and the relevant antibiotics. Alternatively, I used 100 μM bipyridyl A as the chelator. A sterile paper disc (Becton Dickinson and company, France) was placed in the center of the solidified top agar and 10 μ l of 50 μM ferric

siderophore was added to the center of the disc. The plates were incubated overnight at 37°C. The results were expressed as the diameter of the zone of visible growth in mm, around the paper disk.

Siderophore binding

Bacteria expressing wild-type or mutant ligand-gated porins were grown overnight in LB and subcultured into MOPS and allowed to grow for 5.5 to 6.5 hours at 37°C with vigorous aeration and then placed on ice. ⁵⁹Fe-siderophore was prepared with a specific activity of 150-400 cpm/pmol and purified by column chromatography. I carried out the binding reaction (Newton 1999) at 0°C to prevent the uptake of bound ferric siderophore. A 100 µl aliquot of the ice cold culture (~5 x 10⁷ bacteria) was taken in a 50 ml test tube and 10 ml of ice cold MOPS medium containing the different concentrations of ⁵⁹ferric siderophore was poured into the tube to achieve rapid and thorough mixing. The tubes were incubated on ice for 1 min and the mixture filtered through 0.45 µm and washed with 10 ml of 0.9 % LiCl (aq). The bound radioactivity was counted using in a Packard Cobra gamma counter. I tested bacteria not expressing the proteins of interest as negative control and subtracted the values obtained from those of the test strains, to exclude non-specific adsorption. The experiments were generally done in triplicate for each concentration of ferric siderophore used. Aliquots of the bacterial culture were saved for determining the level of protein expression for each mutant strain in the binding experiment. The *K_d* and capacity of binding of wild type and mutant receptors were determined using the one site bound versus free equation in Grafit 5.0.9 (Erithacus).

Siderophore transport

Bacteria expression the receptor proteins were grown overnight in LB and subcultured into MOPS and allowed to grow for 5.5 to 6.5 hours at 37°C with

vigorous aeration. $^{59}\text{FeEnt}$ was prepared with a specific activity of 200-400 cpm/pmol and purified by column chromatography. All the transport procedures (Newton 1999) were performed at 37°C. A 100 μl aliquot ($\sim 5 \times 10^7$ bacteria) of the bacterial culture was taken in a 50 ml test tube and 10 ml of MOPS medium containing the different concentrations of $^{59}\text{FeEnt}$ was poured into the tube. After incubation, the transport reaction was quenched with a 100-fold excess of non-radioactive ferric siderophore. Reactions with very high concentrations of ^{59}Fe -siderophore ($> 100 \text{ nM}$) were not quenched because of the extremely large amounts required to achieve a 100-fold excess of non-radioactive ligand. The mixture was then filtered through 0.45 μM nitrocellulose filters and washed with ice cold 0.9 % LiCl in water. The bound radioactivity (in cpm) was counted using a Packard Cobra gamma counter. Negative controls were also tested when high concentrations of FeEnt were used for the low affinity mutants. The experiments were generally done in triplicate for each concentration of ferric siderophore. Aliquots of the bacterial culture were saved for determining the level of protein expression for each strain in the transport experiment. The initial transport rate was calculated by measuring the difference in the bound cpm between two independent measurements, one incubated for 5 sec and the other for 15 sec, for each concentration of ferric siderophore. The K_m and the V_{max} of transport were determined from these 10 sec uptake rates using the Enzyme Kinetics equation in Grafit 5.0.9 (Erithracus). For mutants with lower uptake capabilities, the kinetic parameters were calculated by measuring the uptake over longer periods of time.

Colicin killing assay

Bacteria were grown overnight in LB medium. A 100 μl sample of the culture was plated on LB agar with 3 ml of tryptone top agar containing the relevant antibiotics. Serial dilutions of Colicins B and D were made fresh in LB and applied on

to the plate using a clonemaster (Immusine). The plates were incubated at 37°C overnight. The susceptibility to colicin killing (Cao 2000) was expressed in arbitrary titration units, defined as the reciprocal of the highest dilution of colicin that caused a clearing of the bacterial lawn. The data was tabulated as the ratio of the mutant titer to the wild type titer in percentage units.

Competition between ferric catecholates

Bacteria expressing FepA were grown overnight in LB and subcultured into MOPS and allowed to grow for 5.5 to 6.5 hours at 37°C with vigorous aeration. ⁵⁹FeEnt was prepared as mentioned above. The bacterial suspension was incubated with premixed ⁵⁹FeEnt and varying concentrations of the competitor. All manipulations were performed on ice. The experiments were done in triplicate for each mixture of competitor with 1 nM ⁵⁹FeEnt. The cells were then collected by filtration through nitrocellulose and washed with 0.9 % lithium chloride to remove unbound ligand. The bound radioactivity (in cpm) was counted using a Packard Cobra gamma counter. KDF541 was also tested as negative control and the values subtracted from those of the test strains, to exclude non-specific adsorption.

Periplasmic incorporation of TEV protease

Periplasmic incorporation of the TEV protease was performed by the methodology described by Brass (Brass, Methods in Enzymology. Vol. 125, 289-302). Bacteria from an overnight culture were subcultured into MOPS medium and grown until the culture reached an Abs₆₀₀ of 0.5 – 0.7. A total of 1×10^9 cells were pelleted down by centrifuging at 10000 to 12000 x g for 2-5 min in a 1.5 ml microcentrifuge tube. The cell pellet was washed first with 1 ml of 100 mM Tris - HCl, pH 7.5 and then with 1 ml of 100 mM potassium phosphate buffer, pH 7.5 at room temperature. The cells are then suspended in 50 µl of ice cold 100 mM Tris-

HCl, pH 7.5 containing 300 mM CaCl₂ and variable amounts of TEV protease (Invitrogen), transferred to 110x10 mm test tubes and shaken vigorously on ice for 30 min using a reciprocal shaker. Alternatively, the bacteria were permeabilized with low-calcium high-sucrose buffers (Zgurskya 1999). The cells are then washed with 0.9% NaCl at room temperature once or twice. The cell pellet is then resuspended in 1 ml of MOPS medium and retained at RT until use (typically 15 min).

Periplasmic expression of TEV protease

Plasmid pCC1 encodes a periplasmically expressed maltose binding protein - TEV protease fusion. The test substrate used was maltose binding protein – TEV site – Alkaline Phosphatase fusion (MBP-TEV site-PhoA), expressed by plasmid pMER1. The substrate protein is also expressed in the periplasm. Both pCC1 and pMER1 were gifts from Michael Ehrmann. For periplasmic coexpression of TEV protease with its targets, I transformed bacteria with plasmids pCC1 and pUC18*fhuA* (wild type or TEV site derivatives) or pMER1 simultaneously. The transformed bacteria were grown overnight in LB with glucose and subcultured into MOPS or MMA medium. After the culture reached an Abs₆₀₀ of 0.4, I induced the expression of the TEV protease with IPTG. The expression of the control substrate was induced with arabinose.

Proteolysis by incorporated TEV-protease

After the periplasmic incorporation of the protease, I incubated the bacteria in the defined medium (containing antibiotics and sulfhydryl reagents) at 37°C with vigorous aeration for 1 to 6 hours. For proteolysis of FhuA targets during the transport cycle, I added variable amounts of Fc. In each case, sufficient Fc was added to sustain transport by bacteria expressing wild type FhuA (V_{max} for KDF541

pHSG575*fhuA*⁺=87 pmol/10⁹ cells/min) for the entire duration of the experiment.

Finally, the cells were pelleted and subjected to SDS-PAGE and immunoblotting.

Proteolysis by co-expressed TEV protease

Overnight cultures of bacteria were subcultured into defined media. After they reached an Abs₆₀₀ of 0.4, inducers, DTT/BAL and Fc were added as required and the culture was further incubated at 30°C or 37°C for 2 to 6 hours. The cells were harvested and processed for immunoblots.

Cloning of FepA-TEV site- PhoA

The fusion protein was cloned into the low copy plasmid vector, pHSG575 producing plasmid pFTPc. The *fepA* gene from pITS23 was amplified with the primers, M13 forward primer (Integrated DNA Technologies) and FepA.C.XbaI. The latter primer carried an XbaI recognition site. The purified PCR product was digested with PstI and XbaI to get insert 1. The TEV site-PhoA segment of pMER1 was digested with the enzymes XbaI and SacI to get insert 2. Plasmid pITS23 was digested with PstI and SacI to obtain the vector segment. The vector and the 2 inserts were ligated with T4 DNA ligase (New England Biolabs) to give pFTPc. The expression of the fusion protein is regulated by *fepA*'s natural promoter. The construct was verified by double stranded sequencing. For expression from the high copy plasmid vector, I transferred the *fepA-TEV site-phoA* gene construct to pUC18. I amplified the fusion gene from pFTPc by PCR with M13 forward and reverse primers (Integrated DNA Technologies). The purified PCR product was digested with MluI and SacI to obtain the insert fragment. Plasmid pITS449 (pUC18*fepA*) was similarly digested to obtain the vector fragment. The vector and the insert fragments were ligated to get pUCFTPc. However, this clone remains to be verified.

Expression of FepA-TEV site-PhoA

The plasmid pFTPc was transformed into strains OKN3 (*fepA*-) and KDL118 (*fepA-phoA*-). Bacteria were grown overnight in LB medium with the relevant antibiotics. They were then subcultured into MOPS medium (OKN3) or T medium (KDL118). After the cells reached stationary phase, cell lysates were prepared and subjected to western blotting. For detecting FepA, I used murine ascites fluid containing monoclonal anti-FepA antibodies, either mab41 (epitope in N domain) or mab45 (epitope in C domain). For PhoA, I used rabbit serum containing polyclonal anti-PhoA antibodies.

FM labeling of bacterial proteins in vivo

In vivo labeling was performed as described previously (Cao 2003). Bacteria were grown in LB medium with the required antibiotics until they reached stationary phase. The culture was used to inoculate complete MOPS medium. When the culture reached exponential phase, 2.5×10^9 cells were harvested by centrifugation and washed with 25 ml of 1x Tris buffered saline, pH 7.4 (TBS). The cells were resuspended in TBS at a cell density of 5×10^8 cells/ml. FM was prepared in N, N-dimethylformamide (Sigma) and added to the cell suspension to a final concentration of 65 μ M. The concentration of the stock fluorophore solution was determined by absorption spectrophotometry. The mixture was then incubated at room temperature protected from exposure to light. After 30 min, the mixture was centrifuged and the cell pellet was washed thrice in ice cold TBS. The cells were then resuspended in ice-cold complete MOPS medium and stored on ice until further manipulation.

Fluorescence spectrophotometry

Fluorimetric measurements were performed as described previously. I used a SLM 8000 fluorospectrophotometer (Rochester, New York) upgraded to SLM 8100.

We recorded the fluorescence of 5×10^7 bacteria in 2 ml of complete MOPS medium. The temperature was equilibrated with a water bath. For FM labeled samples, I recorded the fluorescence intensity at excitation wavelength, 490 nm and the emission wavelength, 518 nm. Background fluorescence was monitored with bacteria expressing wild type FepA, incubated with the fluorophore.

Labeling in the presence of FeEnt

Labeling accessibility was tested using SDS-PAGE. Bacteria were grown as for FM labeling and washed with 1x TBS. However, only $3\text{-}5 \times 10^8$ cells were collected and labeling performed in 1.5 ml centrifuge tubes. After washing, the cells were resuspended at a density of 5×10^8 cells/ml and chilled on ice. FeEnt was added and allowed to equilibrate with the binding site. The cells were incubated on ice for 10 to 15 min. Fluorophore was added and the mixture was either incubated on ice for 30 min or transferred to 37°C. The cells were subsequently washed and processed for SDS-PAGE.

Detection of labeling

For detection of FM or AM labeled proteins, I lysed the cells by suspending them in sample buffer. The cell lysates were boiled for 5 min and centrifuged to remove cell debris for 1 min. The supernatant was resolved by SDS-PAGE. The gel was directly scanned for fluorescent protein bands using the fluorescence detector of the STORM scanner (Molecular Dynamics). I used the blue fluorescence setting to identify FM and AM labeling. In my labeling experiments, I included mutant constructs of FepA such as FepAS271C that have been previously showed to be strongly labeled by the fluorophores (Cao 2003) as controls for the labeling reaction and detection on SDS-PAGE. I also transferred the protein bands to nitrocellulose membranes and scanned the latter, but this method reduced the sensitivity of

detection. Alternatively, I detected the FM labeled protein bands by western blotting polyclonal serum developed in rabbit immunized with a conjugate of bovine serum albumin (BSA) and Fluorescein iodoacetamide. The blots were developed either with ¹²⁵I-Protein A or colorimetrically with alkaline phosphatase substrates. For the latter, I used a dilute conjugate of anti-rabbit Ig immunoglobulin developed in goat and alkaline phosphatase. In each experiment, I also monitored the expression of FepA by western blotting with mouse anti-FepA monoclonal antibodies (Mab 45).

Chapter 3

Results

Aromatic residues in the binding and transport of FeEnt

All the experiments detailed in this section were performed in collaboration with my colleague, Bo Jin.

Identification of candidate residues for mutagenesis

The amino acid sequences of various FeEnt transporters of different Gram-negative bacteria and *E. coli* LGPs were aligned (Cao 2000) by the PILEUP algorithm (Genetics Computer Group, Madison WI) and adjusted based on the crystal structure of FepA (Buchanan 1999) and FhuA (Locher 1998 and Ferguson 1998). The alignments were examined for the presence of conserved aromatic residues in the surface loops and the top of the N domain that could potentially participate in the binding interaction. Residues that were at least 70% conserved among the different receptors were selected for this study, namely tyrosines 472, 478, 481 and 495 (Figure 6). Less conserved tyrosines 217, 488, 540, 553 and 638 in the surface loops and tryptophan 101 in the ‘sensor’ loop NL2 of the N domain (Buchanan 2000) were also included.

Protein expression and localization

The low copy plasmid pITS23 (Scott 2001) is present at a copy number of 2 to 3/per bacterium. pITS23 is a derivative of pHSG575 expression vector (Hashimoto-Gotoh 1981). Under the conditions of iron starvation used in our experiment, the *fepA* gene in pITS23 translates into approximately 43,000 molecules of FepA per cell. The mutations were engineered on pITS23. The expression levels of all the constructs were determined by quantitative ¹²⁵I-Protein A (Kronvall 1970, Newton 1997)

western blotting. All the protein constructs were expressed at levels similar to wild type FepA (Figure 6a). The localization of the protein in the OM was similar to wild type for all the mutants (Figure 7). The localization of the FepA derivatives was also verified by flow cytometric analysis (Annamalai & Jin 2004).

Colicin sensitivity

The susceptibility to colicin killing (Cao 2000) is not only a measure of the protein's localization, but is also an indicator of the protein's proper assembly and functionality. The mutations caused different effects on the sensitivity to colicin B and colicin D. Mutations W101A and Y553A caused more than a 20-fold reduction in colicin sensitivity, while the other mutants had more modest (< 10-fold) reductions. Y472A causes a 90% reduction in susceptibility to colicin B but does not affect susceptibility to colicin D. This suggests that the residue is involved in the reaction with colicin B but not the latter. FepA Y217 A and Y488A also show similar, albeit more modest differences. However, other mutations have similar effects on the interaction with both the colicins. Taken together, the data implies that while the points of interaction between the colicins and FepA overlap as to the identity of the participating residues, there are also significant differences. The interaction between the macromolecules presumably involves large regions of each protein and it is not surprising that these regions encompass several individual amino acid determinants.

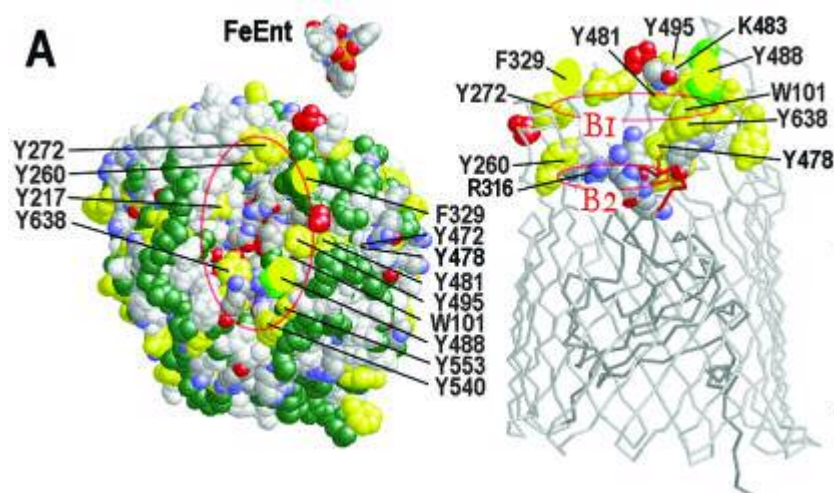


Figure 6. Target residues for alanine mutagenesis (Figure by Klebba in Annamalai and Jin 2004).

On the left is the space-filled representation of FepA (Buchanan 1999) looking from the cell exterior into the barrel. On the right, the protein backbone is viewed in the plane of the membrane bilayer. Tyrosines 217, 472, 478, 481, 495, 540, 553 and 638 are depicted in yellow. Tyrosine 488 was not identified in the crystal structure and the oval symbol indicates its expected position. Residues that were investigated in previous studies are also included. Tryptophan 101 at the top of NL2 was also included in this study. The putative two binding sites, B1 and B2 are marked with red ellipses. It can be seen that B1 contains a zone of aromaticity and lysine 483. B2 has both aromatic and basic including tyrosine 260 and arginine 316 respectively. Also included is the crystal structure of vanadium enterobactin (labeled FeEnt, see text).

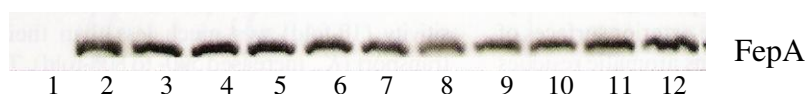


Figure 6a. Expression of FepA and its derivatives. Whole cell lysates of *E. coli* KDF541 harboring plasmid pHSG575 expressing wild type FepA (pITS23) or its derivatives were resolved by SDS-PAGE and immunoblotted with Mouse anti-FepA monoclonal antibody, mab45 and 125 I-Protein A. The bands were revealed by phosphor imaging (Molecular Dynamics). Lane order from for lanes 1 to 12 is KDF541 expressing no FepA, wild type FepA, FepA W101A, Y217A, Y472A, Y478A, Y481A, Y488A, Y495A, Y540A, Y553A and Y638A respectively.

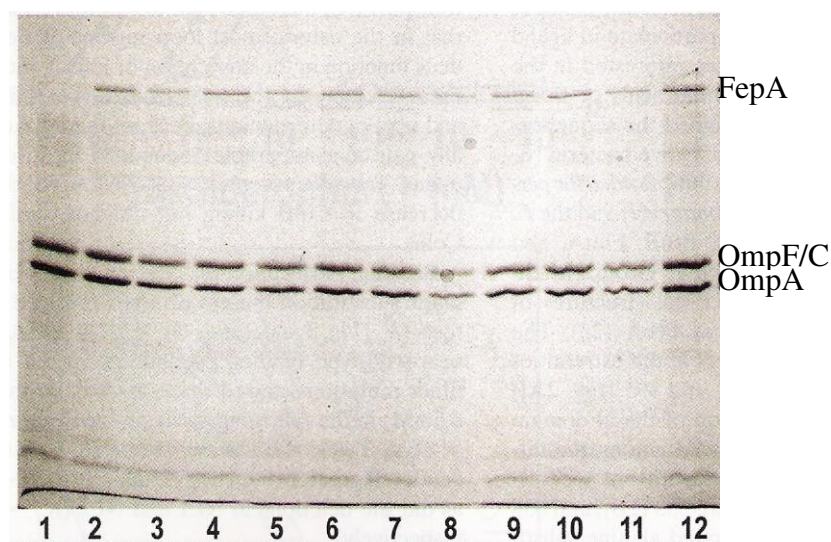


Figure 7. Localization of FepA and its derivatives. OMs of *E. coli* KDF541 harboring plasmid pHSG575 expressing wild type FepA (pITS23) or its derivatives were resolved by SDS-PAGE. The bands were revealed by staining with coomassie blue. Lane order from for lanes 1 to 12 is KDF541 expressing no FepA, wild type FepA, FepA W101A, Y217A, Y472A, Y478A, Y481A, Y488A, Y495A, Y540A, Y553A and Y638A respectively.

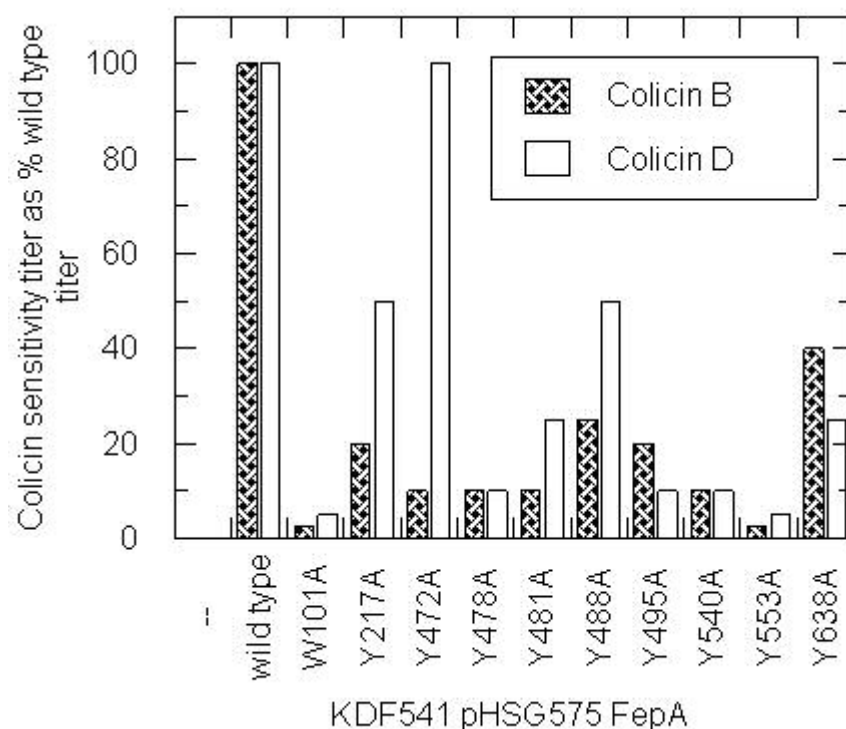


Figure 8. Sensitivity to colicins B and D. KDF541 expressing FepA or its derivatives from pHSG575 was plated on solid media and exposed to serial dilutions of colicins B (shaded bars) and D (open bars). The susceptibility to colicin killing was expressed in arbitrary titration units, defined as the reciprocal of the highest dilution of colicin that caused a clearing of the bacterial lawn. The data was plotted as the ratio of mutant titer to wild type titer in percentage units (see also table).

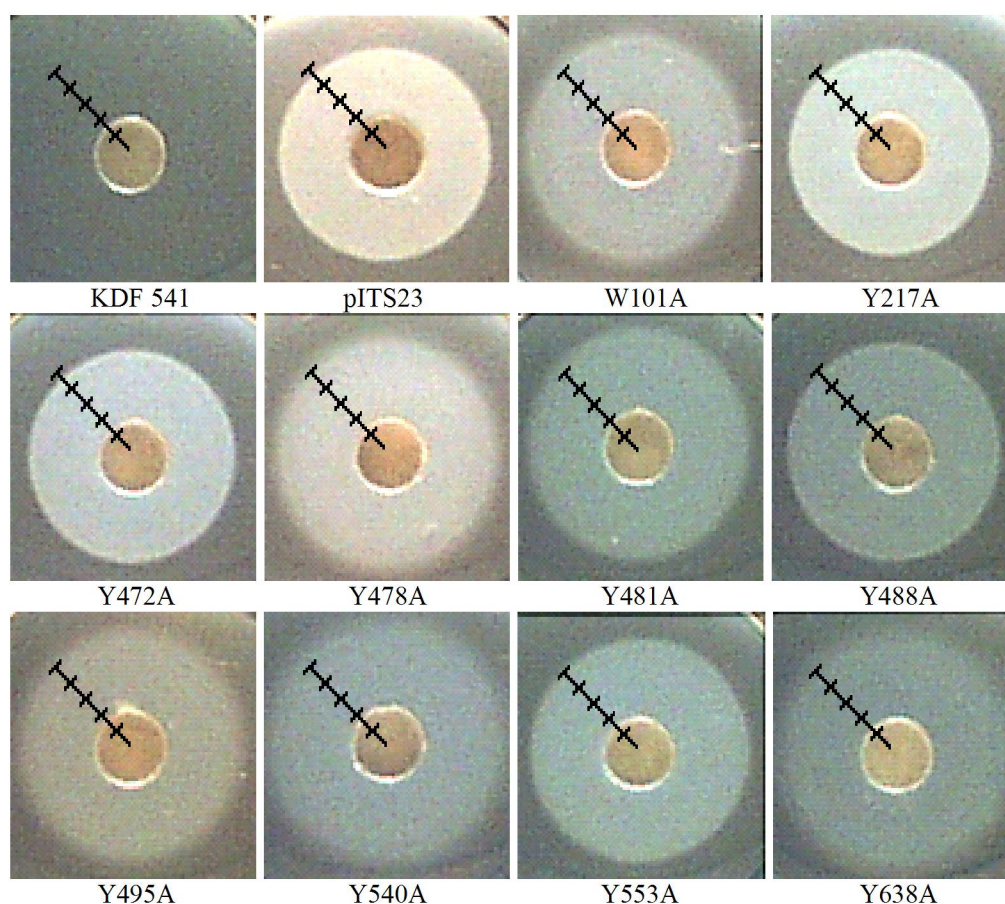


Figure 9. Siderophore nutrition assay of FepA and its derivatives. Bacterial cultures in their logarithmic phase are plated in iron deficient media containing the iron chelator, apoferrichrome A and a paper disc is placed in the center of the agar. 50 pmol of FeEnt is pipetted onto the center of the disc. The plates are incubated overnight. The zone of bacterial growth (halo) is photographed with an Olympus® digital camera. The grid is introduced electronically using Adobe Photoshop® software. *E. coli* KDF541 with no plasmid (top left) or hosting pITS23 (expressing wild type FepA) were tested to provide and positive controls respectively. The aminoacid substitution in the FepA protein is listed under each photograph.

Aromatic residues in the binding interaction:

The in vivo binding capabilities (Newton 1999, Cao 2000) of the aromatic substitution mutants were compared to that of the wild type (Table 5). The difference in their K_d s enabled their classification into different classes. FepA Y217A, Y488A and Y553A showed wild-type binding capabilities. These residues probably play little role in binding. FepAW101A, Y472A, Y478A, Y495A and Y540A demonstrated 3 to 5-fold defects in binding. The order of importance among these residues is Y472 > Y540 > W101 > Y495 > Y478. FepAY481A and Y638A showed more than a 10-fold reduction in binding affinity. Y481A is a significant component of the binding interaction. Its substitution produced the largest defect identified in this study.

The capacities of the mutants, W101A and Y638A were very low, compared to wild-type. The capacity of binding represents the maximum number of available binding sites on FepA proteins expressed on the cell surface. However, these proteins were expressed and localized similar to wild-type FepA. The difference in the capacity therefore does not derive from different numbers of the mature proteins on the protein surface. The replacement of these residues directly affects the formation of the protein's binding site. In the absence of these aromatic residues a large proportion of the receptors do not assume an optimal conformation for binding.

Aromatic residues in the transport of FeEnt

The siderophore nutrition test measures the overall uptake, both binding and transport, capabilities of the protein. All the mutants tested showed a difference in their phenotype, when compared to wild type FepA (Figure 9). Although the assay serves only as a screening test, the diameter and the appearance of the zone of growth (halo) have some correlation to the functionality of the mutant protein (Table 5). The wild type consistently gives a dense zone of growth with sharp borders. Generally,

mutants with the greatest deficiency in transport capabilities gave much fainter and larger (> 2 mm difference) zones of growth, compared to wild type. FepAW101A, Y478A, Y481A, Y495A and Y638A follow this pattern. On the other hand, mutants that showed sharp or fuzzy halos and halos close in size (difference < 2mm) to wild type had moderate deficiencies in their transport capabilities (see below).

FepAY217A, Y488A and Y553A are members of this second set. For example, FepAY540A, which produces a faint halo with the largest diameter among the mutants reported here showed only a moderate reduction in its transport capabilities.

In radioisotopic transport studies, all the mutants studied showed defects in their transport capabilities albeit to different degrees (table 5). The transport defects of Y472A, Y481A, Y488A, and Y540A were commensurate with their binding deficiencies. Among these, Y481A produced the biggest defect. Its K_m was 18 fold higher than the wild type. Such mutations were named class I mutations (Figure 10a, 10b and 10c). The major contribution of these residues was to the binding reaction and the effect of their substitution on transport derived from that on binding.

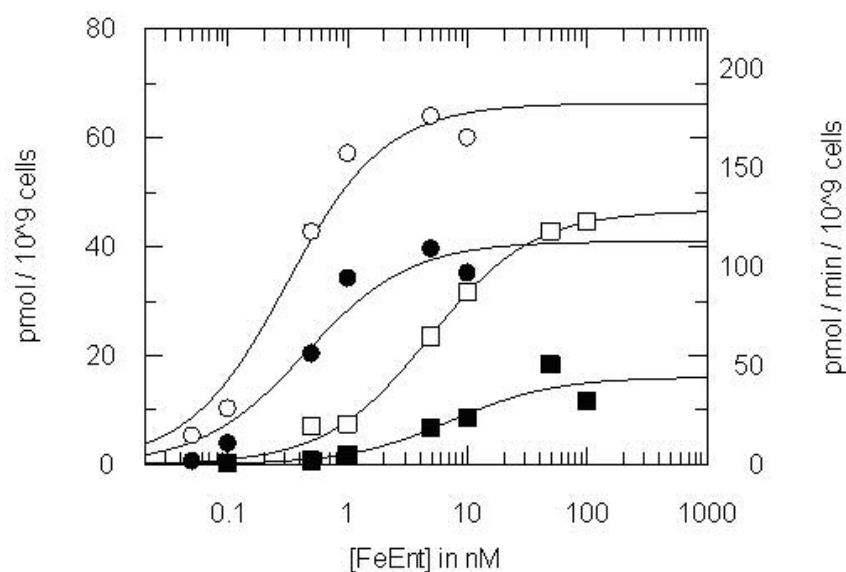


Figure 10a. Binding and transport by class I substitution mutants. Wild type FepA (circles) and FepAY481A (squares) were expressed from pHSG575 in *E.coli* KDF541. The concentration dependence of binding (open symbols) and transport (closed symbols) was determined at six concentrations of $^{59}\text{FeEnt}$. The data was analyzed and plotted by using the bound-versus-total and enzyme kinetics equation of Grafit 5.0.9 (Erithracus).

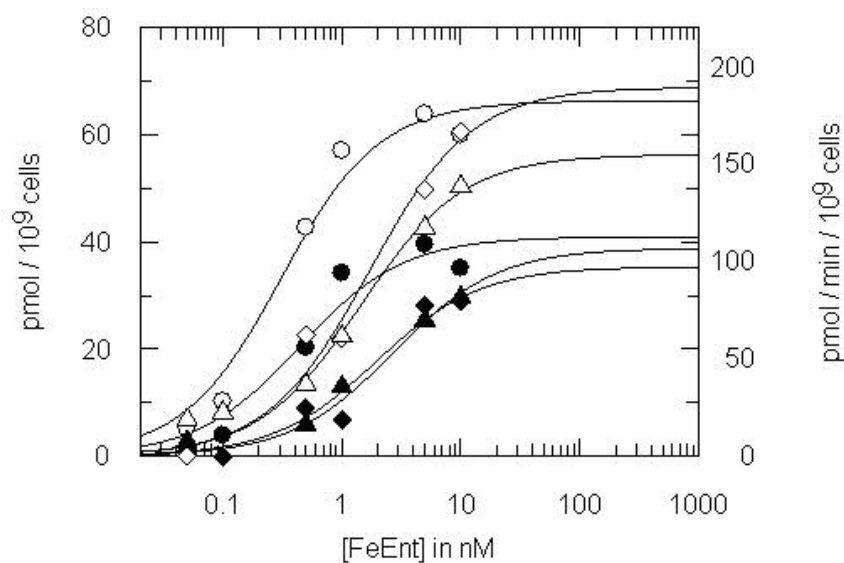


Figure 10b. Binding and transport by class I substitution mutants. Wild type FepA (circles), FepAY472A (diamonds) and Y540A (triangles) were expressed from pHSG575 in *E.coli* KDF541. The concentration dependence of binding (open symbols) and transport (closed symbols) was determined at six concentrations of $^{59}\text{FeEnt}$. The data was analyzed and plotted by using the bound-versus-total and enzyme kinetics equation of Grafit 5.0.9 (Erithracus).

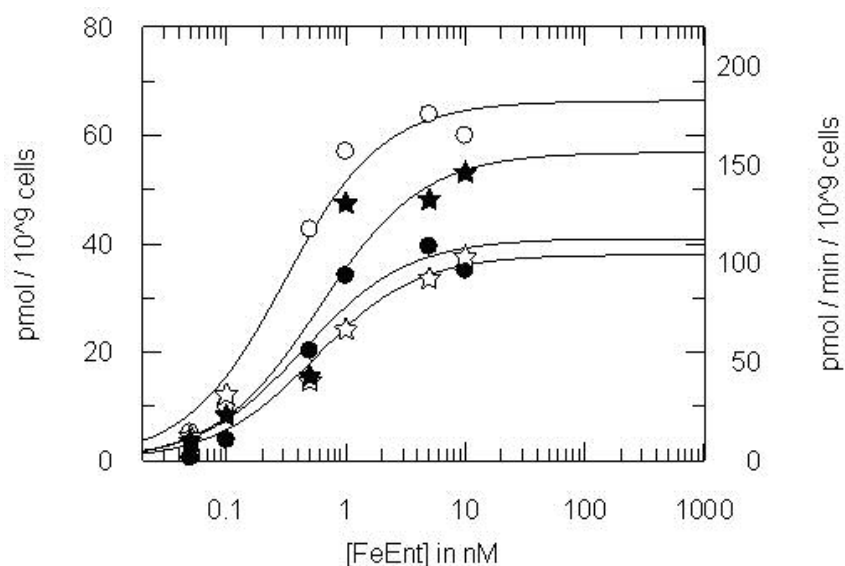


Figure 10c. Binding and transport by class I substitution mutants. Wild type FepA (circles) and FepAY488A (stars) were expressed from pHSG575 in *E.coli* KDF541. The concentration dependence of binding (open symbols) and transport (closed symbols) was determined at six concentrations of $^{59}\text{FeEnt}$. The data was analyzed and plotted by using the bound-versus-total and enzyme kinetics equation of Grafit 5.0.9 (Erithracus).

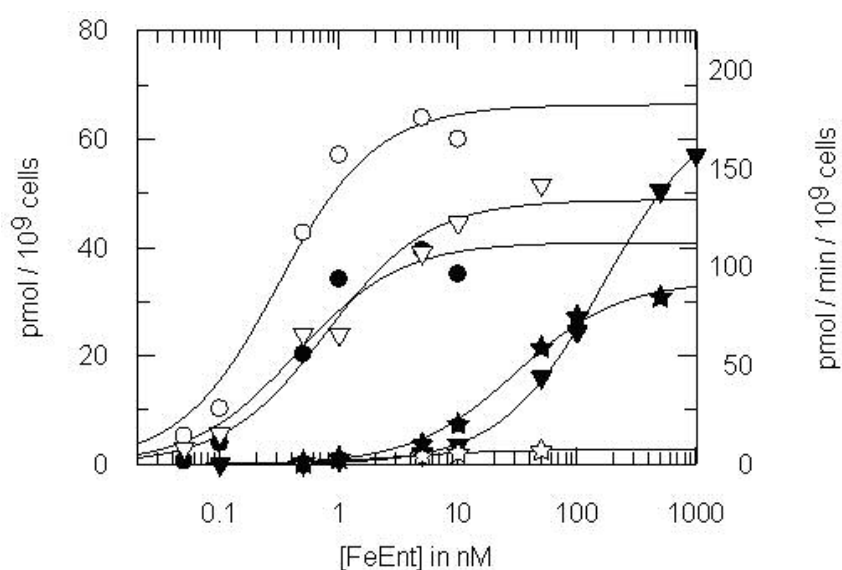


Figure 11a. Binding and transport by class II substitution mutants. Wild type FepA (circles), FepAY478A (inverted triangles) and FepAY638A (stars) were expressed from pHSG575 in *E.coli* KDF541. The concentration dependence of binding (open symbols) and transport (closed symbols) was determined at six concentrations of $^{59}\text{FeEnt}$. The data was analyzed and plotted by using the bound-versus-total and enzyme kinetics equation of Grafit 5.0.9 (Erithracus).

The defects in transport did not always mirror the defects in binding. Y478A and W101A severely affected the transport but not binding. This is evident from their very high K_m of transport. The K_m of W101A is apparently so high that it could not be accurately determined in our experiments. We were unable to measure the maximal velocity of transport at saturating levels of substrate concentration. Y217A, Y553A and Y638A produced smaller increments in the K_m . This group of mutations were classified as class II mutations (Figure 11a, 11b and 11c). The primary contribution of these residues appears to be to the transport process and their substitutions produced disproportionate effects on transport when compared to binding. Y638A produced a 10 fold increase in binding K_d , but resulted in a 77-fold increase in the transport K_m . The residue appears to contribute both to the binding and transport reaction, but has a larger role in the latter process. Its substitution therefore is a class II substitution.

Y495A is the sole example of a class III mutation, with a near wild type K_d , K_m and capacity, but a 5-fold lower V_{max} and therefore a low turnover number, k_8 . This class of mutation affected the efficiency of the transport process (Figure 12a).

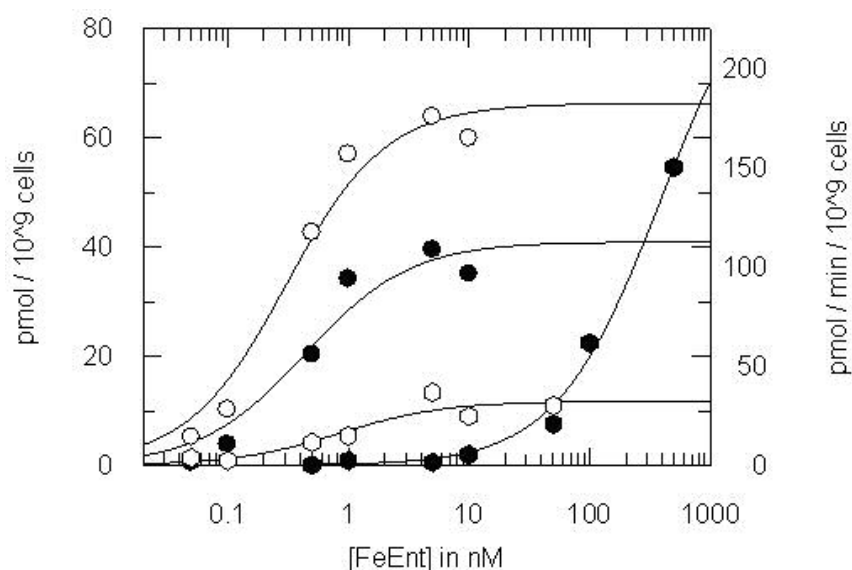


Figure 11b. Binding and transport by class II substitution mutants. Wild type FepA (circles) and FepAW101A (hexagons) were expressed from pHSG575 in *E.coli* KDF541. The concentration dependence of binding (open symbols) and transport (closed symbols) was determined at six concentrations of $^{59}\text{FeEnt}$. The data was analyzed and plotted by using the bound-versus-total and enzyme kinetics equation of Grafit 5.0.9 (Erithracus).

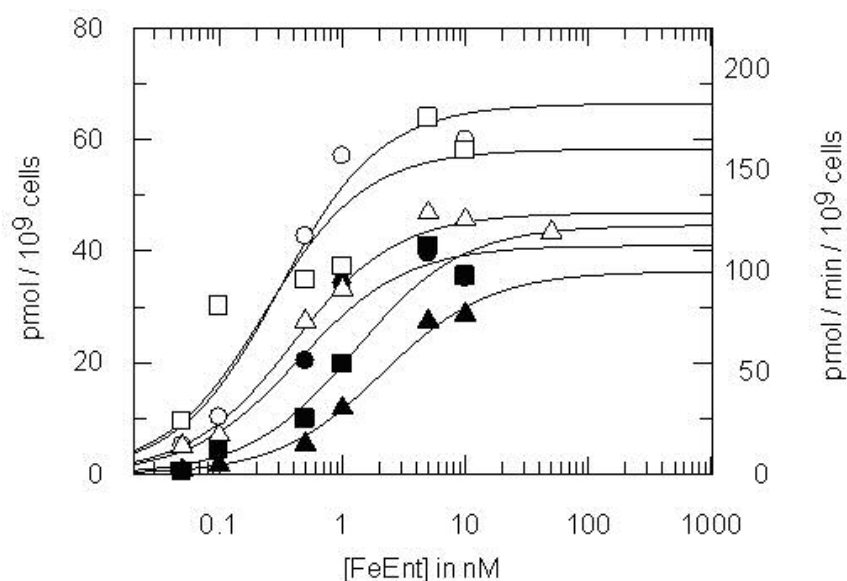


Figure 11c. Binding and transport by class II substitution mutants. Wild type FepA (circles), FepAY217A (squares) and FepAY553A (triangles) were expressed from pHSG575 in *E.coli* KDF541. The concentration dependence of binding (open symbols) and transport (closed symbols) was determined at six concentrations of $^{59}\text{FeEnt}$. The data was analyzed and plotted by using the bound-versus-total and enzyme kinetics equation of Grafit 5.0.9 (Erithracus).

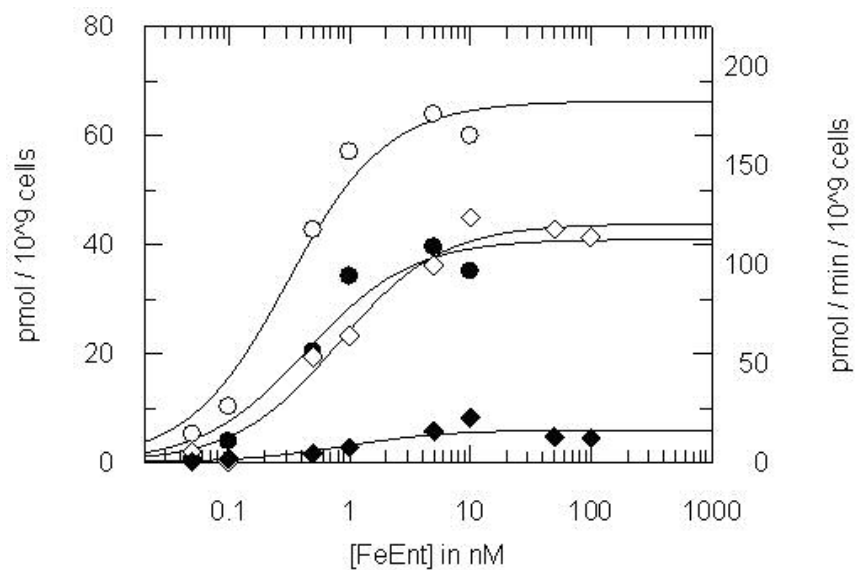


Figure 12. Binding and transport by class III substitution mutant. Wild type FepA (circles) and FepAY495A (diamonds) was expressed from pHSG575 in *E.coli* KDF541. The concentration dependence of binding (open symbols) and transport (closed symbols) was determined at six concentrations of ⁵⁹FeEnt. The data were analyzed and plotted by using the bound-versus-total and enzyme kinetics equation of Grafit 5.0.9 (Erithracus).

FepA	Loop	FeEnt							
		Binding ^a		Transport ^b				Flow cytometry ^d	
		K_d	Capacity	Nutrition	K_m	V_{max}	k_8^c	mab24	mab45
Wild type	NA	0.27	67	18.5	0.4	113	1.7	4.2	45.2
Class I									
Y472A	7	1.5	68	19	2.6	105	1.5	8.34	42.4
Y481A	7	4.8	47	21	7.2	44	0.9	11.3	42.6
Y488A	7	0.5	38	19.5	0.6	156	4.1	3.5	38.5
Y540A	8	1.4	56	23	2.0	98	1.8	10.1	45.9
Class II									
W101A	NL2	0.85	12	20.5	393*	269*	NC	8.8	54.6
Y217A	2	0.20	58	18.5	1.3	122	2.1	3.5	44.1
Y478A	7	0.76	49	21	167	184	3.8	14.2	34.8
Y553A	8	0.40	46	20.5	2.1	100	2.2	7.2	47.3
Y638A	10	2.9	3	22	31	93	31	4.1	38.5
Class III									
Y495A	7	0.79	44	21.5	0.9	17	0.4	8.8	39.1

Table 5. Binding and transport by FepA and its derivatives. The proteins were expressed from pHSG575 in *E. coli* KDF541. Class I, comparable increases in binding K_d and transport K_m ; class II, larger increase in transport K_m ; class III, reduction in transport rate.

a. Binding. K_d (nM) and capacity (pmol bound/ 10^9 cells) were determined from the concentration dependence of FeEnt binding by analyzing the mean values from independent experiments with GRAFIT 5.0.9 (Erithacus), using the 'bound versus total' equation.

b. Transport. Nutrition – the diameter of the zone of bacterial growth is listed in mm (see text for details). K_m (nM) and V_{max} (pmol transported/ 10^9 cells/min) of uptake were determined from the concentration dependence of FeEnt transport using GRAFIT 5.0.9 (Erithacus), using the 'enzyme kinetics' equation.

c – k_8 corresponds to the turnover number of the transporter, a value akin to k_3 , the catalytic turnover number of enzymes (Scott 2001). $k_8 = V_{max}/\text{Capacity}$, molecules/receptor protein/min.

* - We were not able to measure transport rate at saturating concentrations of FeEnt for W101A. K_m and V_{max} values were estimated from trends observed with unsaturated transport rate measurements. NC – Not calculated as V_{max} could not be determined.

d. Data was collected on Elite Coulter cell sorter by Salete Newton. Samples were prepared by incubating bacteria with Mouse anti-FepA antibodies, mab 24 and mab 45, which recognize epitopes on loops L4 and L5 of FepA respectively. The values listed are mean fluorescence intensity of 10^4 bacteria and in parenthesis is the percentage of the bacterial population that gives signals within one standard deviation of the mean (Annamalai and Jin 2004).

Chapter 4

Loops of the N-domain

The experiments in this section were performed in collaboration with my colleague, Bo Jin.

Site directed mutagenesis

The loops of the N domain, NL1 and NL2 (Figure 13) extend from residues 54 to 75 and 91 to 115 of the FepA polypeptide respectively (Buchanan 1999). Carla Taddei, Melissa Simoes, Simone Alves, and Tie Koide constructed *fepA*Δ60-67 in which the central segment of NL1 is deleted. Similarly, Alexandre Moutran, Marcio Lasaro and Solange Nunes constructed *fepA*Δ98-105, which carries the deletion in NL2. The mutations were engineered on pITS449 (pUC18*fepA*⁺). *E. coli* KDF541 served as the host bacterium for the resultant plasmid constructs. The work was carried out under the tutelage of Dr. Klebba, Dr. Newton and Dr. Scott under the auspices of the American Society for Microbiology-sponsored International Training Program for Latin America: “Molecular Biological Approaches to Bacterial Cell Wall Biochemistry,” in April 2002 at Departamento de Microbiologia, Universidade de Sao Paulo, Sao Paulo, Brazil.

Protein expression and localization

The expression levels of all the constructs were determined by quantitative I-¹²⁵I-Protein A western blotting. All the protein constructs were found to be expressed and localized to the OM at levels similar to wild type FepA (Figure 14, Figure 15). The localization of the mutated proteins was also verified by flow cytometric analysis (Annamalai & Jin 2004).

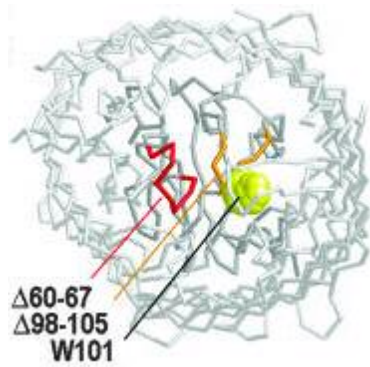


Figure 13. Loops of the N domain of FepA. The segments deleted in the superior portion of NL1 (red) and NL2 (orange) are depicted in the protein backbone of FepA (Buchanan 1999). The view is from the cell exterior looking into the barrel. The backbone is depicted in grayscale. Tryptophan 101 is represented in spacefilled form to identify NL2. The loops are well situated to interact with the ligand (Figure by Klebba in Annamalai and Jin 2004).



Figure 14. Expression of FepA and its derivatives. Whole cell lysates of *E. coli* KDF541 harboring plasmid pUC18 expressing wild type FepA (pITS449) or its derivatives were resolved by SDS-PAGE and immunoblotted with Mouse anti-FepA monoclonal antibody, mab 45 and 125 I-Protein A. The bands were revealed by phosphor imaging (Molecular Dynamics). Lane order from for lanes 1 to 3 is KDF541 expressing wild type FepA, FepA Δ 60-67 and FepA Δ 98 105 respectively (Annamalai and Jin 2004).

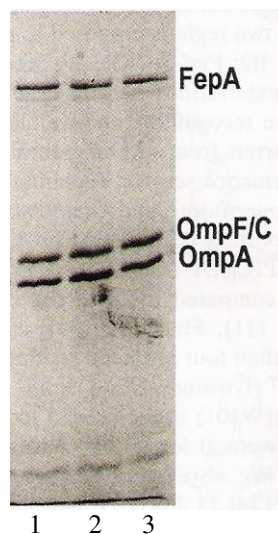


Figure 15. Localization of FepA and its derivatives. OM of *E. coli* KDF541 harboring plasmid pUC18 expressing wild type FepA (pITS449) or its derivatives were resolved by SDS-PAGE. The bands were revealed by staining with coomassie blue. Lane order from for lanes 1 to 3 is KDF541 expressing wild type FepA, FepA Δ 60-67 and FepA Δ 98-105 respectively (Annamalai and Jin, 2004).

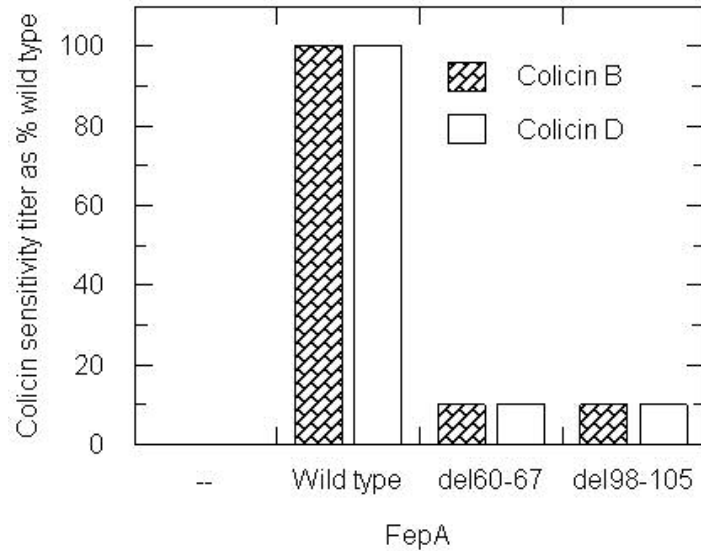


Figure 16. Sensitivity to colicins B and D of N domain loop deletion mutants. KDF541 expressing wild type FepA or its derivatives from pUC18 was plated on solid media and exposed to serial dilutions of colicins B and D. The susceptibility to colicin killing was expressed in arbitrary titration units, defined as the reciprocal of the highest dilution of colicin that caused a clearing of the bacterial lawn. The data was plotted as the ratio of mutant titer to wild type titer in percentage units.

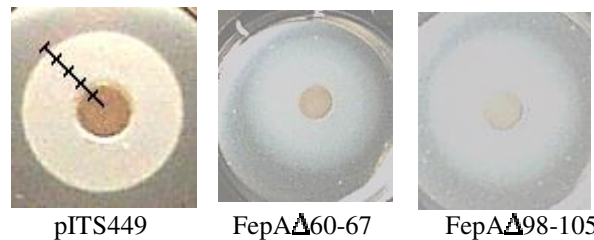


Figure 17. Siderophore nutrition assay of FepA and its derivatives. Bacterial cultures in their logarithmic phase were plated in iron deficient media containing the iron chelator, apoferrichrome A and a paper disc was placed in the center of the agar. 10 μ l of 50 μ M FeEnt was pipetted onto the center of the disc. The plates were incubated overnight. The zone of bacterial growth (halo) was photographed with an Olympus® digital camera. The grid is introduced electronically using Adobe Photoshop® software.

Colicin sensitivity

Both the deletion mutations conferred sensitivity to killing by both colicin B and D upon bacteria expressing the protein constructs. When compared to wild type FepA, the mutant constructs exhibited 10-fold reduced activity (Figure 16).

Binding and transport by N domain loop deletion mutants

The binding and transport of the N domain loop deletion mutants were compared to wild type FepA expressed from pITS449. The plasmids were hosted by *E. coli* KDF541. The deletion mutations gave rise to class II defects in FepA function (Table 6). Siderophore nutrition tests demonstrated larger zones of growth with diffuse borders for the deletion mutants when compared to wild type (Figure 17). When compared to wild type FepA, the K_d of binding was increased 18- and 28- fold by the $\Delta 60-67$ and $\Delta 98-105$ deletions (Table 6). However, transport was impaired 500- and 700-fold as evident from the increase in their K_m of transport. These parameters resemble the defects identified with Y638A, although the loop deletions affected transport more severely.

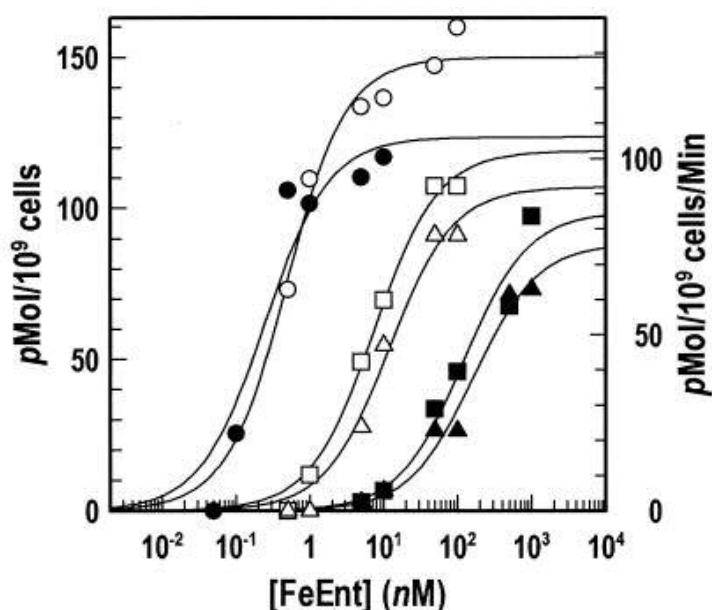


Figure18. Binding and transport by N-loop deletion mutants. (Open symbols) $^{59}\text{FeEnt}$ binding and $^{59}\text{FeEnt}$ uptake (solid symbols) by *E. coli* KDF541 harboring pUC18 plasmids, expressing *fepA*⁺ (circles, pITS449), *fepA*Δ60-67 (squares), and *fepA*Δ98-105 (triangles) alleles. The binding and transport data were analyzed and curves were plotted by using the bound-versus-total and enzyme kinetics equations, respectively, of Grafit 5.09 (Annamalai and Jin 2004).

FeEnt									
FepA	Loop	Binding ^a		Transport ^b				Flow cytometry ^d	
		K_d	Capacity	Nutrition	K_m	V_{max}	k_8^c	mab 24	mab 45
<i>fepA</i> ⁺	NA	0.41	150	18	0.24	123	0.8	4.1 (80)	11.7 (90)
Class II									
<i>Δ60-67</i>	NL1	7.3	119	25	99	119	0.8	6.2 (91)	11.5 (93)
<i>Δ98-105</i>	NL2	11.7	107	25	88	163	0.8	6.57 (91)	12.6 (88)

Table 6. Binding and transport by FepA N domain loop deletion. The proteins were expressed from pUC18 in *E. coli* KDF541. Class II, mutation causing larger increase in transport K_m .

a. Binding. K_d (nM) and capacity (pmol bound/ 10^9 cells) were determined from the concentration dependence of FeEnt binding by analyzing the mean values from independent experiments with GRAFIT 5.0.9 (Erithacus), using the 'bound versus total' equation.

b. Transport. Nutrition – the diameter of the zone of bacterial growth is listed in mm (see text for details). K_m (nM) and V_{max} (pmol transported/ 10^9 cells/min) of uptake were determined from the concentration dependence of FeEnt transport using GRAFIT 5.0.9 (Erithacus), using the 'enzyme kinetics' equation.

c – k_8 corresponds to the turnover number of the transporter, a value akin to k_3 , the catalytic turnover number of enzymes (Scott 2001). It relates the V_{max} of transport to the capacity of binding, $k_8 = V_{max}/\text{Capacity}$, molecules/receptor protein/min.

d. The data was collected on Elite Coulter cell sorter by Salete Newton. Samples were prepared by incubating bacteria with mouse anti-FepA antibodies, mab24 and mab45, which recognize epitopes on loops L4 and L5 of FepA respectively. The values listed are mean fluorescence intensity of 10^4 bacteria and in parenthesis is the percentage of the bacterial population that gives signals within one standard deviation of the mean (Annamalai & Jin 2004).

Chapter 5

Recognition of ferric catecholates by FepA

The experiments in this section were performed in collaboration with my colleague, Bo Jin.

Binding of ferric catecholates

We tested the ability of bacteria expressing FepA to bind the ferric catecholates FeEnt, FeTRENCAM and FeCorynebactin (Figure 19). Among these, FeCorynebactin showed no adsorption to FepA even at a concentration of 1 μ M. FeTRENCAM bound with a K_d of 17 nM, which is about 50 times greater than the K_d of the FepA-FeEnt adsorption. The results are different from previous reports (Thulasiraman 1998), which placed the K_d for binding FeTRENCAM (27 nM) at nearly twice the FeEnt K_d (17 nM). However, subsequent reports (Newton 1999) identified substrate depletion as a distorting factor in the original report. At low concentrations of substrate, the concentration of the unbound ligand decreases as the binding reaction proceeds. At low volumes of the reaction, this leads to a significant decrease in the amount and thereby the concentration of the ligand. By performing the reaction at large volumes, the authors avoided this large depletion in the ligand concentration. The current experiments were performed with the newer protocols.

Transport of ferric catecholates

Among the three ferric catecholates tested (Figure 19), only the native siderophore and FeTRENCAM are transported. The K_m of transport for FeTRENCAM was 4.5 nM, which is 18 times that for FeEnt. Similar to binding, these experiments were performed with the newer protocol to avoid depletion effects.

Competition of FeEnt with other siderophores

We compared the ability of different ferric siderophores to inhibit the binding of $^{59}\text{FeEnt}$ (Figure 20). Among the panel that we studied, we included the catecholates FeEnt (for the identity reaction), FeTRENCAM, FeCorynebactin, FeAgrobactin and the hydroxamate Fc. Only the first three catecholates showed inhibition of $^{59}\text{FeEnt}$ binding. We calculated the IC_{50} (inhibitory concentration) of the binding, using the 4-parameter fit of Grafit 5.0, Erithracus. FeEnt reduced the adsorption of $^{59}\text{FeEnt}$ to 50% of the uninhibited value at a concentration of 0.67 nM (inhibitory concentration 50, IC_{50}). This value is close to its K_d (0.27 nM). The IC_{50} of FeTRENCAM was around 120 nM, reflecting its lower affinity for the receptor. Even at a concentration of 25 μM , FeCorynebactin only showed 50% inhibition of $^{59}\text{FeEnt}$ adsorption. This concentration is nearly 100,000 times the K_d of FeEnt binding. Despite its catecholate structure, FeAgrobactin did not inhibit $^{59}\text{FeEnt}$ binding. The hydroxamate Fc showed no effect either. Neither of these two siderophores supply iron to bacteria through FepA (Thulasiraman 1998, Scott 2001).

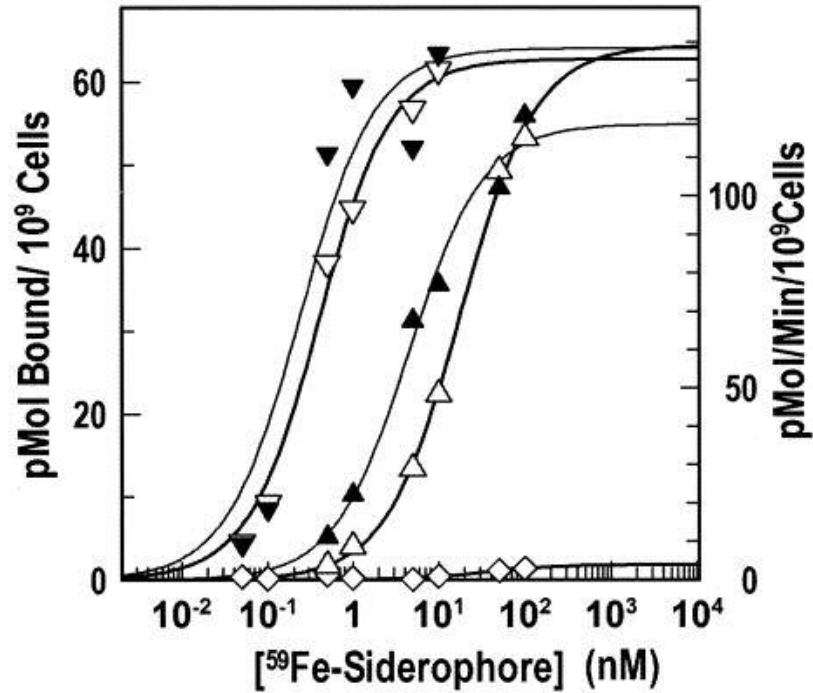


Figure 19. Binding and transport of ferric catecholates. We compared the binding (open symbols) and transport (solid symbols) of $^{59}\text{FeEnt}$ (inverted triangles), $^{59}\text{FeTRENCAm}$ (triangles), and $^{59}\text{FeCorynebactin}$ (diamonds) by *E. coli* strain KDF541/pITS23 (Annamalai & Jin 2004).

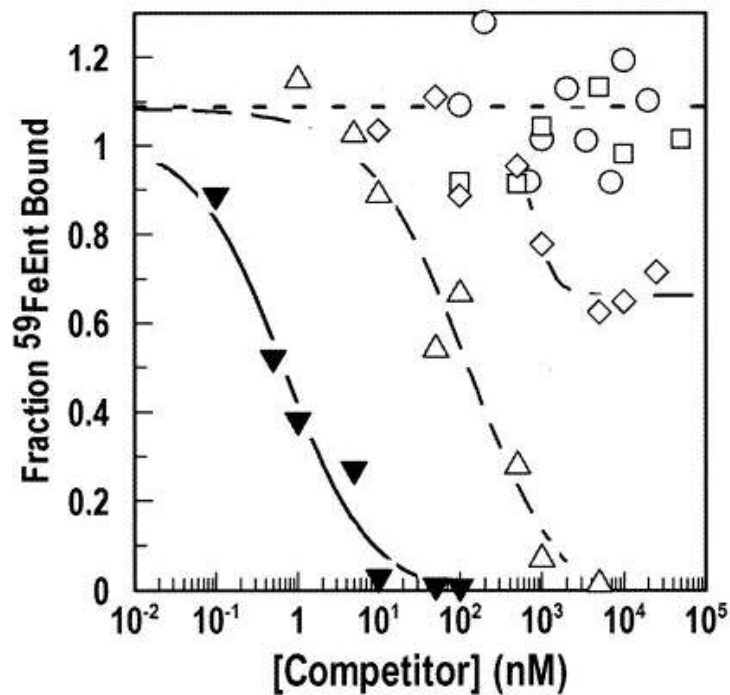


Figure 20. Competition of $^{59}\text{FeEnt}$ binding to FepA by ferric siderophores. We determined the abilities of Fe (\square), FeAgrobactin (\circ), FeTRENCAm (\triangle), FeCorynebactin (\diamond), and FeEnt (\blacktriangledown) to inhibit the binding of $^{59}\text{FeEnt}$ to *E. coli* strain KDF541/pITS23 (*fepA*⁺). The data were analyzed and plotted by the IC50-4 Parameter Logistic of Grafit 5.09 (Annamalai & Jin 2004).

Chapter 6

Complementation between isolated barrel and N domains

Expression of FepA and FhuA protein constructs

E. coli strains carrying precise deletions of the structural genes (see immediately below) of FepA (OKN3) and FhuA (MB97) alone or in combination (OKN73) were transformed with plasmids expressing the N domain deletion mutants of FepA (Fep β) and FhuA (Fhu β) (Scott 2001). Similarly the chimeric FhuNFep β and FepNFhu β protein constructs were expressed in these strains. Further, I retransformed *E. coli* KDF 541 with the same plasmids. I then proceeded to compare the functionality of the different protein constructs when expressed in the different strains.

OKN3 was constructed by Salete Newton following the Datsenko-Wanner method. The strain was constructed by deleting the FepA gene from BN1071 (Klebba 1992). *E. coli* MB97 (AB2847 *fhuA*), constructed using the same methodology was a gift from Volkmar Braun (Braun 2003). We also constructed a *fepA*- derivative of MB97, which we dubbed OKN73. OKN73 is similar to MB99 (Braun 2003).

Colicin susceptibility

FepA derivatives and colicins B and D. I measured the susceptibility of Fep β and the chimeric FhuNFep β to colicins B and D (Table 7). Both these constructs did not confer any colicin B or D sensitivity to strains carrying complete deletions of the *fepA* and *fhuA* genes (OKN73). The presence of genome-encoded FhuA (in OKN3) did not rescue the constructs either. However, the concurrent presence of either genomically encoded FepA₁₋₃₆₃ fragment (in KDF541) or plasmid encoded FepN restored Fep β 's sensitivity to both colicin B and D. FepA₁₋₃₆₃ also complemented FhuNFep β . The complementation did not restore the sensitivity to wild type levels.

FhuA derivatives and colicin M. I measured the susceptibility of strains expressing Fhu β and FepNFhu β to purified colicin M (Table 8). In OKN73 (*fepA-fhuA*-) and MB97 (*fhuA*-), both these constructs had no activity. Coexpression of plasmid encoded FepN (FepA₁₋₁₅₀) did not restore Fhu β 's activity. Nor did OM localized FepA-PhoA fusions with increasing lengths (100, 227, 258, 290 and 352 amino acids) of FepA N terminal segments complement Fhu β . However, Fhu β was active in KDF541 (see below).

FepA protein	Colicin sensitivity as percent wild type titers					
	OKN73		OKN3		KDF541	
	<i>fepA-fhuA</i> -		<i>fepA</i> -		<i>fepA₄₁₋₃₆₃fhuA</i> -*	
	B	D	B	D	B	D
-/-	-	-	-	-	-	-
wt. FepA	100	100	100	100	100	100
Fep β	-	-	-	-	6.25	1
FhuNFep β	-	-	-	-	0.75	0.1
FepN	-	-	-	-	-	-
Fep β + FepN	0.45	0.006	3.25	0.15	6.25	1.5

Table 7. Colicin B and D sensitivity of FepA derivatives. The different protein constructs were encoded on the low copy plasmid vector, pHSG575. pHSG575 carries the Chloramphenicol acetyltransferase (*cat*) gene and confers resistance to the antibiotic chloramphenicol. The isolated N domain of FepA was expressed from high copy pUC18 vector, which confers ampicillin resistance. Bacteria were grown overnight in LB medium with appropriate antibiotics. The culture was plated on LB plates and serial dilutions of purified colicin B and D were applied (see materials and methods) using the clonemaster (Immusine). The plates were then incubated over night at 37°C. The plates were then examined for clearance of the bacterial lawn. The sensitivity to colicin was recorded in arbitrary dilution units or titers defined as the maximum dilution that cleared the bacterial lawn. In the table, the titers are listed as percent wild type titers (derivative titer/wild type FepA titer x 100%) to compare between experiments. * - the *fhuA* locus of KDF541 has not been fully described (see text).

FhuA protein	Colicin M sensitivity as % wild type titer		
	OKN73	MB97	KDF541
	<i>fhuA-fepA-</i>	<i>fhuA-</i>	<i>fepA_{Δ1-363}fhuA-*</i>
-/-	-	-	-
Wild type	100	100	100
Fhuβ	-	-	50
FepNFhuβ	-	-	-
Fhuβ + FepN	-	ND	ND
Fhuβ + FepA ₁₋₁₀₀ ::PhoA	-	ND	ND
Fhuβ + FepA ₁₋₂₂₇ ::PhoA	-	ND	ND
Fhuβ + FepA ₁₋₂₅₈ ::PhoA	-	ND	ND
Fhuβ + FepA ₁₋₂₉₀ ::PhoA	-	ND	ND
Fhuβ + FepA ₁₋₃₅₂ ::PhoA	-	ND	ND

Table 8. Colicin M sensitivity of FhuA derivatives. The different protein constructs were encoded on the low copy plasmid vector, pHSG575. The isolated N domain of FepA was expressed from high copy pUC18 vector, which confers ampicillin resistance. The different FepA-PhoA fusions were previously described (Murphy 1989). The proteins were encoded on high copy plasmid vector, pUC18. The resultant plasmids were named pFPxxx, where xxx indicates the number of residues of FepA retained in the fusion protein. Bacteria were grown overnight in LB medium with appropriate antibiotics. The culture was plated on LB plates and serial dilutions of purified colicin M were applied (see materials and methods) using the clonemaster (Immusine). The plates were then incubated overnight at 37°C. The plates were then examined for clearance of the bacterial lawn. The sensitivity to colicin was recorded in arbitrary dilution units or titers defined as the maximum dilution that cleared the bacterial lawn. In the table, the titers are listed as percent wild type titers (derivative titer/wild type FhuA titer x 100%) to compare between experiments. – No sensitivity. ND – Not performed. * - the *fhuA* locus of KDF541 has not been fully described (see text).

Siderophore nutrition analysis

I tested the ability of the different protein constructs to transport FeEnt (for FepA derivatives, Table 7) and Fc (for FhuA derivatives, Table 10). I found that the proteins Fep β and the chimeric FhuNFep β failed to transport FeEnt in bacteria with complete FepA deletions with (OKN73) or without (OKN3) complete FhuA deletions. However, the concurrent presence of genomically encoded FepA₁₋₃₆₃ fragment (in KDF51) restored Fep β 's activity. FepA₁₋₃₆₃ also complemented FhuNFep β . The coexpression of FepN did not restore the uptake. Fhu β and the chimeric FepNFhu β are inactive in the complete FhuA deletion background with or without the complete FepA deletion. Plasmid encoded FepN (FepA (1-150)) did not restore Fhu β 's activity. Nor did OM localized FepA-PhoA fusions with increasing lengths (100, 227, 258, 290 and 352 amino acids) of FepA N terminal segments complement Fhu β . However, Fhu β and the chimeric FepNFhu β were active in KDF541 (see below).

FepA Protein	Diameter of zone of growth in mm		
	OKN73	OKN3	KDF541
	<i>fepA-fhuA-</i>	<i>fepA-</i>	<i>fepA_{Δ1-363}fhuA-*</i>
-/-	-	-	
Wild type	16	17	17
Fepβ	-	-	21
FhuNFepβ	-	-	21
FepN	-	-	-
Fepβ + FepN	-	-	-

Table 9. FeEnt nutrition of FepA derivatives. – No growth observed. A sample of actively growing bacteria was plated with soft agar and an iron chelator, apoferrichrome A. A paper disk was then placed on top of the solidified agar and 500 pmoles of pure FeEnt was added to the center of the disc. The plates were incubated at 37°C for 6 to 8 hours. The diameter of the zone of bacterial growth around the disc was recorded in mm. * - the *fhuA* locus of KDF541 has not been fully described.

FhuA Protein	Diameter of zone of growth in mm		
	OKN73	MB97	KDF541
	<i>fhuA-fepA-</i>	<i>fhuA-</i>	<i>fepA_{Δ1-363}fhuA-*</i>
-/-	-	-	-
Wild type	15	18	16
Fhuβ	-	-	16
FepNFhuβ	-	-	22
Fhuβ + FepN	-	ND	ND
Fhuβ + FepA ₁₋₁₀₀ ::PhoA	-	ND	ND
Fhuβ + FepA ₁₋₂₂₇ ::PhoA	-	ND	ND
Fhuβ + FepA ₁₋₂₅₈ ::PhoA	-	ND	ND
Fhuβ + FepA ₁₋₂₉₀ ::PhoA	-	ND	ND
Fhuβ + FepA ₁₋₃₅₂ ::PhoA	-	ND	ND

Table 10. Fc nutrition of FhuA derivatives. – No growth observed. ND – No data. A sample of actively growing bacteria were plated with soft agar and an iron chelator, apoferrichrome A. A paper disk was then placed on top of the solidified agar and 500 pmoles of pure Fc was added to the center of the disc. The plates were incubated at 37°C for 6 to 8 hours. The diameter of the zone of bacterial growth around the disc was recorded in mm. * - the *fhuA* locus of KDF541 has not been fully described (see text).

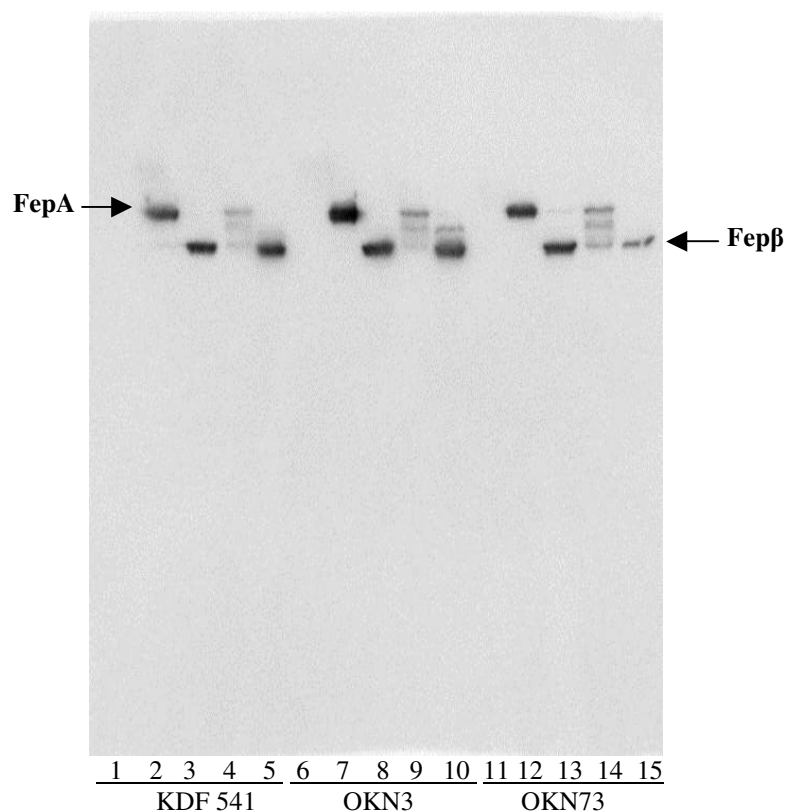


Figure 21. ^{125}I -Protein A immunoblot profiling the expression of FepA derivatives. Bacteria were grown in iron deficient MOPS medium and harvested by centrifugation. The cell pellets were lysed and resolved by SDS-PAGE. The protein bands were electroeluted onto nitrocellulose membranes and a radioimmunoblot was performed. Mab45, a monoclonal antibody that recognizes an epitope on the C domain was used as the primary antibody. In lanes 1-5 are whole cell lysates from KDF541. In lanes 6-10 are samples from OKN3 and in lanes 11-15 are samples from OKN73. For the group from each strain, lane order from left to right are bacteria hosting no plasmid, plasmid expressing wt FepA (pITS23), Fepβ, FhuNFepβ and Fepβ + FepN.

Protein expression

FepA and FhuA derivatives. To investigate whether the differences in the phenotypes observed derived from differences in the expression of the protein constructs, I performed immunoblots on whole cell lysates of bacteria expressing these proteins. I used ascites fluids containing monoclonal antibodies directed against epitopes in the C domain of FepA (between amino acids 290-339, Mab 45, Figure 21) and the N domain of FepA (Mab41, Figure 22) to observe expression of the FepA protein constructs from the different strains. For FhuA derivatives, the expression of FepNFhu β is profiled in figure 22a. MB97 expresses native FepA from its genome. Mab41 will therefore recognize the protein in addition to FepNFhu β . We did not have access to an antibody that recognizes FhuA C domain. We did not therefore have a direct method to observe Fhu β bands. On the other hand, the construct confers sensitivity to colicin M at a different level from wild type FhuA in KDF541, indicating the localization to OM. FhuA and Fhu β have also been reported to localize to the OM when expressed in MB97 and MB99 (similar to OKN73) (Braun 2003). We also observed expression of FhuA derivatives in KDF541 and MB97 as part of the TEV protease experiments (Figures 23 and 28).

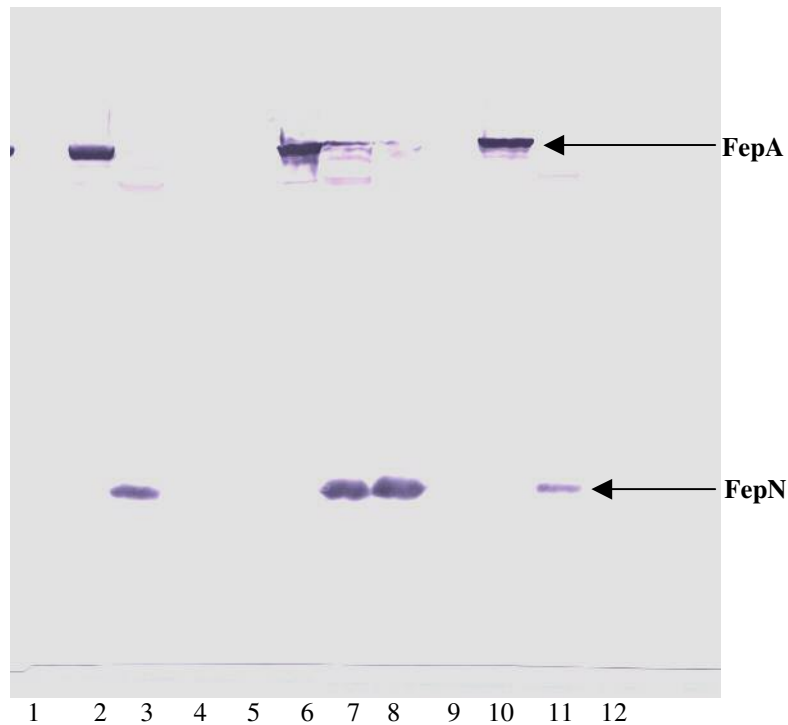


Figure 22. Western blot profiling the expression of FepA derivatives. Bacteria were grown in iron deficient MOPS medium and harvested by centrifugation. The cell pellets were lysed and resolved by SDS-PAGE. The protein bands were electroeluted onto nitrocellulose membranes and a radioimmunoblot was performed. The blot was performed using mab41, a mouse anti-FepA Ig which recognizes an epitope in the N domain. In lanes 1-4 are whole cell lysates from KDF541. In lanes 5-8 are samples from OKN3 and in lanes 9-12 are those from OKN73. For the group from each strain, lane order from left to right are bacteria hosting no plasmid, plasmid wt FepA (pITS23), plasmid FepN+Fep β and plasmid FepN.

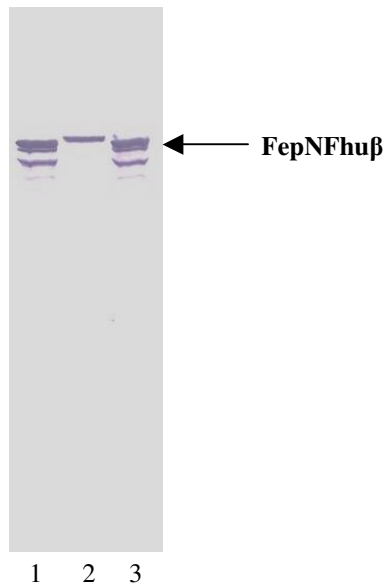


Figure 22a. Expression of FepNFhu β . Whole cell lysates of *E. coli* KDF541 (lane 1), MB97 (lane 2) and OKN73 (lane 3) expressing FepNFhu β from pHSG575 (Scott 2001) were resolved by SDS-PAGE and western blotted with Mouse anti-FepA N domain antibody, Mab 41. MB97 also expresses native FepA from the genome.

Chapter 7

Disposition of the N domain during transport

Protease accessibility of the N domain

Introduction of TEV protease into the periplasm

Bacteria expressing wild type FhuA and FhuA_{TEV site 113-119} were grown overnight in LB medium with the appropriate antibiotics. The culture was used to inoculate complete MOPS medium at a dilution of 1 in 100. After growth to stationary phase, the bacteria were permeablized using the Calcium-Phosphate buffer with or without 5 units of TEV protease (See materials and methods). Calcium-Phosphate permeabilization delivers proteins into the periplasm of *E. coli*. After the permeabilization, the bacteria were washed twice with isotonic saline. The cells were resuspended in complete MOPS medium. The permeablized cells were either subjected to transport assays (see below) or lysed by boiling in sample buffer.

For detection of protease in cells, nitrocellulose membranes containing the SDS-PAGE resolved whole cell-lysates were subjected to western blotting. I used antibodies directed against TEV protease to detect the protein. Rabbit serum containing anti-TEV protease antibodies was a gift from Michael Ehrmann. Antibody X1E2 recognizes an epitope in the N domain of FhuA. The epitope is located on loop NL2 (amino acid residues 98-101) of FhuA (Crystal Archer, Rob Keely and Sarah Weiss). To recognize the above primary antibodies, I used anti-mouse Ig or anti-Rabbit Ig developed in goat (Sigma). The secondary antibodies are conjugated to alkaline phosphate. I developed the blots colorimetrically. In figure 23, lanes 3 and 4 show the presence of extraneous TEV protease in the bacterial cells. The absence of the band in lanes 1 and 2 demonstrates that it did not arise because of the

permeablization procedure. That the band did not arise due to spontaneous degradation of FhuA_{TEV site 113-119} is indicated by its absence in lane 5.

Although the exact mechanism of this process is not clear, it is believed to involve fusion of membranes promoted by the calcium and phosphate ions (Brass 1986). The hyperosmolar buffer may also shrink the cytoplasm of the cell widening the periplasmic space (Neu 1965). The net result is the creation of large, transient pores in the OM. This allows protein molecules as large as 50 kDa to enter the periplasm (Brass, Methods in enzymology) by simple diffusion. The molecular weight of TEV protease (Invitrogen) is ~30, 000. The protease equilibrates between the extracellular fluid and the periplasm. The permeablization requires ice-cold temperatures. The low temperature presumably delays the closure of these pores. Upon transferring the suspension to room temperature, the pores reseal rapidly trapping the protease in the periplasm. After the permeablization, the bacteria were washed twice with isotonic saline. These washes remove only the protease loosely adherent to the surface of *E. coli*. The periplasmic protease is not removed.

Proteolysis of control substrate by introduced TEV protease:

In order to demonstrate that the TEV protease is active in the periplasm of the bacteria, I tested the proteolysis of control substrate, MBP-TEVsite-PhoA. MBP-TEVsite-PhoA is a soluble fusion of *E. coli* maltose binding protein (MBP), a linker containing the TEV recognition amino acid sequence, ENLYFQG (TEV site) and *E. coli* alkaline phosphatase (PhoA). The fusion protein was encoded from plasmid pMER1, a gift from Dr. Micheal Ehrmann. The fusion protein was expressed in *E. coli* CC118 (*F*- Δ (*ara-leu*)7697 *araD* 139 Δ *lacX*74 *galE galK* Δ *phoA*20 *thi rpsE rpoB argE* (*A_m*) *recA*1 *appR*1) (Manoil 1985). Bacteria were permeablized and 50 units of TEV protease was introduced into the periplasm. The introduced enzyme cleaved the

fusion protein, liberating PhoA from the fusion protein. This is evidenced by the appearance of a band of the PhoA protein in the western blot (Figure 24).

The gene for MBP-TEV site-PhoA fusion also encodes the signal sequence for *malE*. Therefore, it is expressed in the periplasm of bacteria. Since the host strain CC118 lacks the *phoA* gene, the appearance of PhoA serves as an indicator for proteolysis. This reaction can be either mediated by the introduced TEV protease or unknown proteases or spontaneously. The latter two scenarios are excluded by the absence of detectable proteolysis in the absence of introduced TEV protease. The introduced TEV protease cleaves the target. This reaction could occur in the periplasm or the cytoplasm. In this regard, the permeabilization procedure that I employed delivers the enzyme primarily into the periplasm and not into the cytoplasm (Brass, methods in enzymology). Therefore, the proteolysis probably happens in the periplasm and not in the cytoplasm.

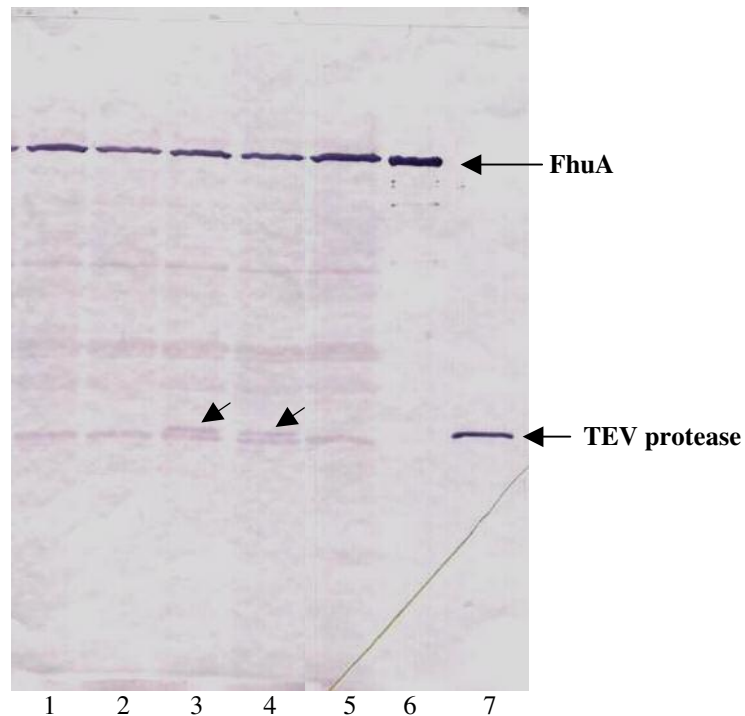


Figure 23. Western blot showing the retention of TEV protease by permeablized cells. I used a mixture of diluted X1E2 (Mouse anti-FhuA Ig) and Rabbit anti-TEV protease Ig as primary antibodies. The secondary antibodies were alkaline phosphatase conjugates. The blots were developed colorimetrically using substrates NBT and BCIP. Lanes 1-5 contains samples from KDF541 pHSG575 *fhuA*_{TEV site 113-119}. In lanes 6 and 7, I ran purified FhuA and TEV protease respectively. Sample in lane 5 is from nonpermeablized cells. In lanes 1 to 4 are cells from permeablized cells with TEV protease (Lanes 3, 4) and without protease (Lanes 1, 2,). The TEV protease bands can be seen in lanes 3 and 4.

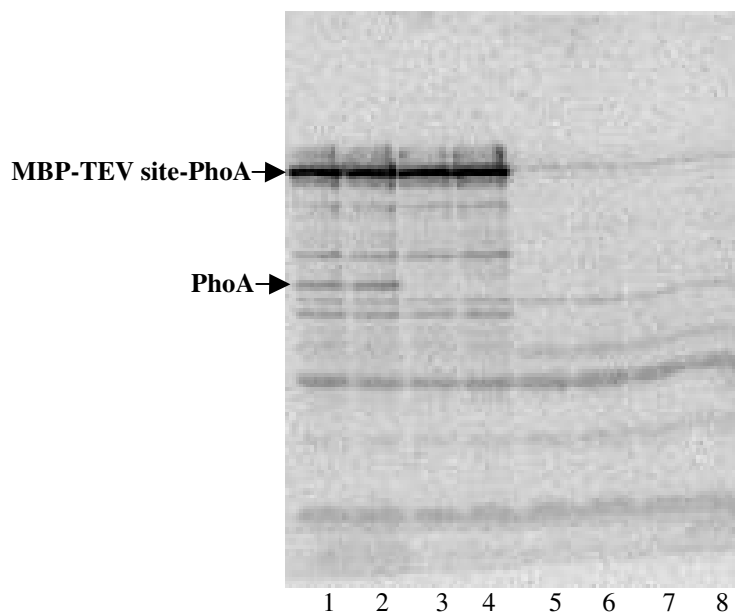


Figure 24. Western blot showing the proteolysis of periplasmic substrate, MBP-TEV site-PhoA by introduced TEV protease. CC118 with (lanes 1-4) and without (lanes 5-8) plasmid pMER1 (expressing MBP-TEV site-PhoA fusion) were grown overnight in LB and inoculated into complete MOPS medium and grown until the culture reached stationary phase. Acetate was used as a carbon source for the MOPS culture to avoid catabolite repression of expression from pMER1. Bacteria were permeablized and TEV protease was introduced into the periplasm (lanes 1,2,5,6). After washing, the cells were suspended in MOPS medium containing dimercaptopropanol. Fc was added to samples in lanes 1, 3, 5 and 7. The suspensions were incubated at 37°C for 3 hours. The cells were then harvested

and processed for western blot. Serum containing the primary antibody, polyclonal rabbit anti-PhoA Ig and ^{125}I -Protein A was used for the radioimmunoblot.

Proteolysis of control substrate by expressed TEV protease

In order to test the activity of the TEV protease in our strains, I transformed bacteria CC118 with plasmids, pCC1 (encoding the enzyme, MBP TEV protease) and pMER1 (encoding the substrate, MBP-TEV site-PhoA). Expression of MBP-TEV protease was induced with IPTG. MBP-TEV site-PhoA expression was induced with arabinose. The expression of the two fusion proteins results in the cleavage of the substrate protein by the TEV protease. The coexpression (Figure 25) delivered slightly more proteolytic activity than permeabilization (Fig 24) as evidenced by the increased cleavage (~50% of total substrate protein) of the fusion protein. The addition of even 3 μM Fc, the natural ligand for FhuA did not affect the proteolysis.

The carbon source acetate reportedly induces catabolite derepression and hence was used during induction (Oh 2002). Glucose was used in specific cases as a repressor (see Fig 21 legend). With coexpression, the observed proteolysis can happen in the periplasm as well as the cytoplasm. This may explain why there is increased cleavage of the substrate with coexpression than with periplasmic introduction. Alternatively, this may just result from a higher concentration of the protease in the former case.

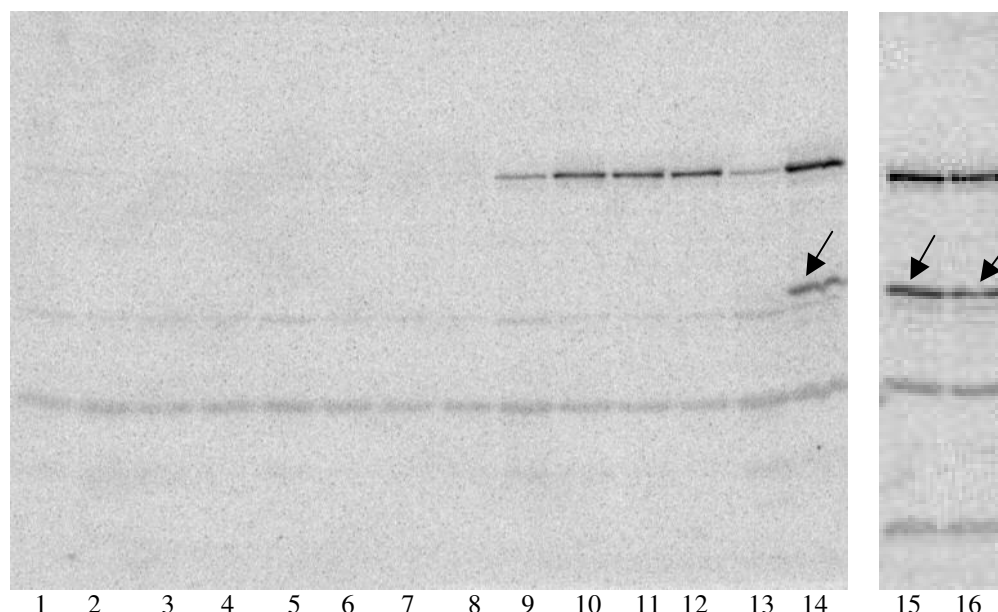


Figure 25. Western blots showing the degradation of periplasmic substrate by coexpressed TEV protease. Bacteria were grown overnight in LB and inoculated into complete MOPS medium and grown until the culture reached stationary phase. The bacteria were harvested by centrifugation and suspended in fresh MOPS medium. IPTG (samples in lanes 2-4, 6-8, 10-12 and 14-16) and arabinose (samples in lanes 3&4, 7&8, 11&12 and 15&16) was added to induce the expression of the enzyme and the substrate fusion proteins respectively. Fc was added to cultures (in lanes 4, 8, 12 and 16) to check for any effect on the proteolysis (inhibition) by the FhuA ligand. The carbon source in lanes 1, 5, 9 and 12 was glucose to repress any expression of MBP-TEV protease fusion. All the other cultures contained acetate as the source. The cultures were shaken at 37°C for 3 hours. Lanes 1-4 contain samples from the host strain CC118 with no plasmids. In lanes 5-8 are samples from CC118 expressing the enzyme, MBP-TEV protease fusion protein (from plasmid pCC1) only and in lanes 9-12 are those from bacteria expressing the substrate, MBP-TEV site-PhoA fusion protein (from plasmid pMER1) alone. Samples from CC118 coexpressing the enzyme and the substrate fusion proteins were run in lanes 13-16. The coexpressed enzyme cleaves the expressed substrate. Serum containing the primary antibody, polyclonal rabbit anti-PhoA Ig and 125 I- Protein A was used for the radioimmunoblot. The arrows indicate bands corresponding to PhoA generated by the proteolysis.

Control substrate in the OM

The control substrate MBP-TEV site-PhoA is expressed in the periplasm. The peptidoglycan layer in gram-negative bacteria is linked to the OM by lipoprotein moieties. The murein layers the periplasmic face of the inner leaflet of the OM. Demchick and Koch (1996) estimated that this multilayered sieve has a pore diameter of about 2.06 nm and is freely permeable to globular proteins, weighing about 22 to 25 kilodaltons. This limit is only a rough estimate and the authors reiterate that even proteins as big as 50 kilodaltons may still pass through the layer. The molecular weight of the purified TEV protease is 29000. The MBP-TEV protease fusion weighs approximately 60,000. This raises the question whether protein targets in the OM are accessible to TEV protease.

In order to test whether the protease can attack targets in the OM, we constructed a FepA-TEV site-PhoA fusion. Murphy et al. (1989) showed that FepA-PhoA fusions containing more than the first 210 amino acids of FepA localize to the OM. Since the fusion protein contains the entire length of FepA, it will localize to the OM.

Expression of FepA-TEV site-PhoA

KDL118 (CC118*fepA-phoA*-) hosting the plasmid pFTPc failed to grow in iron deficient MOPS medium. However, KDL118 expressing other FepA-PhoA fusions were grown successfully in T medium (Murphy 1990). Therefore, I grew the bacteria KDL118 in T media. Although OKN3 expresses no wild type FepA, the western blot revealed a FepA band when the bacterium carries pFTPc (Lane 5 and lane 1a in figure 26). No expression of the fusion protein was detected in KDL118, although it expresses wild type FepA from pITS23 (lane 2, figure 26). This suggests that the fusion protein is unstable. In figure 26, lane 3 shows that the FepA 710::PhoA

fusion protein (Murphy 1989) is expressed from KDL118. This indicates that the instability of FepA-TEV site-PhoA is probably not a result of culture conditions. The FepA band in lanes 5 and 1a appears to be the full-length polypeptide. This suggests that the fusion protein is getting cleaved at or around the TEV site. However, no TEV protease was present in the system. The cleavage may be due to autolysis or other cellular proteases.

Proteolysis of OM substrate

I tested the ability of introduced TEV protease to cleave the FepA-TEV site-PhoA fusion protein. Since the protein is unstable and only a faint band was seen even without the protease, no specific cleavage could be detected (Figure 26a).

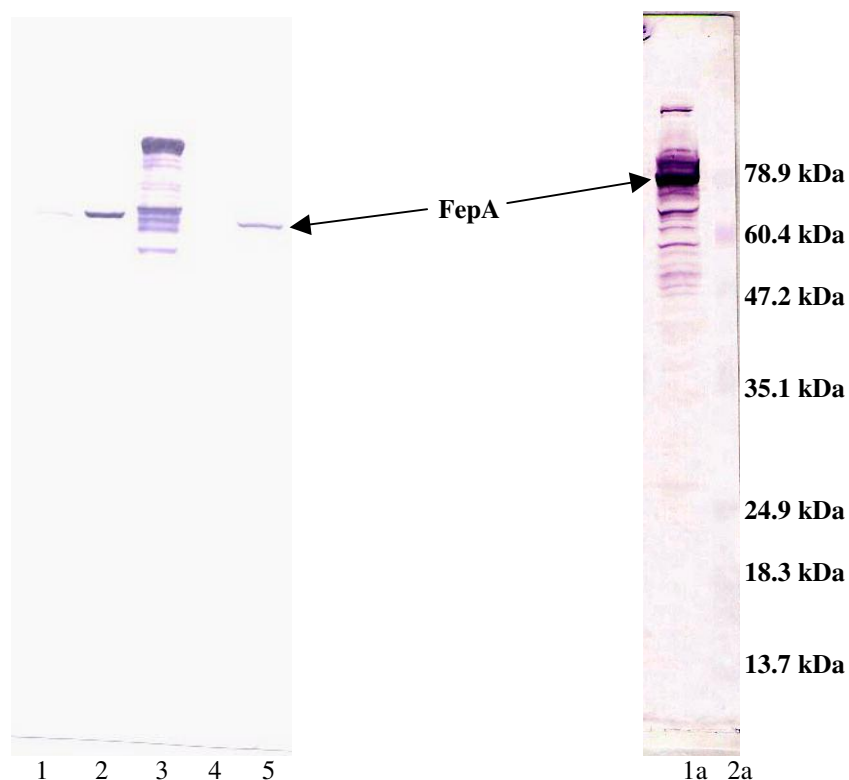


Figure 26. Expression of FepA-TEV site-PhoA fusion protein. Bacteria were grown in iron deficient MOPS medium and whole cell lysates of the cultures were resolved with SDS-PAGE and mouse anti-FepA antibody, mab41 (Left) or mab 45 (Right) was used for western blotting. The blots were developed colorimetrically. From left to right, the lane order is sample from KDL118, KDL118 + pITS23 (*fepA*+), KDL118 + pFP710 (*fepA*1-710-*phoA* fusion), KDL118 + pFTPc (FepA-TEV site-PhoA fusion), OKN3 + pFTPc (FepA-TEV site-PhoA fusion, lane 5 in left figure, lane 1a in right figure) and Benchmark prestained protein marker (Invitrogen®), lane 2a).

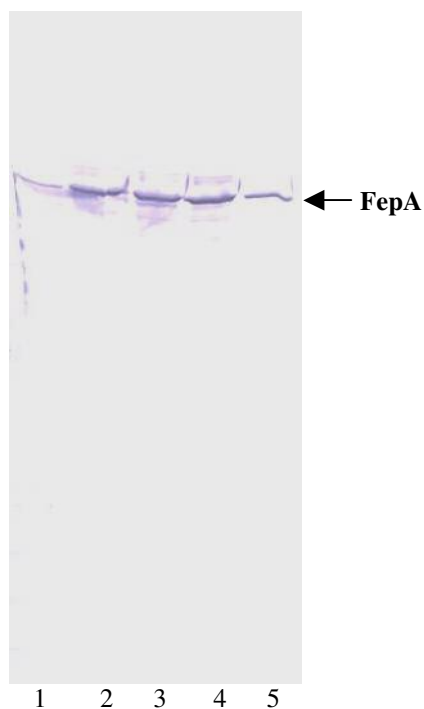


Figure 26a. Proteolysis of OM substrate by periplasmic TEV protease. *E. coli* OKN3 expressing pFTPc was grown in iron deficient MOPS medium. The cells were harvested and either left untreated (lane 5) or permeabilized with (lanes 1,2) or without (lanes 3, 4) TEV protease. The cells were then incubated at 37°C with (lanes 1, 3) or without (lanes 2,4) FeEnt to allow proteolysis. After incubation

whole cell lysates of the cultures were resolved with SDS-PAGE and mouse anti-FepA antibody, mab 45 (Right) was used for western blotting. The blots were developed colorimetrically. The fusion protein is barely visible in lane 4 (not seen in the photograph). Even in the absence of the TEV protease, the fusion protein appears to be cleaved to give off FepA.

Expression of FepA-TEV site-PhoA in protease deficient strains

The control substrate was unstable in our regular strains. We therefore tried to express the construct in strains, SF120 and SF130 deficient in multiple cellular proteases (Table 3). The strains were a gift from George Georgiou. Although the genotype of these strains does not list any mutations in the *fepA* gene, I found that the strains were resistant to colicins B and D. The strains were sensitive to colicin M. It is not clear what alterations are in *fepA*. The fact that both SF120 and SF130, its derivative carries the *fepA*- phenotype suggests that this is a stable change. The strains contain a cassette of a chloramphenicol resistance gene inactivating the protease gene. The plasmid vector, pHSG575 also carries the cat gene (chloramphenicol acyltransferase). This overlap interfered with the selection of pFTPc transformed SF120 or SF130. I tried serial passage in chloramphenicol-free medium to make the strains sensitive to the antibiotic. Even after five passes, the bacteria retained the resistance gene. More passes may be required before the resistance is lost. However, the effects of such a loss on the *ptr*- genotype are unknown.

I tried to select for the transformed bacteria with very high concentrations of the bacteria. However, even a 250 µg/ml concentration of chloramphenicol (more than 100 times the minimum inhibitory concentration (MIC)) did not inhibit the growth of the parent strains. Alternatively, I tried to express the fusion protein in pUC18 plasmid vector with ampicillin resistance without success.

Proteolysis of Fhu targets by introduced TEV protease

I was not able to observe the cleavage of FhuA targets by permeabilization or coexpression approaches. X1E2, the anti-FhuA antibody recognizes an epitope on the

N domain of FhuA. This epitope is located between amino acid 98 and 101. The TEV sites are located on the FhuA amino acid sequence such that proteolytic degradation of the protein would give rise to a smaller N-terminal fragment and a larger C-terminal fragment. For FhuATEV site 71-77, the proteolysis will give rise to a C-terminal fragment, which will retain the epitope for X1E2. Western blots with X1E2 should reveal a truncated FhuA band if proteolysis occurs. For the other two FhuA derivatives with TEV sites at amino acid location 113-119 and 136-142, X1E2 will be unable to recognize the C-terminal fragment as the epitope will be a part of the N-terminal fragment.

The molecular weight of the largest N terminal fragment with the latter 2 mutants would be less than 15,510. We use 0.45 μ M pore size nitrocellulose membranes (Protran) for our western blots. Polypeptides of this length are routinely observed on such membranes in our laboratory. Since the membranes are multilamellar structures, they are expected to bind even the smaller polypeptide fragments. However, in order to exclude the possibility that the smaller fragments pass through the membranes, I performed the blots using 0.2 μ M pore size membranes. However, I did not observe any bands such as might arise due to specific TEV protease mediated proteolysis. Further, periplasmic proteases may digest the N terminal fragments as they arise. Since I did not have access to an antibody recognizing an epitope on the C domain, I was unable to observe the larger C terminal fragment on western blots.

Attempts were made in our laboratory to prepare a monoclonal antibody against the C domain of FhuA by immunizing mice with purified FhuA. However, most of the clones produced antibody directed against epitopes in the N domain of FhuA. Two of the isolates appeared to be directed against FepA epitopes. This may be

due to cross reactivity or heterophilic generation or maybe due to contamination of our FhuA preparation with FepA. Moreover, numerous species of *E. coli* colonize the murine gut. This may explain the origin of FepA specific clones in our preparation. Together, these factors forced me to rely on observing the disappearance of FhuA bands as an indicator of proteolysis for TEV site mutants FhuA_{TEV site113-119} and FhuA_{TEV site136-142}.

Figure 27 depicts the immunoblot of the apparently successful transport/proteolysis experiment. We see a near complete disappearance of the FhuA band in lane 11 (arrow).

However, subsequent similar permeabilization experiments did not match these results. In light of the possible hindrance from peptidoglycan (see above), I introduced both TEV protease and lysozyme into the periplasm of bacteria expressing FhuA_{TEV} site targets. The cell wall of the bacteria, LPS and OM shield the murein from digestion by extraneous lysozyme. If introduced into the periplasm, the enzyme is then able to digest the peptidoglycan. However, as seen in figure 28, no cleavage of the FhuA targets is observed for all three TEV site constructs. Fig 24 depicts the coexpression proteolysis experiment. No difference is observed between lanes containing wild type FhuA and FhuA_{TEV site 113-119}.

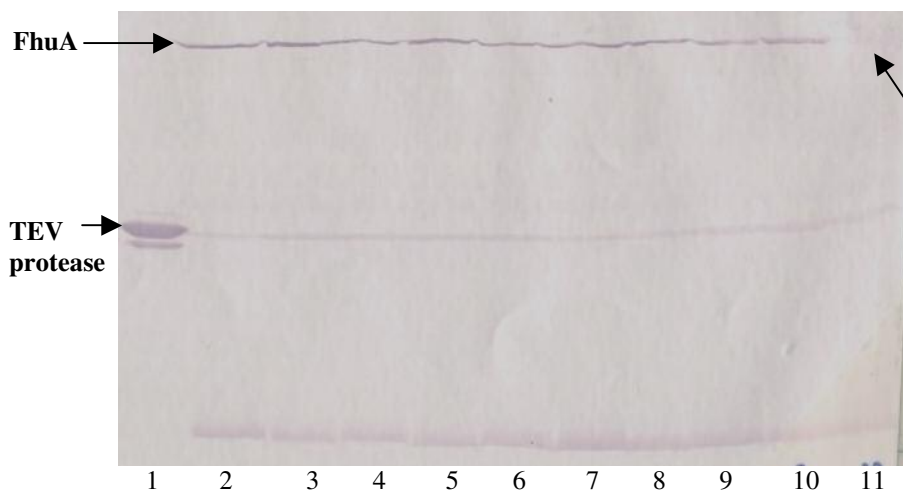


Figure 27. Proteolysis of Fhu targets by introduced TEV protease. *E. coli* KDF541 expressing wild type FhuA (lanes 2-6) and FhuA_{TEV site 113-119} from pHSG575 were untreated or permeabilized (3-6, 8-11) with (5,6 and 10,11) or without (3,4 and 8,9) TEV protease. Subsequently, the cells were incubated with (4, 6 and 9, 11) or without (2, 5, 8 and 11) Fc. Whole cell lysates were resolved on SDS-PAGE and immunoblotted with Mouse anti-FhuA monoclonal antibody (X1E2) and Rabbit anti-TEV protease antibody (Michael Ehrmann). The western blots were developed colorimetrically. The arrow over lane 11, points to the near complete absence of the FhuA protein band.

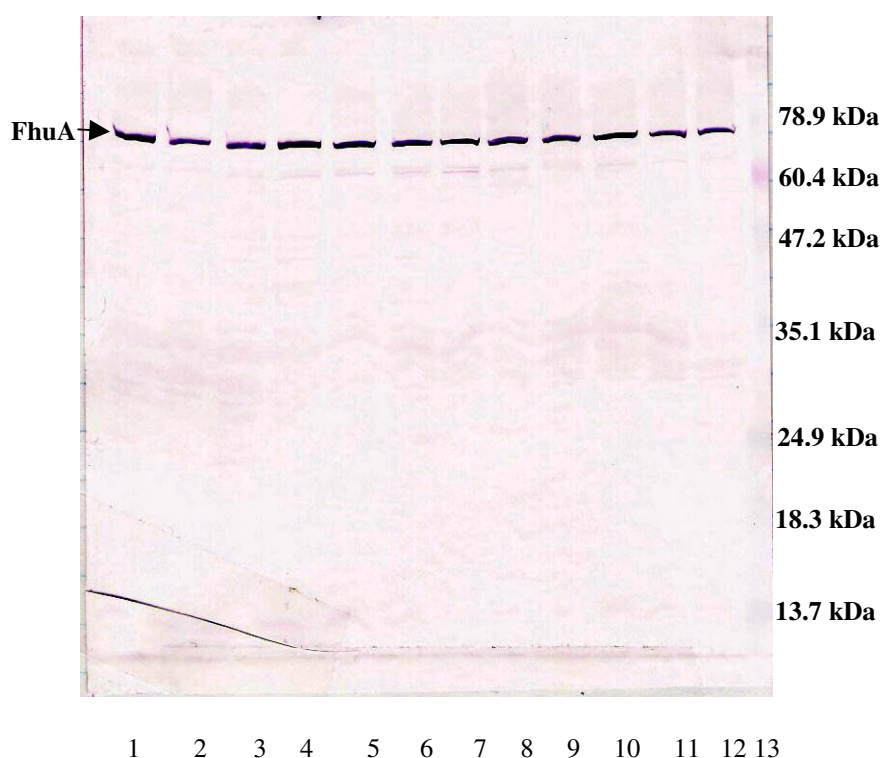


Figure 28. Protease accessibility assay with FhuA and its TEV site derivatives. *E. coli* MB97 (*fhuA*) hosting plasmid pHSG575 expressing wild type FhuA (lanes 1-3), FhuA with TEV sites at 71-77 (lanes 4-6), 113-119 (7-9) and 136-142 (10-12) were either untreated (lanes 1, 4, 7 and 10) or permeabilized and TEV protease and lysozyme introduced into the periplasm (all other lanes). The cells were subsequently incubated with (lanes 3, 6, 9 and 12) and without (2, 5, 8 and 11) Fc. Whole cell lysates were resolved by SDS-PAGE and western blots performed with mouse anti-FhuA antibody, X1E2. No cleavage of the FhuA band is observed in any of the lanes. In lane 13, Benchmark prestained marker was run and the molecular weights of the bands are indicated to the right (Invitrogen®).

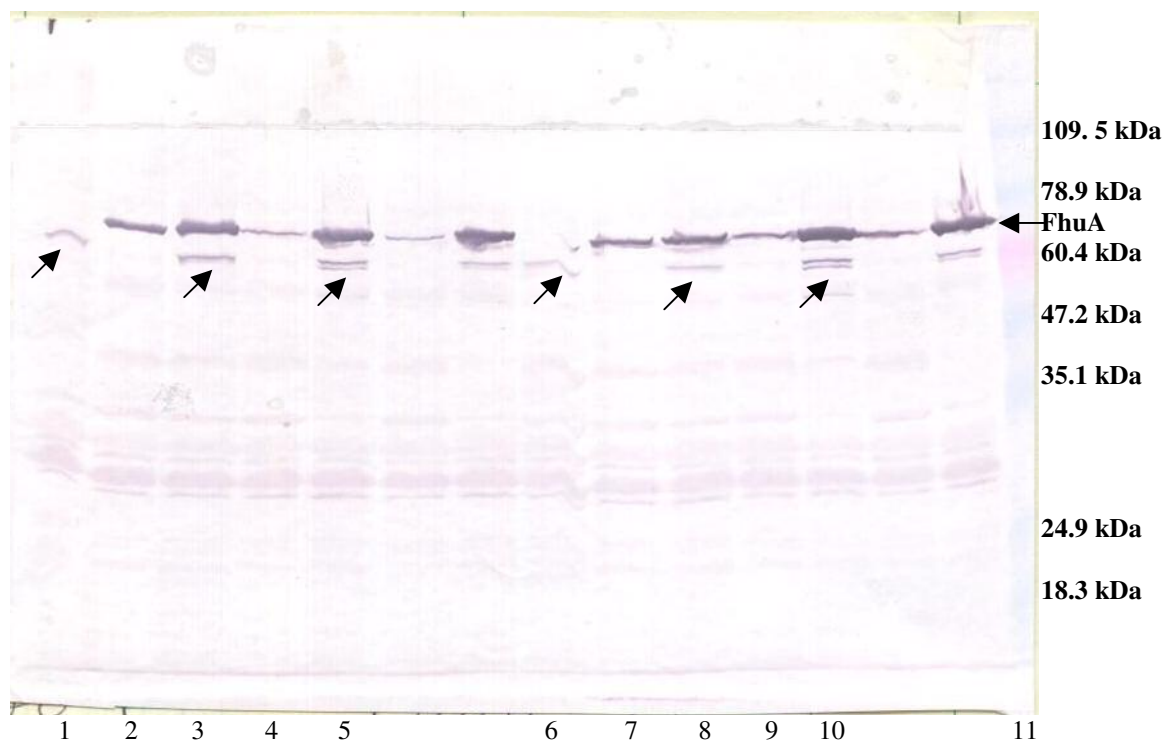


Figure 29. Western blot showing the coexpression of FhuA derivatives and the MBP-TEV protease fusion by *E. coli* KDF541. Bacteria were grown overnight in LB and inoculated into complete MOPS medium and grown until the culture reached stationary phase. The bacteria were harvested by centrifugation and suspended in fresh MOPS medium with no glucose or acetate. IPTG was added to induce the expression of the protease fusion protein (in lanes 1, 3, 5, 6, 8 and 10) and the cultures were shaken at 37°C for 3 hours. DTT was also added to all the cultures to support protease activity. Fc was added to samples in lanes 6 to 10 to allow transport by FhuA derivatives. In lanes 1 and 6 are samples from KDF541pCC1 expressing only the fusion protein. Lanes 2, 3, 7 and 8 carry samples from KDF541pUC18*fhuA* expressing wild type FhuA with (2 & 7) and without (3 & 8) the MBP-TEV protease fusion. Similarly lanes 4, 5, 9 and 10 carry samples from KDF541pUC18*fhuA*_{TEV site 113-119}. A mixture of X1E2 (Mouse anti-FhuA Ig) and Rabbit anti-TEV protease Ig were used for the immunoblot. Arrows indicate the MBP-TEV protease bands.

Experiments in FhuA target proteolysis

I attempted several variations in the protocols to increase the activity of the TEV protease and achieve FhuA target proteolysis. These included changes in the medium, reaction conditions and the chemical composition of the buffers.

Sulfhydryl agents. TEV protease is a cysteine protease. In cysteine proteases like Papain, the active site contains a thiolate imidazolium pair (Polgar 1974). The cysteine of the dyad is sensitive to oxidation. Therefore, thiol reductive compounds are added to the proteolysis reaction mixture. These include compounds like 2-mercaptoethanol (β -ME), dithiothreitol (DTT) and dimercaptopropanol. In the past, we (Bo Jin and I) have found that we can add β -ME and DTT up to a concentration of 1 mM to bacterial cultures without any deleterious effects on cell growth. I therefore added 1 mM DTT to the reaction mixture to maintain the active site sulfhydryl in the reduced state. As expected, I found no difference in cell survival or protein expression. However, these agents did not affect the enzyme activity and no cleavage of the FhuA targets was detected.

Reaction conditions. The physiological temperature for TEV protease activity is $\sim 30^{\circ}\text{C}$. I tested the proteolysis at both 30 and 37 degrees. TEV protease functioned comparably, if not better at 37°C in our experiments. Changes in centrifugation speeds or temperature had no impact. Changes in the washing procedure like the frequency of washes and the temperature of the buffers did not influence the outcome.

Medium. For co-expression experiments, which involved bacteria with multiple plasmids, I found that overnight cultures in LB medium required at least 1% glucose as a supplement for proper cell growth. I also tried different defined media for the subculture and the proteolysis. However, the different defined media did not affect the proteolysis except the cell yield of the subcultures.

TEV protease is inhibited by high concentrations of copper and zinc ions. MOPS medium usually includes solutions containing copper and zinc ions. However, these ions are present at much lower concentrations in MOPS medium. Nevertheless, I prepared MOPS medium without Copper and Zinc. However, use of this altered MOPS medium did not produce visible proteolysis.

In order to remove even trace amounts of copper and zinc, I added chelators that sequester Copper and Zinc. In vitro proteolysis with TEV protease usually involves the use of EDTA (Ethylenediamine tetraacetic acid). EDTA is not only a chelator of zinc and copper ions, but also sequesters magnesium ions. The structural integrity of the lipopolysaccharide and in turn the cell wall of *E. coli* depends on the crosslinking salt bridges formed by magnesium ions. Therefore, we decided against adding EDTA as a chelator. The search of literature for a more specific chelator yielded dimercaprol (Dimercaptopropanol, British anti-Lewisite, BAL). Dimercaprol also has the added advantage of being a sulfhydryl reducing agent. I therefore used dimercaprol as a dual agent in our reactions. D-penicillamine is another chelator of these two metal ions. However, it did not produce any detectable results. None of these modifications led to detectable proteolysis of FhuA.

Buffers. I originally employed the permeablization technique described in Zgurskaya et al. (1999), which uses permeablization buffers with high sucrose concentrations. The original protocol devised by Brass et al. employed high concentrations of calcium. The sucrose technique was only a modification suggested for proteins affected by calcium. Therefore, I switched to sucrose free permeablization buffers (see above). However, no difference was seen between samples that were treated with the two different buffers.

Enzyme concentration. I tried to increase the concentration of the TEV protease in the experiments. Even increasing the amount of TEV protease introduced, from 10 units to 50 units and then 200 units per 10^9 cells failed to show hydrolysis of the FhuA targets.

Protein expression. I used rifampicin at a concentration of 200 $\mu\text{g/ml}$ to block bacterial transcription. This enabled us to study the effects of the proteolysis on only the protein molecules that are fully folded and localized. However, this did not change the outcome in that I was not able to detect any proteolysis.

Oxamates. Dougherty et al. (1988) reported that oxamates inhibit the activity of cysteine proteases at concentrations above 1 μM . Fc, the natural ligand for FhuA is a hydroxamate ferric siderophore. It is probably transported intact into the cytoplasm of the cells. Nevertheless, I tested the activity of the TEV protease on the control substrate in the presence of Fc. I found that concentrations as high as 3 μM did not affect the proteolytic activity.

Fluorophore labeling of residues in the N domain

Selection of fluorophores

I selected the thiol reactive fluorophore conjugate, FM (Molecular probes, Invitrogen) to label the introduced cysteines in vivo. Several considerations dictated the selection of the fluorophore. Cao et al. (2003) described the optimal conditions for labeling mutant FepA proteins in vivo with the FM. The OM contains water-filled channels that allow the free diffusion of molecules smaller than 600 Da (Nikaido and Vaara 1985). Specifically, the protein OmpF provides a 7 by 11 Å eyelet (Cowan 1995). From sugar diffusion studies, the estimated diameter of the pore is about 12 Å. The molecular weight of FM is 427 (Molecular probes). Further, the largest diameter of the fluorescein molecule is about 9 Angstrom. The conjugate is therefore small enough to traverse the OM (OM) of the bacterium and enter the periplasm. We do not expect FM to travel through FepA, unless a conformational change in the N domain creates a channel.

In addition to FM, I also used ALEXA Fluor 488 C5-maleimide (AM, Molecular probes, Invitrogen). ALEXA Fluor 488 is a derivative of fluorescein of molecular weight 720.66. The crystal structure of AM is not available. The larger size of this molecule suggests that it will not traverse the OM. However, the structure of this molecule resembles fluorescein and its larger weight may not necessarily increase its largest diameter in solution.

Entry of fluorophores into the periplasm

In order to assess the ability of the fluorophores to enter the periplasm, I tested the labeling of cysteines introduced in lipid-deficient derivative of AcrA (Zgurskaya 1999). The derivative is present in the periplasm and is free of cysteines. Therefore, the mutation A15C (Ip 2003) introduces an unbonded cysteine.

I tested the labeling of AcrAA15C expressed from pUZ11 (pUC18 derivative) in AG100A. While wild type AcrA was unmodified, both FM and AM modified AcrA A15C (figure 30) indicating that the agents enter the periplasm. The strain and the relevant plasmids were a gift from Helen Zgurskaya (Department of Chemistry & Biochemistry, University of Oklahoma, Norman, OK, USA).

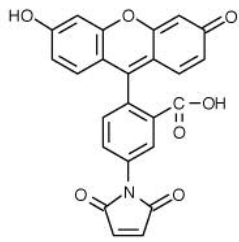
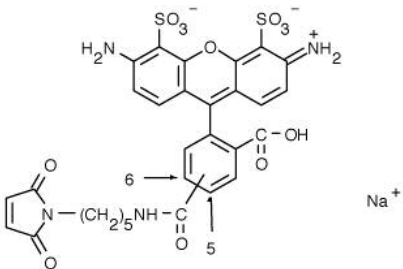
Fluorophore	Fluorescein 5-maleimide (FM)	Alexa Fluor® 488 C ₅ -maleimide (AM)
Formula	C ₂₄ H ₁₃ NO ₇	C ₃₀ H ₂₅ N ₄ NaO ₁₂ S ₂
Molecular weight	427.37	720.66
Structure		

Table 11. Comparison between FM and AM.

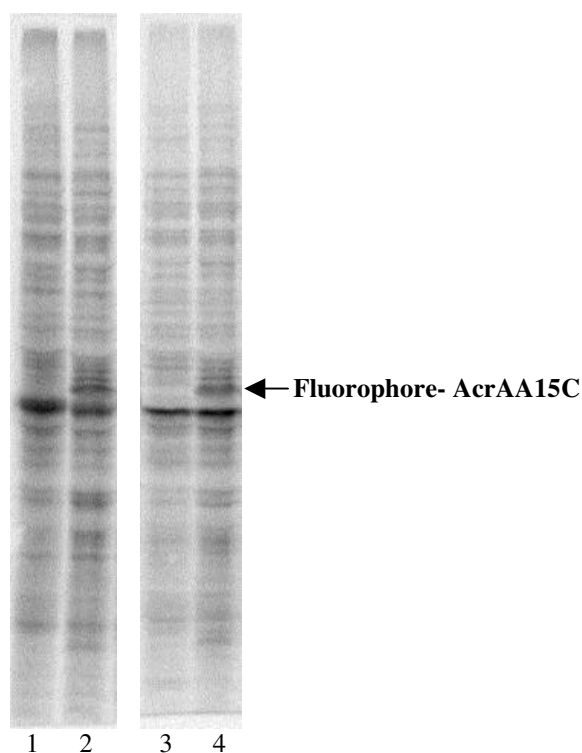


Figure 30. Labeling of AcrA by FM and AM. AG100A expressing AcrA wild type (lanes 1 and 3) or AcrA A15C (lanes 2 and 4) were labeled with 65 μ M FM (lanes 1 and 2) or AM (lanes 3 and 4) for 30 min at 37°C. The cells were lysed in sample buffer and resolved by SDS-PAGE. The gel was scanned for fluorescence in a STORM SCANNER (Molecular Dynamics). The arrow indicates the position of AcrA.

Location of the introduced cysteines

The amino acid sequence of the FepA polypeptide contains two cysteines at positions 487 and 494. Prior research (Liu 1994) established that these cysteines form a disulfide bond. Accordingly, neither of these two cysteines are labeled by fluorophores (Cao 2003, figure 31). We selected residues for mutagenesis based on their crystal structure coordinates. Glycine 54 is located on the lateral surface of the N domain away from the hinge in FepA. Glycine 54 also initiates loop NL1 of FepA. In the crystal structure, it is not visible from the surface opening of the barrel and barely observed through the periplasmic opening. Therefore, the residue is apparently inaccessible from the cell surface or the periplasm. In close proximity to glycine 54 is glycine 565 in the barrel wall. The side-chains of its flanking amino acids, leucine 566 and glutamate 564 point towards the membrane bilayer in the crystal structure. Since the residues are in β strand 16 of the barrel, the side chain of G565C probably points inwards into the lumen of the barrel. The reverse orientation will likely disrupt the beta strand and compromise the protein's structure.

At the top of the N domain, tryptophan 101 is located in NL2. FepAW101C is labeled with FM (Cao 2003) implying that this residue is freely accessible from the cell surface. At the periplasmic face of the N domain is residue isoleucine 14. Isoleucine14 is also a member of the 'TonB box'. It is located in close apposition to the barrel, specifically to residue glycine 300. Daniel Scott prepared FepAG54C as part of a study involving disulfide bond formation. For a similar objective, Paul Warfel constructed FepAI14C and FepAG300C. Bo Jin and I constructed FepAW101C for the in vivo labeling study described above (Cao 2003). Li Ma introduced the mutation G565C in FepA.

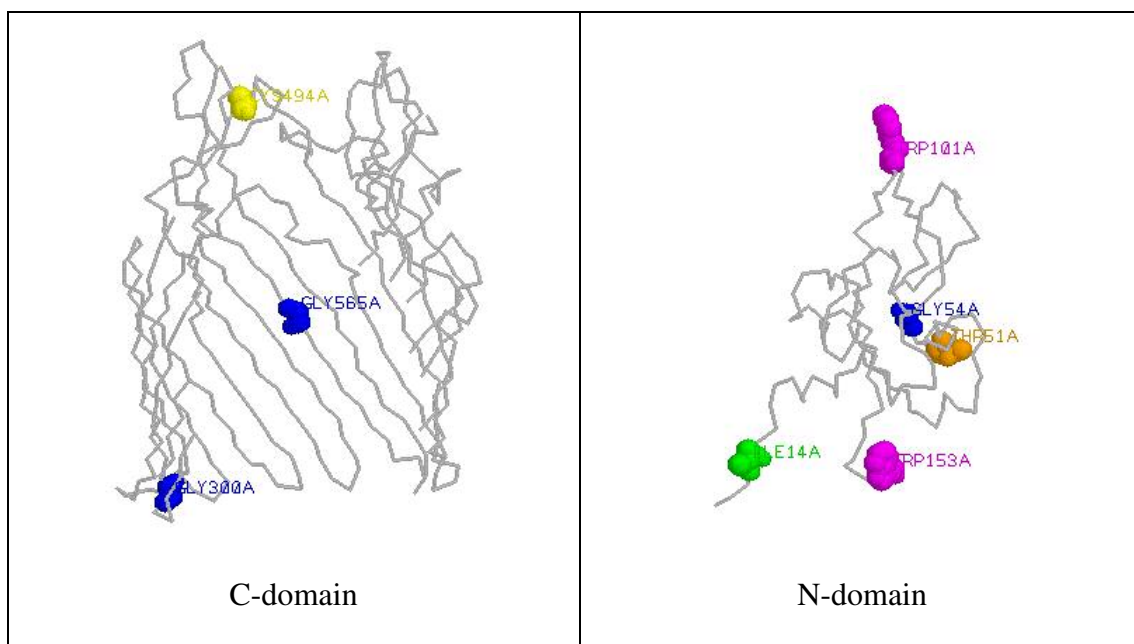


Figure 31. Target residues for cysteine mutagenesis. The residues were selected based on their location in the crystal structure of FepA. The views are in the plane of the lipid bilayer with the cell exterior on top and the periplasm at the bottom. The protein backbone of both N- and C- domains is depicted in grayscale. On the left, the C domain is shown in slab mode to reveal the location of glycine 565. Glycines 54, 300 and 565 are depicted in blue. Isoleucine 14 is depicted in green, threonine 51 in orange and tryptophans 101 and 153 are depicted in pink. One of the native cysteines, 494 is depicted in yellow. The other cysteine, 487 was not mapped in the crystal structure. Tryptophan 153 is shown to indicate the position of the hinge between the N domain and the C-domain β -barrel.

FepA	Diameter of halo in mm	
	OKN3	OKN13
--	0	0
Wild type	16	0
I14C	18	0
T51C	18	0
G54C	19	0
W101C	17	0
G300C	19	0
G565C	19	0

Table 12. Siderophore nutrition assay of cysteine substitution mutants. The diameter of the zone of growth (halo) of bacteria around the disc containing the ferric siderophore is expressed in millimeters. Differences are also noted in the opacity of the halos which reflect the density of the bacterial growth.

Siderophore nutrition assay.

I tested the ability of the protein constructs to transport FeEnt. All the mutant proteins transported FeEnt into OKN3. As expected, none of the constructs supplied iron to strain OKN13 lacking TonB. FepAW101C produced a lower density of cell growth than wild type FepA (Table 12).

Colicin killing

All the mutant proteins conferred sensitivity on OKN3 to colicins B and D. None of the proteins was active in OKN13. FepAW101C was only 10% as active as wild type FepA in this assay (Table 13).

Protein expression

All the mutant constructs expressed FepA from its natural promoter (Figure 32).

Labeling with FM

Initial fluorophore labeling was performed with FM and the FepA proteins expressed in OKN3. For samples labeled with FM and also AM, the best results were obtained by directly scanning the wet gel for fluorescent bands (STORM scanner). Transferring the bands onto nitrocellulose before scanning led to a loss of sensitivity (Figure 33). Although we had antibodies against fluorescein, immunoblotting did not give greater sensitivity and reduced specificity.

I experimented with different concentrations of FM. Of the concentrations that I tried, 65 μ M gave the best labeling at FepAG54C (Figure 33). I observed no labeling with wild type FepA (Figure 34). This is consistent with earlier reports (Cao 2003).

FepA protein	Colicin sensitivity titer as percent wild type titers			
	OKN3		OKN13	
	B	D	B	D
--	0	0	0	0
Wild type	100	100	0	0
I14C	100	100	0	0
T51C	100	100	0	0
G54C	100	100	0	0
W101C	10	10	0	0
G300C	100	100	0	0
G565C	100	100	0	0

Table 13. Colicin sensitivity of cysteine substitution mutants. Titers correspond to the reciprocal of the maximum dilution of the colicin that clears the bacterial lawn. Results are expressed as a percentage of the titers calculated for killing of OKN3/pITS23 expressing wild type FepA.

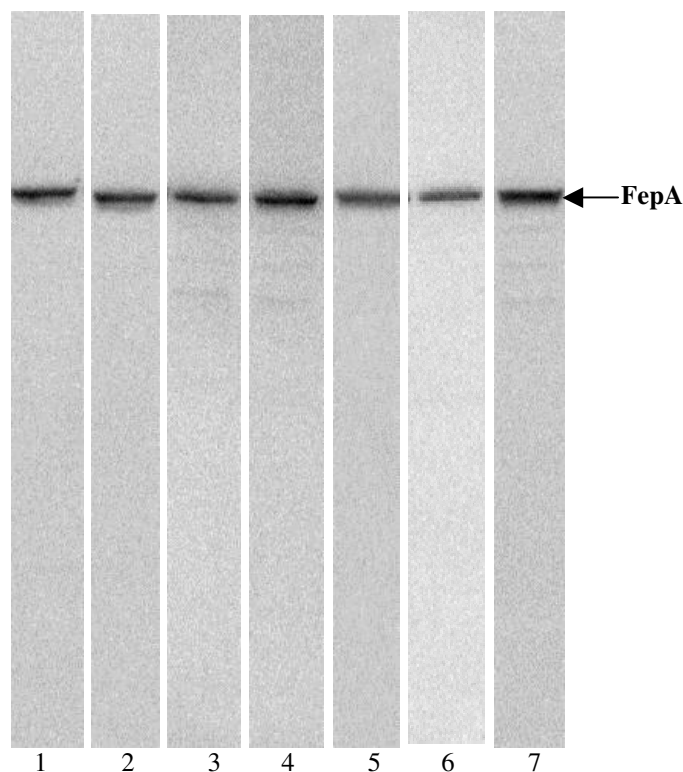


Figure 32. ¹²⁵I-Protein A immunoblot profiling the expression of FepA derivatives. Bacteria were grown in iron deficient MOPS medium and harvested by centrifugation. The cell pellets were lysed and resolved by SDS-PAGE. The protein bands were electroeluted onto nitrocellulose membranes and a radioimmunoblot was performed. Mab45, a monoclonal antibody that recognizes an epitope on the C domain was used as the primary antibody. All the constructs were expressed in OKN3. The picture is a composite of pictures taken of immunoblots performed for each mutant construct. The samples in strips 1 to 7 were wild type FepA, FepA I14C, T51C, G54C, W101C, G300C and G565C.

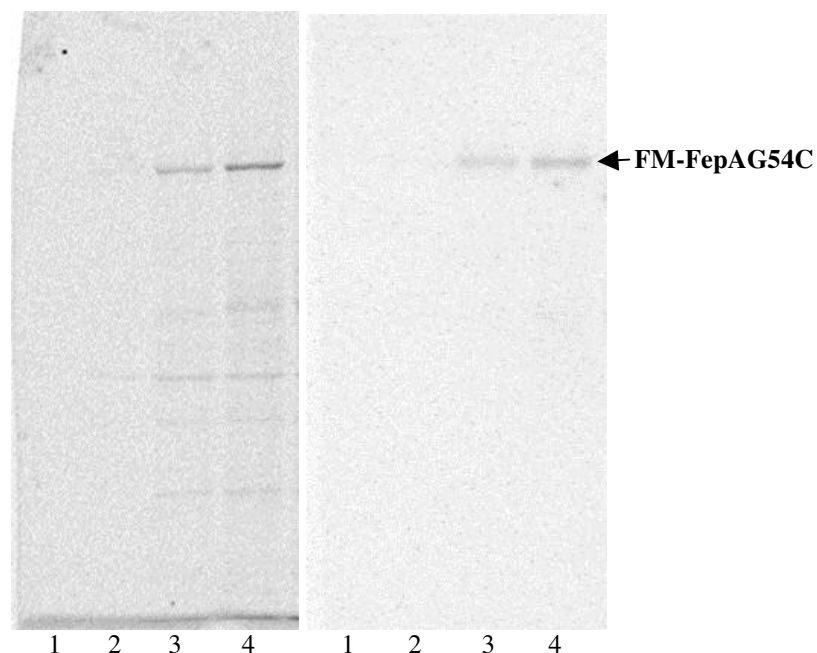


Figure 33. Detection of FM labeled FepAG54C. FepAG54C expressed in from plasmid pHSG575 in KDF541 were labeled with increasing concentrations of FM. From samples in lanes 1 to 4, the concentrations employed were 1.3 μ M, 6.5 μ M, 13 μ M and 65 μ M respectively. The bands were detected by scanning the gel (left) or by radioimmunoassay with rabbit serum containing anti-fluorescein antibodies (anti-BSA-fluorescein iodoacetamide Cao 2003) and 125 I-Protein A. The arrow indicates labeled FepAG54C.

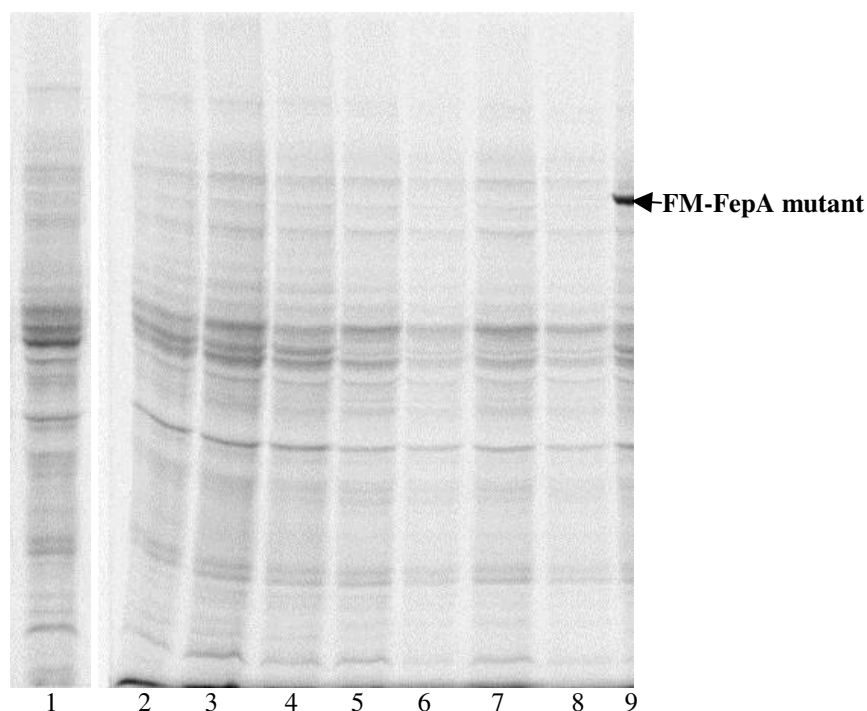


Figure 34. Labeling of wild type FepA by FM. OKN3 (lanes 1, 3, 5 and 7) and OKN13 (lanes 2, 4, 6 and 8) expressing wild type FepA from pHSG575 were labeled with 65 μ M FM for 30 min at 37°C (1, 2, 3 and 4) or 0°C (lanes 5, 6, 7 and 8). Samples in lanes 3, 4, 7 and 8 were pre-incubated with 10 μ M FeEnt at 0°C for 10 min. The cells were lysed in sample buffer and resolved by SDS-PAGE. The gel was scanned for fluorescence in a STORM SCANNER (Molecular Dynamics). In lane 9 is FepA cysteine mutant labeled with FM.

FepAW101C showed strong labeling (Figure 35). In the crystal structure, the β carbon of tryptophan 101 is located at a distance of 9.56 angstrom from the β carbon of cysteine 494 (Figure 36, Buchanan 1999). Cysteine 487 is not described in the crystal structure. However, since the disulfide does form (Liu 1994), it is probably in close proximity to the other residues. The resultant sulfhydryl triad can possibly form one of three disulfide bonds namely C487-C494, W101C-C487, or W101C-C494. This will leave the odd cysteine to be labeled by FM. The fact that none of the other cysteine mutants exhibited this pattern indicates that this shuffling of the disulfide bond does not happen during maturation of the protein.

With wild type FepA, the presence or absence of β -mercaptoethanol does not affect the migration of the protein on SDS-PAGE. This is because the loop subtended by disulfide formation in the native polypeptide is only 7 amino acids long. This does not visibly alter the extended conformation of the solublized protein. However, if the disulfides form between W101C and either of the natural cysteines, the loop is between 386 to 393 residues long. Such a looped conformation presumably affects the gel migration of the SDS solublized polypeptide. In the presence of the reducing agent, labeled FepAW101C migrates as a single band. In the absence of the thiol reagent, labeled FepAW101C migrated as two different bands. The larger size of the aberrant band indicates that this is probably not a result of degradation or protein instability. Theoretically, the protein may get labeled at any of the three cysteines. The smaller band migrates at the level of other labeled FepA proteins. One explanation is that the larger band is the protein with the loop formed either by W101C-C487 or W101C-C494 bonding and the smaller is that with the natural C487-C494 cystine. The latter presumably represents the population labeled at residue 101.

This implies that the looped polypeptide migrates slower despite a presumably more compact conformation.

The presence of only two rather than three labeled bands raises another possibility. Neither of the bands may have label attached to W101C. Instead, the protein may be labeled only at C487 or C494. The labeling of FepAW101c in OKN13 (*tonB*-) even in the presence of FeEnt supports this conclusion. Such a concentration will saturate the binding site and also induce closure of the surface loops of FepA. It is expected that such closure would prevent FM from accessing W101C. Two factors confront this conclusion. The difference in the gel migration caused by the addition of only seven amino acids to the loop is surprising. Even more intriguing is the migration of the smaller at the same rate as native FepA. This model suggests that W101C is not accessible to fluorophores. This is also consistent with the absence of labeling at S211C (Cao 2003). In other words, the interior of the barrel is not accessible to fluorophores.

I also observed strong labeling of I14C (Figure 38). In contrast, I observed only weak labeling of T51C (Figure 39), although threonine 51 is clearly visible on the periplasmic face of the N domain in the crystal structure. The gamma carbon in the side chain of this threonine points towards the barrel (Buchanan 1999). The sulfhydryl group of the substituted cysteine may take a similar orientation and steric hindrance may hinder its modification. Alternatively, the cysteine may assume a buried conformation. Threonine 51 is not part of a helix or a β sheet. The amino acid and its substitute are probably not subject to the constraints of these secondary structures. Therefore, it is not clear what alterations that this mutation will make to the local conformation and what effects will result.

The residue glycine 54 is on the lateral surface of the N domain. I found that FM labeled G54C (Figure 40). Glycine 54 is barely visible from the periplasm and invisible from the surface in the space filled representation of FepA's crystal structure. Yet, it was accessible to modification.

Among the residues substituted in the C domain, G300C was weakly labeled with FM (Figure 41), whereas G565C was not modified (Figure 42), despite its proximity to glycine 54. In light of the protein's wild type sensitivity to colicins B and D and its ability to transport FeEnt, it is imaginable that the mutation G565C did not disrupt FepA structure. This supports the conclusion that the substitution did not compromise β strand 16. In the absence of any such disruption, the sulfhydryl group of the cysteines side chain is not modified despite its location in the lumen. This suggests that the fluorophore does not enter this part of the barrel but that G54C is labeled when the residue and the N domain moves out of the barrel. Such movement may be directed towards the surface or the periplasm.

The same labeling pattern was found when the reaction was performed at 37 °C or 0°C.

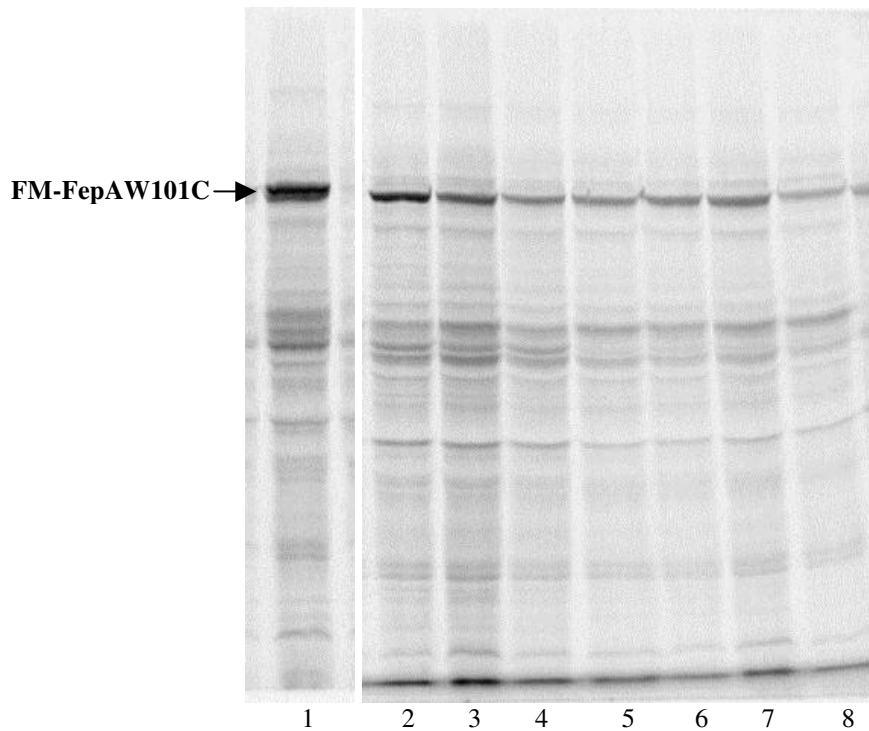


Figure 35. Labeling of FepAW101C by FM. OKN3 (lanes 1, 3, 5 and 7) and OKN13 (lanes 2, 4, 6 and 8) expressing FepAW101C from pHSG575 were labeled with 65 μ M FM for 30 min at 37°C (1, 2, 3 and 4) or 0°C (lanes 5, 6, 7 and 8). Samples in lanes 3, 4, 7 and 8 were incubated with 10 μ M FeEnt at 0°C for 10 min. The cells were lysed in sample buffer and resolved by SDS-PAGE. The gel was scanned for fluorescence in a STORM SCANNER (Molecular Dynamics).

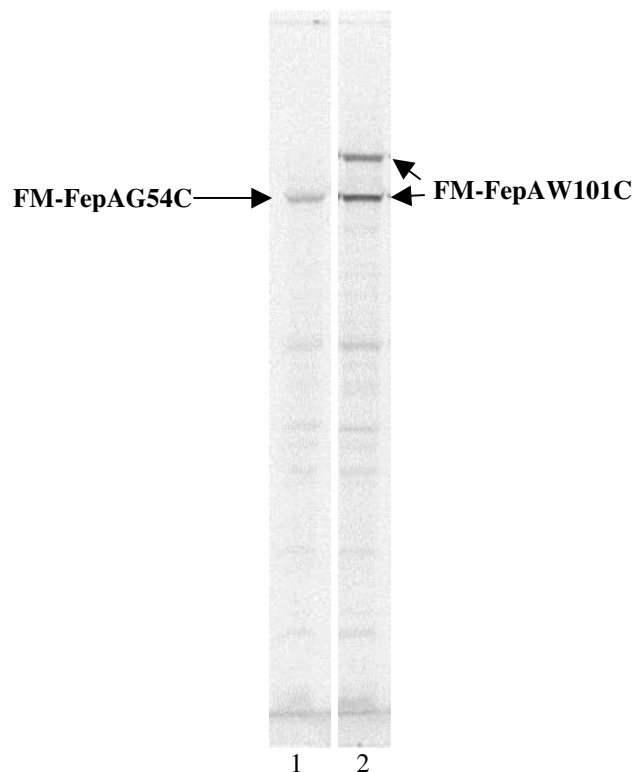


Figure 36. Detection of FM-FepAW101C in the presence and absence of sulfhydryl reagents. KDF541 expressing FepAG54C (lane 1) and FepAW101C (lane 2) from pHSG575 were labeled with 65 μ M FM for 30 min at 37°C. The cells were lysed in sample buffer without adding 2-mercaptoethanol and resolved by SDS-PAGE. The gel was scanned for fluorescence in a STORM SCANNER (Molecular Dynamics).

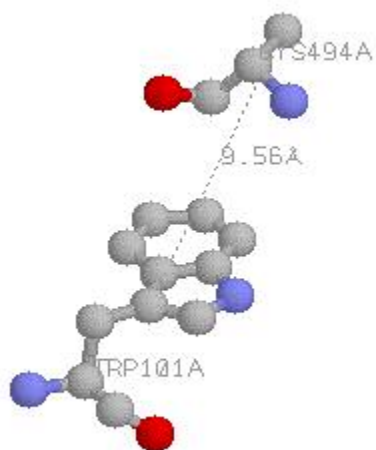


Figure 37. Distance between W101 and C494 in the crystal structure.

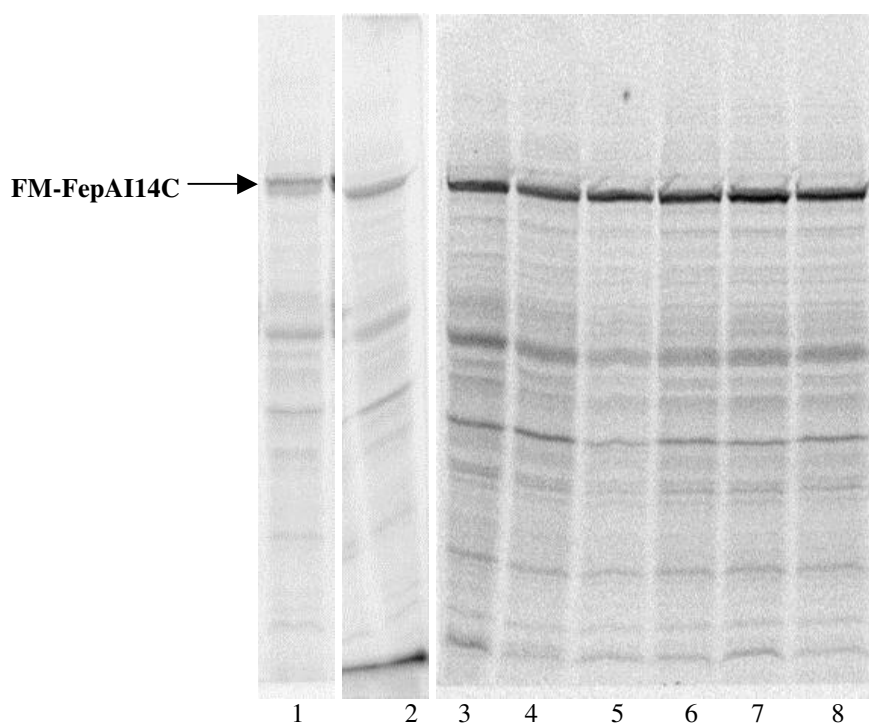


Figure 38. Labeling of FepAI14C by FM. OKN3 (lanes 1, 3, 5 and 7) and OKN13 (lanes 2, 4, 6 and 8) expressing FepAI14C from pHSG575 were labeled with 65 μ M FM for 30 min at 37°C (1, 2, 3 and 4) or 0°C (lanes 5, 6, 7 and 8). Samples in lanes 3, 4, 7 and 8 were incubated with 10 μ M FeEnt at 0°C for 10 min. The cells were lysed in sample buffer and resolved by SDS-PAGE. The gel was scanned for fluorescence in a STORM SCANNER (Molecular Dynamics).

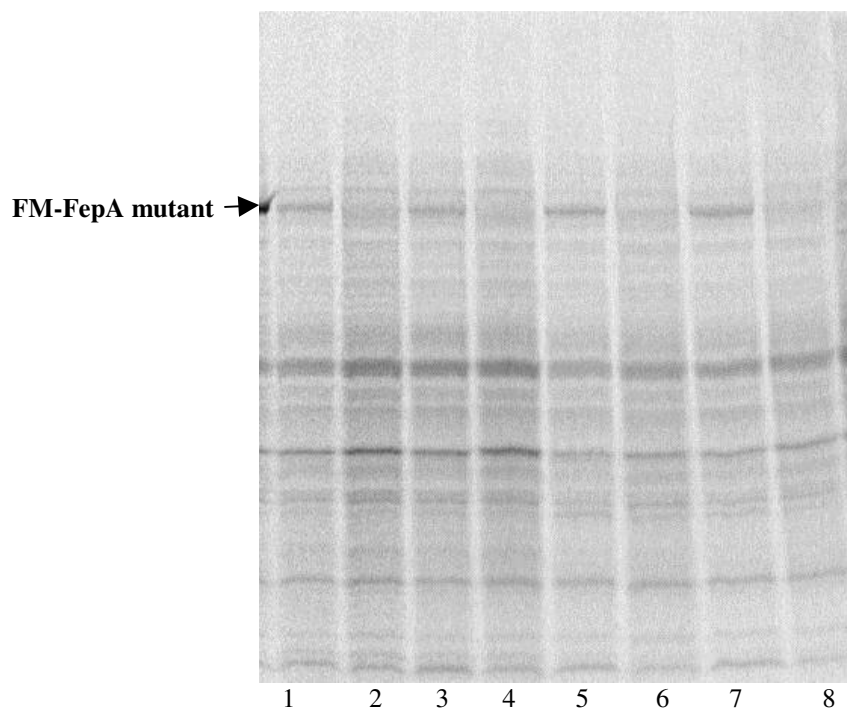


Figure 39. Labeling of FepAT51C by FM. OKN3 (lanes 1, 3, 5 and 7) and OKN13 (lanes 2, 4, 6 and 8) expressing FepAT51C from pHSG575 were labeled with 65 μ M FM for 30 min at 37°C (1, 2, 3 and 4) or 0°C (lanes 5, 6, 7 and 8). Samples in lanes 3, 4, 7 and 8 were incubated with 10 μ M FeEnt at 0°C for 10 min. The cells were lysed in sample buffer and resolved by SDS-PAGE. The gel was scanned for fluorescence in a STORM SCANNER.

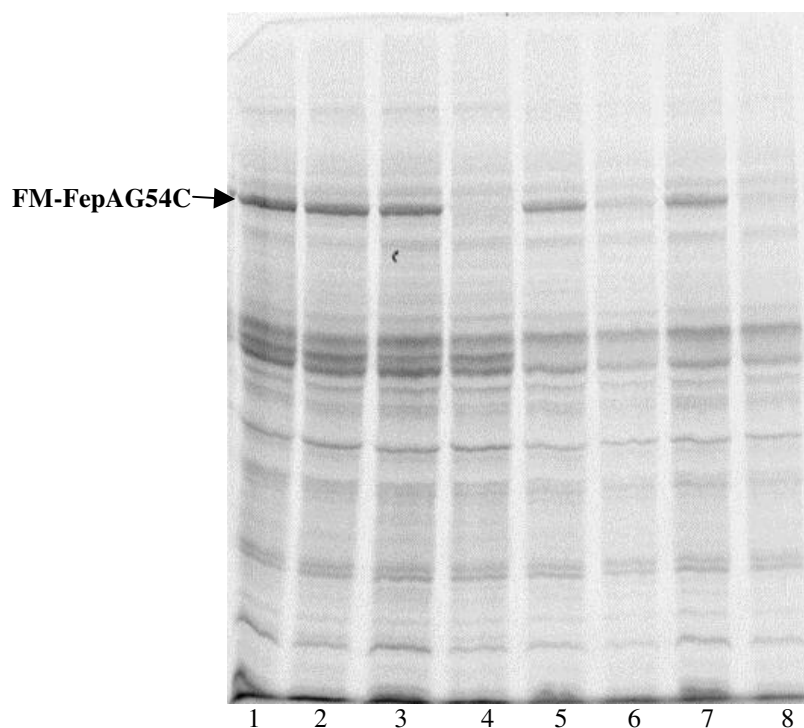


Figure 40. Labeling of FepAG54C by FM. OKN3 (lanes 1, 3, 5 and 7) and OKN13 (lanes 2, 4, 6 and 8) expressing FepAG54C from pHSG575 were labeled with 65 μ M FM for 30 min at 37°C (1, 2, 3 and 4) or 0°C (lanes 5, 6, 7 and 8). Samples in lanes 3, 4, 7 and 8 were incubated with 10 μ M FeEnt at 0°C for 10 min. The cells were lysed in sample buffer and resolved by SDS-PAGE. The gel was scanned for fluorescence in a STORM SCANNER (Molecular Dynamics).

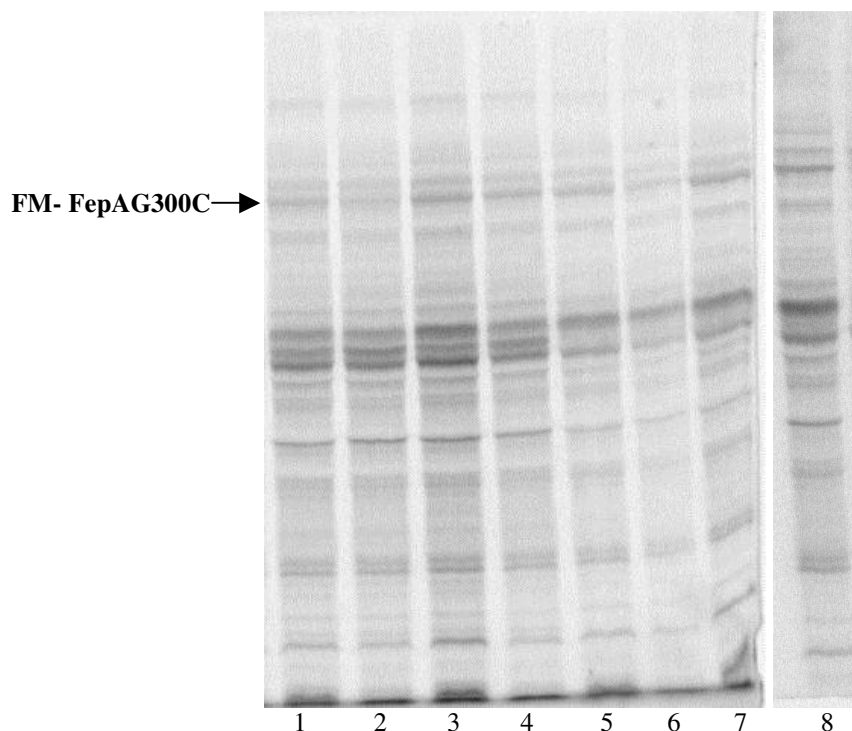


Figure 41. Labeling of FepAG300C by FM. OKN3 (lanes 1, 3, 5 and 7) and OKN13 (lanes 2, 4, 6 and 8) expressing FepAG300C from pHSG575 were labeled with 65 μ M FM for 30 min at 37°C (1, 2, 3 and 4) or 0°C (lanes 5, 6, 7 and 8). Samples in lanes 3, 4, 7 and 8 were incubated with 10 μ M FeEnt at 0°C for 10 min. The cells were lysed in sample buffer and resolved by SDS-PAGE. The gel was scanned for fluorescence in a STORM SCANNER (Molecular Dynamics).

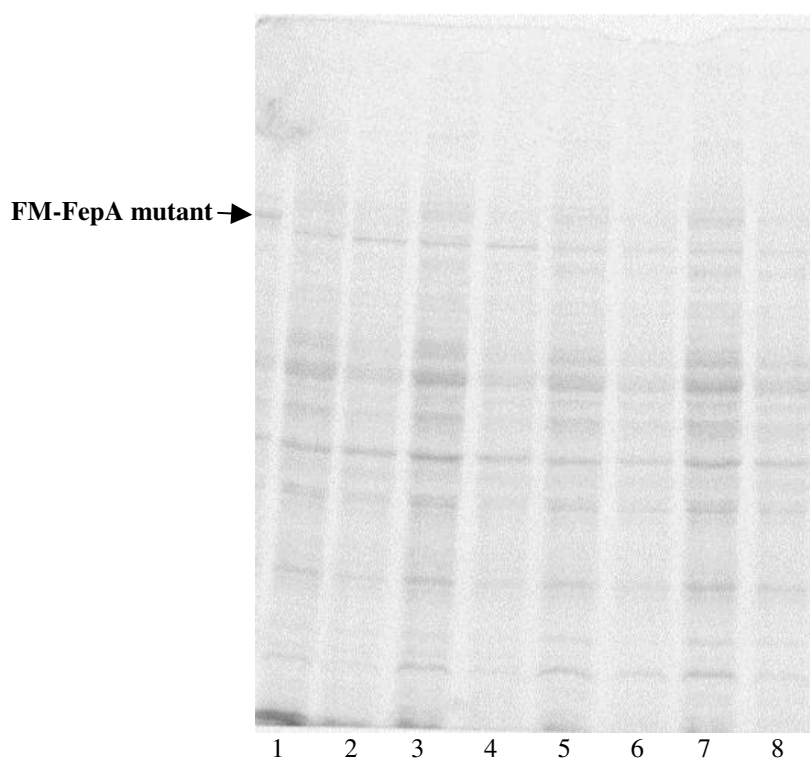


Figure 42. Labeling of FepAG565C by FM. OKN3 (lanes 1, 3, 5 and 7) and OKN13 (lanes 2, 4, 6 and 8) expressing FepAG565C from pHSG575 were labeled with 65 μ M FM for 30 min at 37°C (1, 2, 3 and 4) or 0°C (lanes 5, 6, 7 and 8). Samples in lanes 3, 4, 7 and 8 were incubated with 10 μ M FeEnt at 0°C for 10 min. The cells were lysed in sample buffer and resolved by SDS-PAGE. The gel was scanned for fluorescence in a STORM SCANNER (Molecular Dynamics).

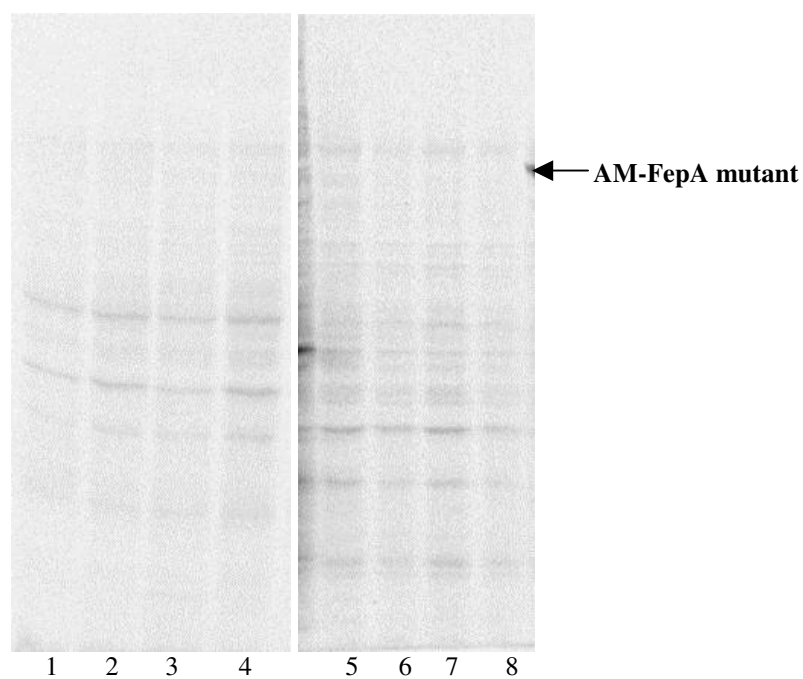


Figure 43. Labeling of wild type FepA by AM. The data was obtained as detailed for FM above.

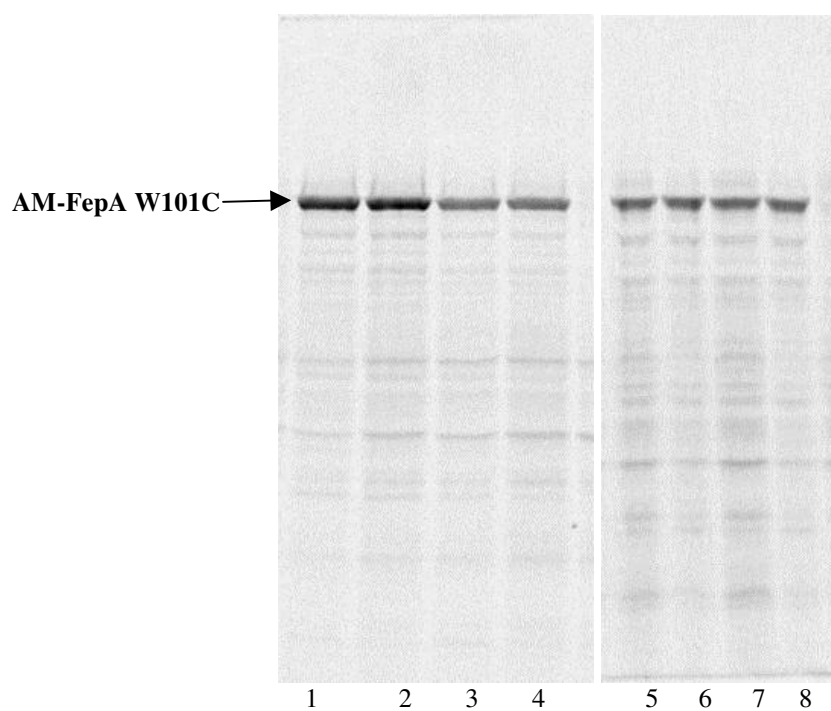


Figure 44. Labeling of FepAW101C by AM. The data was obtained as detailed for FM above.

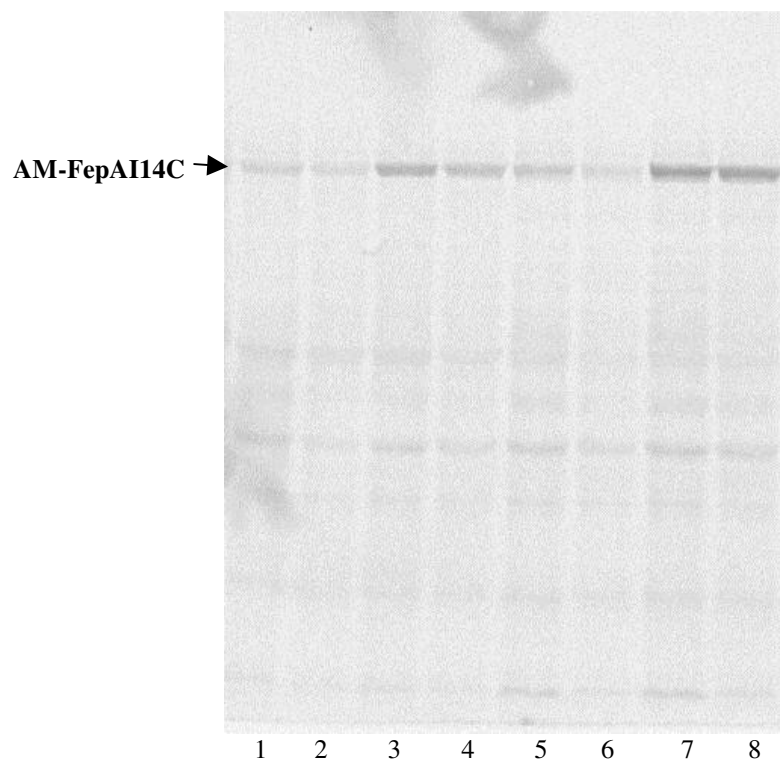


Figure 45. Labeling of FepAI14C by AM. The data was obtained as detailed for FM above.

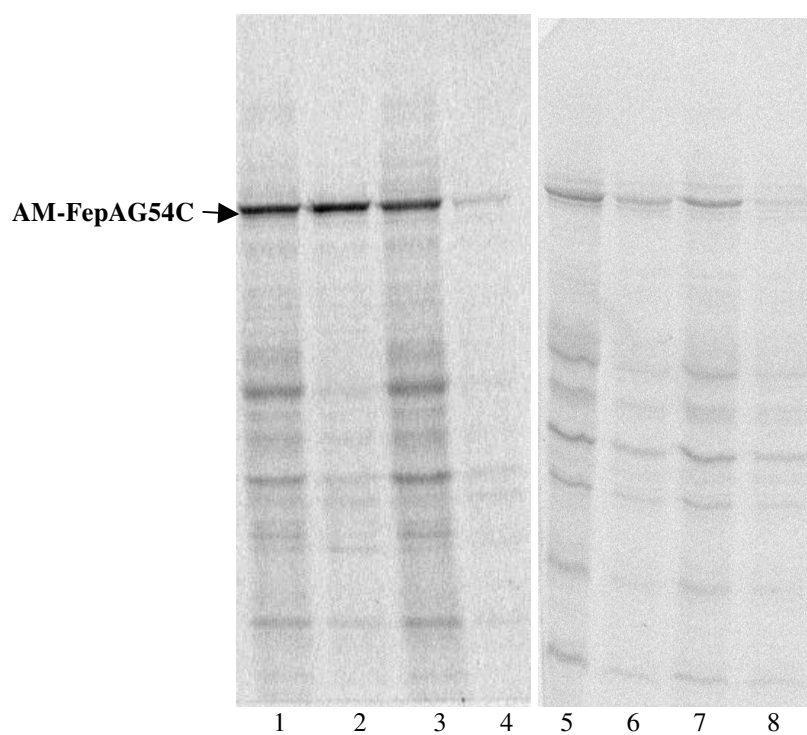


Figure 46. Labeling of FepAG54C by AM. The data was obtained as detailed for FM above.

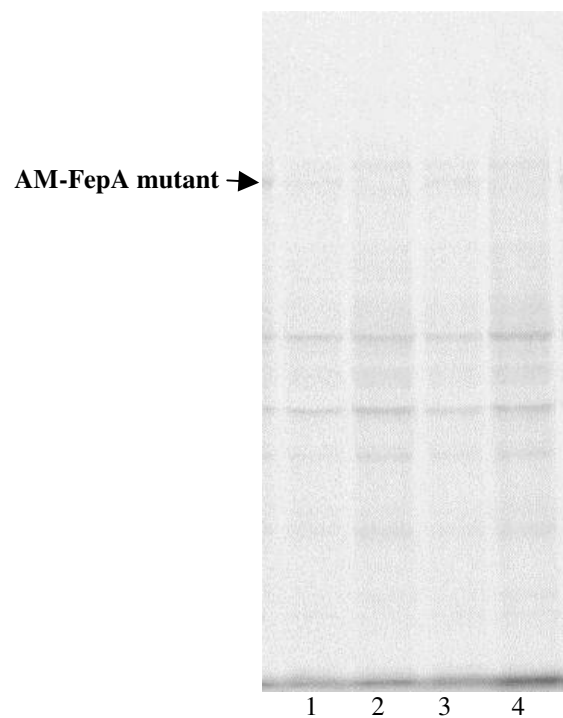


Figure 47. Labeling of FepAT51C by AM. The data was obtained as detailed for FM above. However, labeling was only performed at 37°C.

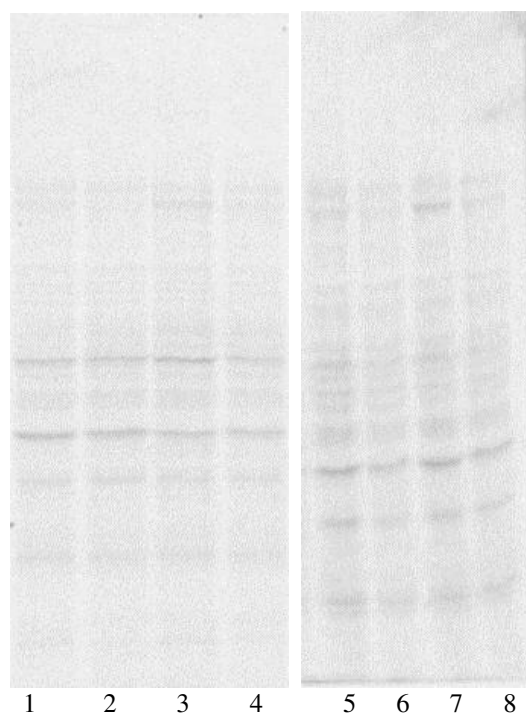


Figure 48. Labeling of FepAG300C by AM. The data was obtained as detailed for FM above. No labeling of FepA G300C is observed in any of the four lanes.

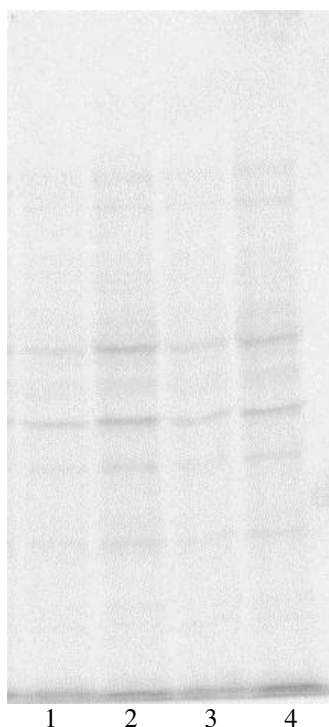


Figure 49. Labeling of FepAG565C by AM. OKN3 (lanes 1, 3) and OKN13 (lanes 2, 4,) expressing FepA G565C from pHSG575 were labeled with 10 μ M AM for 30 min at 37°C. Samples in lanes 3 and 4 were pre-incubated with 10 μ M FeEnt at 0°C for 10 min. The cells were lysed in sample buffer and resolved by SDS-PAGE. The gel was scanned for fluorescence in a STORM SCANNER (Molecular Dynamics). No labeling of FepA G565C is observed in any of the four lanes.

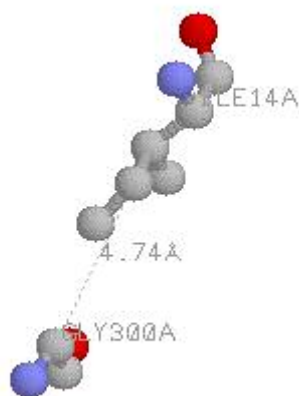


Figure 50. Distance between isoleucine 14 and glycine 300 in the barrel wall.

Labeling with AM

I tested the ability of AM to label the cysteines of FepA in OKN3. The fluorophore did not label wild type FepA (Figure 43). But it modified W101C (Figure 44). However, this may be subject to the same considerations as FM labeling (see above).

G54C is also labeled (Figure 46). G565C is not labeled (Figure 49). The labeling of G54C and not G565C by AM suggests that the fluorophore gains access to the former residue when it is outside the barrel.

AM labeled I14C poorly (Figure 45) and did not label G300C (Figure 48). The β carbon of isoleucine 14 is 4.74 Angstrom away from the alpha carbon of glycine 300 in the barrel wall (Figure 50). Stearic hindrance may block or reduce labeling at these sites. Unlike FM, AM did not modify T51C (Figure 47). The difference in labeling with FM and AM at these three sites suggest that steric factors influence the reaction with fluorophores.

No difference was noted in the labeling pattern between conducting the labeling at 37°C or 0°C. T51C was not tested at 0°C.

Labeling and TonB

The next consideration was the relationship between labeling and the presence or absence of the cofactor TonB. All the different FepA constructs are expressed in OKN13 at wild type FepA levels.

The labeling of G54C in OKN13 was sensitive to the temperature of the reaction. While the labeling of G54C in OKN13 resembled OKN3 at 37°C, when labeled at 0°C, the intensity of labeling in OKN13 decreased. FepAG54C also showed the difference with AM, albeit to a lesser degree. Labeling at other residues did not show this temperature dependence. The absence of tonB in some way affects the

labeling at G54C at 0°C. FepAT51C is not labeled by FM in the absence of tonB. In the absence of TonB, T51C apparently does not attain a labeling competent orientation.

Labeling and FeEnt

I compared the ability of the fluorophores to modify G54C in the presence and absence of FeEnt. The experiment was performed with both OKN3 and OKN13. Both FM and AM were tested at 0°C and 37°C. I found that the prior addition of FeEnt concentrations as high as 100 μ M did not compromise labeling in the transport competent strain (Figure 51). The minimum concentration that could be tested with the transport competent strains was 10 μ M (Table 14). Lower concentrations were affected by substrate depletion and transport was not sustained throughout the duration of labeling (Newton 1999). The ferric siderophore in the extracellular medium was transported into the cell during the reaction and conditions resemble experiments conducted in the absence of FeEnt. On the other hand, concentrations as low as 1 nM decreased or blocked labeling of G54C in OKN13. The latter strain does not allow transport. The K_d of wild type FepA is around 0.2 nM. At subnanomolar concentrations, the receptor proteins are not saturated. This scenario leaves a population of receptors unbound by FeEnt and open to attack by FM. As the concentration of the ligand increases, the receptor proteins become saturated. In this situation, the label is not able to attack the target cysteine. This explains why there is a difference in the labeling at different concentrations of FeEnt. Similar results were obtained with both FM and AM. The same pattern was noted with incubation at 0°C and 37°C. The binding of FeEnt blocks labeling at G54C.

The addition of 10 μ M FeEnt did not affect the labeling of W101C by FM or AM. Even in the tonB⁻ strain, W101C got labeled. No difference in FM labeling was noted

at either temperature of incubation. With G565C, no labeling was detected in the presence or absence of FeEnt. This was true of both the fluorophores. The presence or absence of tonB or the change in the temperature made no difference.

With G300C, the addition of FeEnt increased the labeling with FM. This was noted in both tonB⁺ and tonB⁻ situations at both 0°C and 37°C. In contrast, no labeling was detected with AM even in the presence of FeEnt.

With I14C, the addition of FeEnt appeared to increase the labeling by FM slightly in the transport competent strain, OKN3. In OKN13, the proteins were labeled comparably with and without FeEnt. With AM, the addition of FeEnt markedly increased the labeling of I14C in both tonB⁺ and tonB⁻ strains. The above pattern was noted at both the temperatures of incubation.

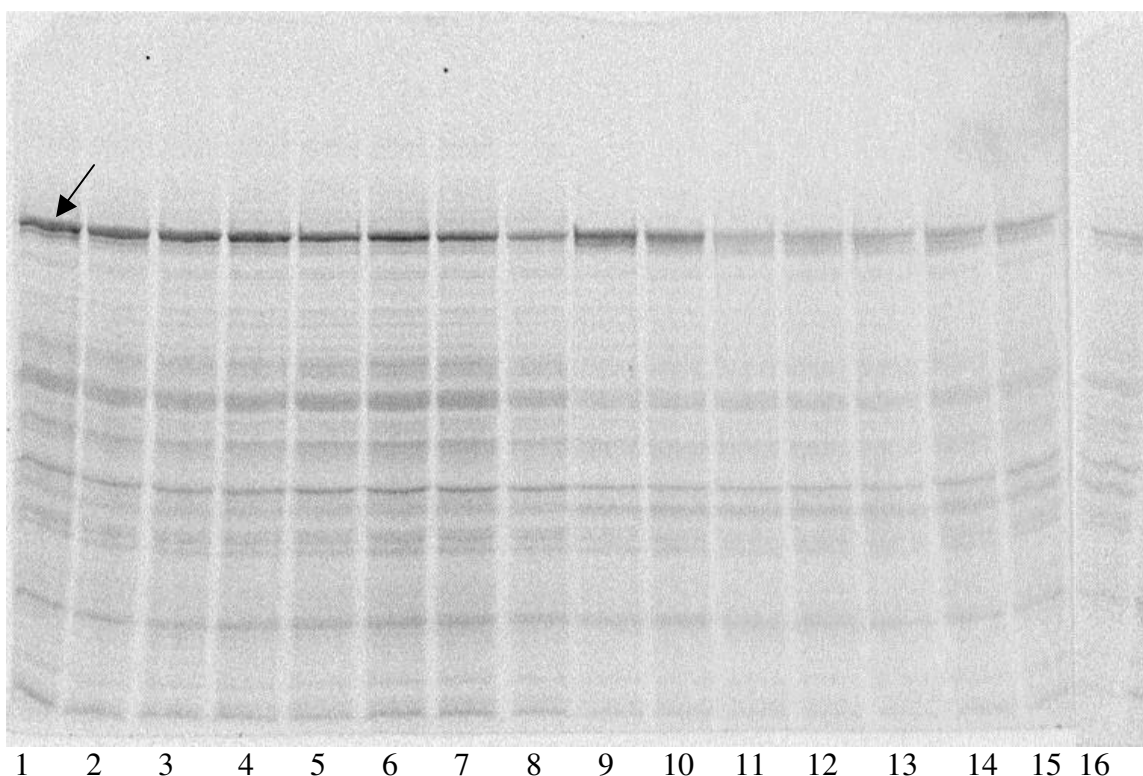


Figure 51. Labeling of FepAG54C by FM in the presence of increasing concentrations of FeEnt. OKN3 (lanes 1-8) and OKN13 (lanes 9-16) expressing FepAG54C from pHSG575 were labeled with 65 μ M FM for 30 min at 37°C. Samples in lanes 1 and 9 were not exposed to FeEnt. Samples in lanes 2-8 and lanes 10-16 were each incubated with 10-fold increasing concentrations of FeEnt from 0.1 nM up to 100 μ M at 0°C for 10 min before exposure to the fluorophore. The cells were lysed in sample buffer and resolved by SDS-PAGE. The gel was scanned for fluorescence in a STORM SCANNER (Molecular Dynamics). The arrow points to FM labeled FepAG54C.

Volume of reaction in ul	Concentration of FeEnt	Amount of FeEnt in pmoles	Duration of transport*	Substrate depletion
600	0.1 nM	0.06	0.00038	Yes
„	1 nM	0.6	0.0038	Yes
„	10 nM	6	0.038	Yes
„	100 nM	60	0.38	Yes
„	1 μ M	600	3.8 min	Yes
„	10 μ M	6000	38 min	No
„	100 μ M	60,000	380 min	No

Table 14. Duration of FeEnt transport at different concentrations of FeEnt. The V_{max} of transport of FeEnt by wild type FepA expressed in OKN3 is 160 pmol transported/ 10^9 cells/min (Salette Newton, Raj Annamalai and Bo Jin). It can be seen that concentrations of FeEnt higher than 10 μ M are required for observing the labeling reaction in the presence of the ferric siderophore.

Chapter 8

Discussion

Recognition of ferric catecholates

Siderophore receptors differ in their specificities of metal complexes that they recognize. From the data observed, it appears that FepA rejects not only the hydroxamate Fc but also the dicatecholate ferric agrobactin. Furthermore, it discriminates between the three tricatecholate compounds FeEnt, FeTRENCAM, and FeCorynebactin. One possible binding mechanism for LGP recognition of ferric siderophores is that FepA initially adsorbs hydrophobically iron complexes in a nonspecific interaction and then rejects unrecognized metal chelates as the binding equilibrium progresses further. However, the complete inability of Fc and ferric agrobactin to inhibit $^{59}\text{FeEnt}$ adsorption suggests that no such initial interaction happens. The first measurable stage of ferric siderophore binding has specificity, in that it was only impaired by ferric catecholate complexes that are structurally similar to FeEnt. This specificity likely derives from the aromatic amino acids in the B1 region of the vestibule mouth.

The selectivity of FepA for FeEnt provides more information about the determinants of ligand recognition. Ent, TRENCAM, and Corynebactin all form tricatecholate, hexadentate, octahedral complexes with iron (III), but they differ in size and in their chemistry. Unlike FeEnt, which has a trilactone backbone, the synthetic compound FeTRENCAM contains three alkyl chains linked to a central amine that connect by amide bonds to its dihydroxybenzoic acid groups. Therefore FeTRENCAM (604 Da) is smaller than that of FeEnt, and with a pK_a of 5 its central amine is essentially unprotonated at neutrality. The 50-fold reduction in the affinity of FeTRENCAM binding, and 20-fold reduction in the affinity of its transport indicate

that the face of its iron center, which is identical to that of FeEnt, is not the only determinant of its recognition by FepA. The structural alterations behind the iron center impair its binding, relative to that of FeEnt. The six oxygens of the natural siderophore's lactone ring provide many potential H-bond acceptors that are absent in FeTRENCAM, suggesting a reason for its lower affinity. These data concur with the model in which the receptor's loops surround the ferric siderophore at binding equilibrium and thereby interact with the backbone.

Different considerations may explain the partial binding observed with FeCorynebactin. Both FeEnt and FeCorynebactin have a cyclic ester backbone, formed by serine and threonine, respectively, from which dihydroxybenzoic acid moieties project. The latter siderophore also contains glycine spacer groups between the backbone and the chelating groups. These differences make FeCorynebactin heavier and larger than FeEnt (933 versus 719 Da). Besides its greater mass, the metal center of FeCorynebactin has opposite chirality (Λ) to that of FeEnt (Δ) and FeTRENCAM (Δ) (Raymond 2003). However, although FepA recognizes the iron center of ferric siderophores, chirality does not govern the receptor-ligand interaction. FeEnt binds with comparable affinity as FeEnt (Thulasiraman 1998). Thus, the rejection of $^{59}\text{FeCorynebactin}$ was surprising and implied that its increased dimensions preclude productive adsorption to the receptor. The partial inhibition of $^{59}\text{FeEnt}$ binding by FeCorynebactin and the nonretention of $^{59}\text{FeCorynebactin}$ by cells expressing FepA suggest that the ferric siderophore begins to bind but does not reach a stable equilibrium. The larger size of FeCorynebactin may interfere with loop closure and hence its passage from B1 to B2.

Aromatic amino acids in FepA function

The eleven surface loops of FepA form a large external vestibule through which FeEnt enters. The solution of the crystal structure of FepA did not reveal a binding site for the siderophore, although the occurrence of an iron-like electron density was found in the extremities of the surface loops (Buchanan 1999). However, accumulating evidence gathered in the past two years suggests that gated porins are not static structures that passively bind and transport their ligands, but instead, they may undergo quite extensive changes in conformation during ligand binding and subsequent uptake. Indeed, we observed biphasic binding kinetics compatible with the existence of either two "passive" binding sites located at the surface and deeper in the vestibule, or of a conformational change in the loops that would move the siderophore from its initial site to a secondary region of the porin (Payne 1997).

Evidence for conformational changes in FepA was first obtained by ESR (electron spin resonance spectroscopy) analyzes of nitroxide probes attached at site E280C (Jiang 1997). By monitoring the mobility of covalently bound nitroxide spin labels, the opening and closing of the gated-porin channels during membrane transport was visualized *in vivo*. *In vivo* cross-linking experiments demonstrated that loop7 undergoes dramatic displacement upon ligand binding: it changes from an initially open conformation (not revealed in the crystal structure), to a closed version (probably similar to that of the crystallized version). This change is not exclusive to FepA, as another gated porin, FecA (transporter of ferric citrate), showed major conformational changes of extracellular loops 7 and 8 upon ligand binding (Ferguson 2002). Loop 7 moves as much as 11 Å in FecA upon ligand binding. The binding of ferric citrate causes conformational changes in the extracellular loops, such that the

siderophore becomes solvent-inaccessible. It is likely that such form resembles the closed phase of the surface loops of FepA when FeEnt binds.

The distinct chemical nature of the two siderophores, FeEnt and Fc precludes the direct extrapolation of those residues subtending the binding site in the Fc-FhuA complex to that of FeEnt-FepA. In this scenario, site-directed mutagenesis enables the study of the importance of selected amino acids in the structure and function of the protein. Single mutation or double substitutions involving the aromatic components of two FeEnt binding sites in FepA, Y260, Y272, and F329, severely impaired the adsorption of FeEnt (Cao 2000). For Y260A and Y272A, the decreased affinity caused comparable decreases in transport efficiency, suggesting that they primarily act in ligand binding. However, F329A, as well as R316A in a positive charge cluster on the receptor surface, showed greater impairment of transport than binding, intimating mechanistic involvement during ligand internalization. Along with the position of these aromatic and positive charged residues in the crystal structure of FepA, the mutagenesis results suggested the existence of two ligand binding site, with aromatic residues mainly in B1 and both aromatic and positive charged residues in B2.

The data presented in this study enables the consideration of the primary role of each aromatic residue studied, in the overall function of FepA. Broadly, the effects of the mutations can be classified into three major classes. Class I mutations are of residues which are primarily involved in binding. The result of their substitution on transport derived from their effects on binding. Y472, Y481, Y488 and Y540 belong to this class. Among these substitutions, Y481A produced the largest defect namely a 17-fold increase in K_d and a 18-fold increase in K_m . Among these residues, Y481

appears to be a major component of the binding site. Its well-exposed location on the protein's surface further supports this conclusion.

All the aromatic residues, presented here, with the possible exception of W101, were selected as putative constituents of the FeEnt binding sites and were expected to be primarily involved in the binding interaction. However, Class II mutations caused no or only moderate defects on binding but greater results on the transport process. These observations suggest that the aromatic residues, in spite of their location in the surface loops of FepA, contribute significantly to the transport mechanism. These residues may participate in the transmission of conformational signals, to initiate the transport sequence, to either the N domain or the β barrel or both, or may directly interact with crucial residues, which accomplish the transport process.

Among the residues producing class II defects, Y478 is part of loop 7 of FepA. This loop undergoes a large 11 Å translocation upon ligand binding and closes off FeEnt from the surface solvent (Scott, Ferguson). The resultant increase in local concentration of FeEnt may drive the transport of ligand into the periplasm. The considerable increase in the thermal factor of mapped residues distal to L480 in loop 7 of FepA also suggests that this region of the protein undergoes dynamic transitions (Buchanan 1999). Y478A is deeper in the vestibule and may serve as the essential anchor for further signaling that will accomplish the transport process, which may explain the 500-fold increase in K_m of Y478A over the wild type. Other residues in this group are amino acids W101 and Y638. In addition to their effects on transport K_m , they also demonstrate a severe reduction in their capacity of binding. In light of their wild type level expression on the surface, this reduction in the capacity of binding reflects the functional importance of these residues. One possible explanation

is that these residues are key participants in the optimization of the binding site for FeEnt. In their absence, the binding site in a majority of the receptor proteins may not adopt its functional conformation. Y217 and Y553 are other members of this group. The varied location of these residues underscores the multi-determinant nature of the binding and uptake process.

A class III mutation was uncovered with Y495A. The substitution produced small defects in the K_m of transport but severely reduced the V_{max} of the receptor protein. FepA Y495A also had a low turnover number of 0.4. The turnover number relates the number of molecules transported per minute. The mutation therefore affects the rate-limiting step in the transport reaction.

Of the surface exposed residues in the crystal structure, tyrosines 481, 495 and 638 are located centrally in the vestibule, whereas residues 217, 540 and 553 are located more peripherally. Mutagenesis of the former group of residues caused large defects in the binding and/or transport, while mutagenesis of the latter produced modest defects. The difference in the location of these residues may explain their differential effects on the protein function. Residue 488 falls in an unresolved portion of the crystal structure. The location of the nearest resolved residues indicates that tyrosine 488 may be well exposed to the surface. However, FepAY488A produced a zone of growth very close to that of wild type FepA in the siderophore nutrition assay. The presence of the disulfide bond between C487 and C494 and the resultant conformational constraints may explain the limited role of Y488 in spite of its location.

Loops of the N domain in FepA function

The N domain loop deletions produced large class II effects. Their effect on the transport process far exceeded the effect on binding. It is noteworthy that the

replacement of tryptophan 101 with alanine precluded the calculation of maximal velocity of transport, but the deletion in NL2, which also removes tryptophan 101, still allowed the same measurements. This underscores the importance of this residue to native FepA. In the deletions, the local rearrangements of the protein structure especially the truncated loop NL2, apparently allow the protein to compensate. In other words, the change in NL2 produces a scenario different from the substitution of one of its residues W101 with alanine.

N domain of ligand gated porins

The N domain of the ligand-gated porins is a novel fold. This globular domain occupies the barrel formed by the C domain. Initial studies suggested that this structure is less important in the transport of the ferric siderophores (Scott 2001, Braun 1999). The authors found that the K_m of transport for Fep β and Fhu β , the proteins without their N domains was similar to that of the full length FepA and FhuA respectively. However, later studies have questioned this conclusion. The latter suggested that the host strains for these protein constructs produced one or more complementing factors that restored activity to the N domain deleted proteins. These constructs were shown to be inactive in host strains lacking these complementing fragments (Vakharia 2002, Braun 2003). In this study, I repeated some of the experiments with the N domain deletions. I investigated the activity of these deletion constructs in the different host strains. Furthermore, I investigated the activity of the chimeric protein constructs, FepNFhu β and FhuNFepB.

Fhu β is inactive in OKN73, the strain with the complete deletion of genomically encoded FepA and FhuA. The construct is inactive in MB97 (*fhuA*). It is however active in KDF541. The *fhuA* locus of KDF541, the original host of Fhu β constructs, has not been sequenced and therefore the exact nature of its *fhuA*-

phenotype has not been characterized. I obtained a wild type length PCR product from the genome of KDF541 using primers that anneal upstream and downstream of the *fhuA* gene. However, the strain does not express any detectable FhuA protein. This implies that the mutation is likely a frameshift mutation rather than a deletion in the gene. The exact location of the mutation is unknown. The strain also contains a residual 363 amino acid N terminal fragment of FepA (see below). The uncharacterized FhuA fragment and/or the FepA fragment may complement the Fhu β protein. The fact that Fhu β is inactive in MB97, which does contains full length active FepA, implies that the protein needs the FhuA fragment. It has been reported that a 352 amino acid FhuA fragment is present in one of the original two strains used for studies on Fhu β and has later been postulated as the complementing factor (Braun 2003).

Regarding Fep β , the proteins are inactive in the strain (OKN73) with complete *fepA* and *fhuA* deletions. The presence of wild type FhuA (in OKN3) failed to complement the construct. In KDF541, the original host for these constructs, they are active. The *fepA*- phenotype of KDF541 was engineered by selecting for spontaneous colicin B resistance. The strain however contains a residual 363 amino acid N terminal fragment of FepA. This fragment or a similar uncharacterized FhuA fragment (see above) is apparently able to complement the activity of Fep β . The coexpression of plasmid encoded FepN also accomplished complementation, although not as well as the FepA₁₋₃₆₃ fragment.

The chimeric protein constructs present a more complicated picture. FepNFhu β behaves like Fhu β in that it is not active in *fepA-fhuA*- OKN73 or *fhuA*- MB97. Like Fhu β , it is active in KDF541. FhuNFep β behaves like FepB. It is not active in *fepA-fhuA*- OKN73 or *fepA*- OKN3. However, like Fep β it is active in

KDF541. This implies that the chimeras also undergo complementation by genomically encoded fragments.

The disposition of the attached N domain is relevant to this discussion. The domain may be inserted into the barrel or may remain suspended in the periplasm. In the latter case, the chimeras will exist as hollow barrels like the deletion constructs. While this may explain their functional similarity to the deletions, evidence exists that argues against this theory. In strain KDF541, Fhu β confers increased susceptibility and hence, permeability to the antibiotic bacitracin, but FepNFhu β does not. In the same vein, Fep β and FhuNFep β confer different antibiotic sensitivities to KDF541. When compared to Fep β , FhuNFep β shows reduced permeability to bacitracin and erythromycin (Scott 2001). In both cases, the antibiotic susceptibility profile of chimeric proteins mirrored that of the wild type LGPs but not the deletions. This suggests that the chimeric protein does not exist as a hollow barrel. The barrel is filled with either the attached N domain or the N domain from the complementing factor. If the latter is true, then it suggests that the final configuration of even the chimeras resembles wild type LGPs. However, the chimeras function with a reduced capacity of binding and the V_{max} of transport just like the deletions. Vakharia et al. postulated that the lower values detected with the deletions may reflect the lower efficiency of the complementation (Vakharia 2002). If that is true, it is imaginable that the chimeras are complemented with comparable or even lower efficiencies. This would leave most of the chimeric barrels empty. The difference in the antibiotic sensitivities between the deletion and the chimera argues against this possibility. It is therefore likely that the barrels are filled with their attached N domains. In light of these considerations, it is not clear how the genomically encoded fragments displace the preexisting N-domains and complement the chimeras. The probable location of the

genomically encoded fragments further complicates the picture. Murphy et al. found that N terminal segments of FepA (like the genomically encoded FepA1-363) longer than 210 amino acids localize to the OM (Murphy 1989). From this tethered location, the N domains from the fragments would have to complement the empty barrels. Unlike lamB and other specific porins, no reliable evidence exists that LGPs like FepA and FhuA form trimers. In the absence of such oligomerization, it is not apparent how the fragments attain the proximity needed to complement the deletion or chimerical proteins. The said complementation may not happen at the level of the mature proteins but at the level of protein expression. The current evidence also does not rule out this possibility.

Disposition of the N domain of FhuA during transport

The N domain of ligand-gated porins completely seals off the barrel in the crystal structure, prompting the denomination ‘plug’ domain (Buchanan 1999). However, this description suggests that this domain blocks transport through the barrel. The absence of LGP transport in its absence (Vakharia 2002, Braun 2003, this study), its independent binding of FeEnt (Usher 2001) and its complementation of the empty barrels (Braun 2003, this study) indicates that the N domain plays the role of an usher than a bouncer. However, it may be the plug against bacterial toxins including antibiotics and bile acids. In light of its specific role, the best description therefore lies in the name, N domain.

The first step in the mapping of the N domain’s disposition is to identify its orientation when the transporter is quiescent. Does the N domain reside inside the barrel? Or is it suspended in the periplasm? In other words, does the crystal structure describe the receptor *in vivo*? The complementarity between the ion pairs of the two domains argues against an artifactual localization of the N domain. Biochemical

evidence exists that help to support and interpret the structural data. The disruption of the native disulfide by W101C, the absence of similar observations with other cysteine mutants which do not have anatomic proximity to the native cystine in the mature protein and the difference in the antibiotic permeabilities of the native protein and the beta barrel (Scott 2001, Braun 1999) indicates that the N domain does reside inside the barrel in vivo. However, it does not indicate whether this arrangement is transient or continuous. If the N domain is within the barrel, then transport requires a change in its conformation. We attempted to determine such conformational changes with the TEV protease experiments. The permeabilization of the *E. coli* cell wall delivers the TEV protease into the periplasm.

Our experiments with the control substrate show that the introduced TEV protease is active in the periplasm of *E. coli*. The techniques employed delivered TEV protease activity to the target location. However, I did not observe proteolytic cleavage of our FhuA TEV site constructs. This suggests that there is no accessibility of the TEV sites in the N domain to TEV protease. However, other technical factors may affect this conclusion.

Even with the soluble target substrate, less than 50% of the target is cleaved in our strains. Therefore, the N terminal fragment of the OM protein may not be generated in sufficient concentration to be visible on an immunoblot. Most experiments in our laboratory are performed using the ¹²⁵I-Protein A immunoblotting. This is a specific technique that also has the added advantage of being precisely quantitative. However, in order to detect the proteolytic fragments even at lower concentrations, I used the more sensitive but less specific colorimetric western blotting. However, these experiments were not successful. I also experimented with

several variables to increase the activity of the TEV protease, but did not achieve FhuA target proteolysis.

I was not able to demonstrate a control reaction at the inner surface of the OM. In the absence of demonstrated activity at this location, the TEV protease experiments do not allow any conclusions about the disposition of the N domain. With limited success with protease methodologies, I shifted to other approaches.

Disposition of the N domain of FepA during transport

The accessibility to fluorophore labeling is an indicator of a residue's disposition in vivo (Henderson 2004). G54C exhibits differential labeling accessibility in vivo under different physiological conditions. Glycine 54 exists in a buried location in the crystal structure. The mutation G54C does not affect the functionality of FepA. Therefore, any change in the disposition of glycine 54 would be expected to indicate the spatial orientation of the N domain. The fluorophores labeled FepAG54C in OKN3 both in the presence and absence of FeEnt. This happened both at 37°C and 0°C. In OKN13, it labeled only in the absence of FeEnt.

AM penetrates the periplasm. Nevertheless, stearic hindrance presumably interferes with labeling at I14C and G300C in the absence of FeEnt. When the ferric siderophore is added, the change in conformation of the tonB box or the entire N domain exposes I14C. This is consistent with the movement in the tonB box described in the FhuA and FecA crystal structures (Locher 1998, Ferguson 2002). The continued absence of G300C labeling under the latter conditions implies that this cysteine is still shielded.

If a pore develops in the presence of transport or ligand binding, it may allow AM to attack the cysteines from either the surface or the periplasm. However, the fluorophores do not enter the barrel as evident from the results with G565C. The

observed labeling at G54C and the absence of the same at G565C is not consistent with the formation of a pore.

A pore is not inconsistent with, albeit not essential to, the increase in I14C labeling by AM in the presence of FeEnt. However, it raises the question why the pore does not support labeling by AM at G300C. Alternatively, the N domain may traverse superiorly and expose I14C to AM upon ligand binding. However, such a movement will expose G300C to AM labeling from the periplasm, which is not observed. .

Another alternative will be the creation of a crescent shaped pore in the barrel which will allow both the ferric siderophore and the fluorophore to enter the protein simultaneously. Since I14C and G54C are located on different faces of the N domain, this may explain the absence of labeling at G54C and the opposite at I14C in tonB- strains. FeEnt may block the fluorophore from reaching G54C but not I14C. The depth of penetration may not give the fluorophore access to G300C. On the contrary, in OKN3, transport may unblock the fluorophore from G54C. However, this scenario will not account for lack of G565C labeling. This leaves us only the solitary conclusion that the labeling of G54C takes place in the periplasm.

The model (Figure 52) that develops out of these experiments involves the movement of the N domain in and out of the barrel. In the absence of tonB and/or ligand, the N domain either stays inside the barrel or cycles between inserted and periplasmically suspended states. In the suspended state, the surface loops may slope towards each other and guard the channel. This is consistent with the absence of Fep β cross-linking to OmpA (Scott 2003). Upon ligand binding, the loops close over FeEnt and make it solvent inaccessible from the exterior of the cell. Further movement ceases until the transport signals are transmitted by the loops. The N domain leaves

the barrel alone or with attached ligand. In the former case, the ligand diffuses out of the barrel as its local concentration in the confines of the barrel will be of the order of 50 M. In the latter case the release of the ligand may happen by transient denaturation of the N domain. After the ligand is transported into the periplasm, presumably into the reaches of FepB, the reassembly of the protein occurs and the surface loops attain the open, ligand binding conformation.

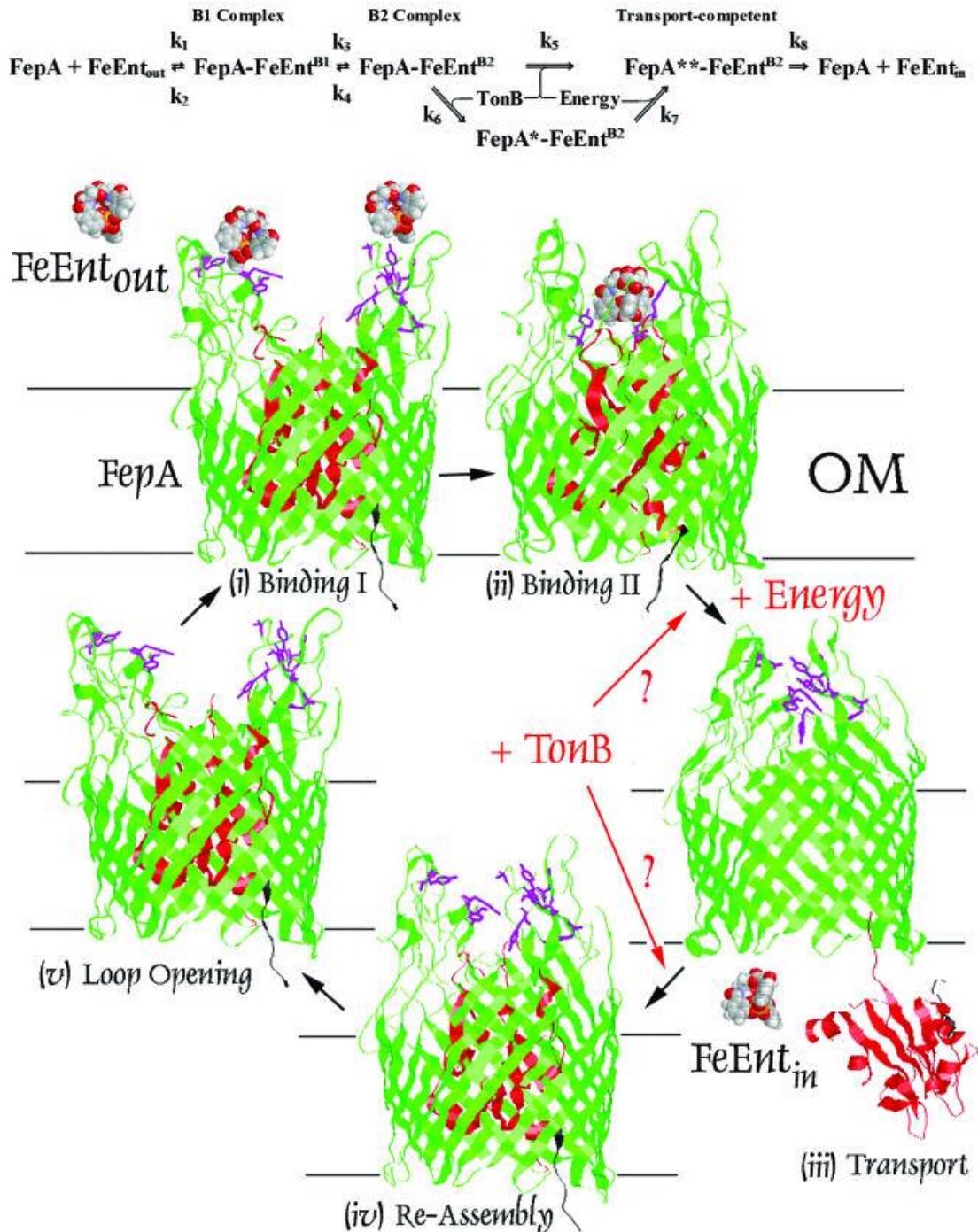


Figure 52. Model of FeEnt transport through FepA. (Top) Formal representation of the FepA transport process. Constants k_1 to k_4 are experimentally defined (Cao 2003, Annamalai and Jin 2004). (Bottom) FepA's transport cycle is depicted as a series of conformational stages that result in binding and internalization of FeEnt. The representations of FepA are based on the crystal structure, but the stages are postulated models not crystallographically demonstrated. FeEnt binding causes the surface loops to close over the ligand. Subsequently, the N domain exits the barrel. The ligand passes through the C-domain channel (Transport). TonB and/or energy may function during this phase of the transport reaction. After transport the receptor reassembles by reinsertion of the N domain into the β -barrel, another potential phase for the input of energy and/or TonB. Lastly, the loops reopen to achieve a binding competent conformation (Figure by Klebba in Annamalai and Jin 2004).

References

1. Ames, G. F. (1974) *J Biol Chem* **249**(2), 634-644
2. Annamalai, R., Jin, B., Cao, Z., Newton, S. M., and Klebba, P. E. (2004) *J Bacteriol* **186**(11), 3578-3589
3. Armstrong, S. K., Francis, C. L., and McIntosh, M. A. (1990) *J Biol Chem* **265**(24), 14536-14543
4. Barnard, T. J., Watson, M. E., Jr., and McIntosh, M. A. (2001) *Mol Microbiol* **41**(3), 527-536
5. Bassford, P. J., Jr., Bradbeer, C., Kadner, R. J., and Schnaitman, C. A. (1976) *J Bacteriol* **128**(1), 242-247
6. Bayer, M. E. (1991) *J Struct Biol* **107**(3), 268-280
7. Blaylock, B. A., and Nason, A. (1963) *J Biol Chem* **238**, 3453-3462
8. Brass, J. M. (1986) *Methods Enzymol* **125**, 289-302
9. Braun, M., Endriss, F., Killmann, H., and Braun, V. (2003) *J Bacteriol* **185**(18), 5508-5518
10. Braun, V., Braun, M., and Killmann, H. (2000) *Adv Exp Med Biol* **485**, 33-43
11. Braun, V., Hancock, R. E., Hantke, K., and Hartmann, A. (1976) *J Supramol Struct* **5**(1), 37-58
12. Breusch, F. (1937) *Hoppe-Seyl. Z.* **250**, 262
13. Brickman, T. J., and McIntosh, M. A. (1992) *J Biol Chem* **267**(17), 12350-12355
14. Brown, N. C., Eliasson, R., Reichard, P., and Thelander, L. (1968) *Biochem Biophys Res Commun* **30**(5), 522-527
15. Buchanan, S. K., Smith, B. S., Venkatramani, L., Xia, D., Esser, L., Palnitkar, M., Chakraborty, R., van der Helm, D., and Deisenhofer, J. (1999) *Nat Struct Biol* **6**(1), 56-63
16. Budzikiewicz, H., Bössenkamp, A., Taraz, K., Pandey, A. and Meyer, J. M. (1997) *Z. Naturforsch. Sect. C* **52**, 551-554.
17. Bullen, J. J., Rogers, H. J., and Griffiths, E. (1978) *Curr Top Microbiol Immunol* **80**, 1-35
18. Cao, Z., Qi, Z., Sprencel, C., Newton, S. M., and Klebba, P. E. (2000) *Mol Microbiol* **37**(6), 1306-1317
19. Cao, Z., Warfel, P., Newton, S. M., and Klebba, P. E. (2003) *J Biol Chem* **278**(2), 1022-1028
20. Carl, J. C. a. R., K. N. (1979) *J. Am. Chem. Soc.* **101**, 5401-5404
21. Carrano, C. J., and Raymond, K. N. (1978) *J Bacteriol* **136**(1), 69-74
22. Chakraborty, R., Lemke, E. A., Cao, Z., Klebba, P. E., and van der Helm, D. (2003) *Biometals* **16**(4), 507-518
23. Chen, R., Schmidmayr, W., Kramer, C., Chen-Schmeisser, U., and Henning, U. (1980) *Proc Natl Acad Sci U S A* **77**(8), 4592-4596
24. Chenault, S. S., and Earhart, C. F. (1992) *J Gen Microbiol* **138**(10), 2167-2171
25. Chenault, S. S., and Earhart, C. F. (1991) *Mol Microbiol* **5**(6), 1405-1413
26. Cooper, S. R., McArdle, J. V., and Raymond, K. N. (1978) *Proc Natl Acad Sci U S A* **75**(8), 3551-3554
27. Coulton, J. W., Mason, P., Cameron, D. R., Carmel, G., Jean, R., and Rode, H. N. (1986) *J Bacteriol* **165**(1), 181-192
28. Cowan, S. W., Garavito, R. M., Jansonius, J. N., Jenkins, J. A., Karlsson, R., Konig, N., Pai, E. F., Pauptit, R. A., Rizkallah, P. J., Rosenbusch, J. P., and et

- al. (1995) *Structure* **3**(10), 1041-1050
29. de Lorenzo, V., Giovannini, F., Herrero, M., and Neilands, J. B. (1988) *J Mol Biol* **203**(4), 875-884
30. Dickman, S. R., and Cloutier, A. A. (1950) *Arch Biochem* **25**(1), 229-231
31. Dickman, S. R., and Cloutier, A. A. (1951) *J Biol Chem* **188**(1), 379-388
32. Dougherty, W. G., Carrington, J. C., Cary, S. M., and Parks, T. D. (1988) *Embo J* **7**(5), 1281-1287
33. DuPont, H. L., Formal, S. B., Hornick, R. B., Snyder, M. J., Libonati, J. P., Sheahan, D. G., LaBrec, E. H., and Kalas, J. P. (1971) *N Engl J Med* **285**(1), 1-9
34. Dutzler, R., Wang, Y. F., Rizkallah, P., Rosenbusch, J. P., and Schirmer, T. (1996) *Structure* **4**(2), 127-134
35. Ecker, D. J., Matzanke, B. F., and Raymond, K. N. (1986) *J Bacteriol* **167**(2), 666-673
36. Eick-Helmerich, K., Hantke, K., and Braun, V. (1987) *Mol Gen Genet* **206**(2), 246-251
37. Elkins, M. F., and Earhart, C. F. (1989) *J Bacteriol* **171**(10), 5443-5451
38. Emery, T. (1971) *Biochemistry* **10**(8), 1483-1488
39. Evans, J. S., Levine, B. A., Trayer, I. P., Dorman, C. J., and Higgins, C. F. (1986) *FEBS Lett* **208**(2), 211-216
40. Fecker, L., and Braun, V. (1983) *J Bacteriol* **156**(3), 1301-1314
41. Ferguson, A. D., Chakraborty, R., Smith, B. S., Esser, L., van der Helm, D., and Deisenhofer, J. (2002) *Science* **295**(5560), 1715-1719
42. Ferguson, A. D., Hofmann, E., Coulton, J. W., Diederichs, K., and Welte, W. (1998) *Science* **282**(5397), 2215-2220
43. Fischer, E., Gunter, K., and Braun, V. (1989) *J Bacteriol* **171**(9), 5127-5134
44. Fiss, E. H., Stanley-Samuelson, P., and Neilands, J. B. (1982) *Biochemistry* **21**(18), 4517-4522
45. Frost, G. E., and Rosenberg, H. (1975) *J Bacteriol* **124**(2), 704-712
46. Gibson, F., and Magrath, D. I. (1969) *Biochim Biophys Acta* **192**(2), 175-184
47. Golden, C. A., Kochan, I., and Spriggs, D. R. (1974) *Infect Immun* **9**(1), 34-40
48. Griggs, D. W., Tharp, B. B., and Konisky, J. (1987) *J Bacteriol* **169**(12), 5343-5352
49. Gunter, K., and Braun, V. (1990) *FEBS Lett* **274**(1-2), 85-88
50. Hancock, R. E., Hantke, K., and Braun, V. (1976) *J Bacteriol* **127**(3), 1370-1375
51. Hantke, K., and Braun, V. (1978) *J Bacteriol* **135**(1), 190-197
52. Harris, W. R., Weitz, F. L., Raymond, K. N. (1979) *J. Chem. Soc. Chem. Commun.*, 177-178
53. Heidinger, S., Braun, V., Pecoraro, V. L., and Raymond, K. N. (1983) *J Bacteriol* **153**(1), 109-115
54. Heller, K. J., Kadner, R. J., and Gunther, K. (1988) *Gene* **64**(1), 147-153
55. Henderson, N. S., So, S. S., Martin, C., Kulkarni, R., and Thanassi, D. G. (2004) *J Biol Chem* **279**(51), 53747-53754
56. Hollifield, W. C., Jr., and Neilands, J. B. (1978) *Biochemistry* **17**(10), 1922-1928
57. Ip, H., Stratton, K., Zgurskaya, H., and Liu, J. (2003) *J Biol Chem* **278**(50), 50474-50482
58. J.H., M. (1972) *Experiments in molecular genetics.*, Cold Spring Harbor

- Laboratory, Cold Spring Harbor, New York.
59. Jiang, X., Payne, M. A., Cao, Z., Foster, S. B., Feix, J. B., Newton, S. M., and Klebba, P. E. (1997) *Science* **276**(5316), 1261-1264
 60. Jurado, R. L. (1997) *Clin Infect Dis* **25**(4), 888-895
 61. Karpishin, T. B., Raymond, K. N. (1992) *Angewandte Chemie International Edition in English* **31**(4), 466 - 468
 62. Kellogg, D. S., Jr., Cohen, I. R., Norins, L. C., Schroeter, A. L., and Reising, G. (1968) *J Bacteriol* **96**(3), 596-605
 63. Killmann, H., Benz, R., and Braun, V. (1993) *Embo J* **12**(8), 3007-3016
 64. Klebba, P. E. (1981) *Thesis/dissertation/manuscript, University of California, Berkeley*
 65. Klebba, P. E. (2003) *Front Biosci* **8**, 1422-1436
 66. Klebba, P. E., McIntosh, M. A., and Neilands, J. B. (1982) *J Bacteriol* **149**(3), 880-888
 67. Klebba, P. E., Rutz, J. M., Liu, J., and Murphy, C. K. (1993) *J Bioenerg Biomembr* **25**(6), 603-611
 68. Kochan, I. (1973) *Curr Top Microbiol Immunol* **60**, 1-30
 69. Koster, W., and Braun, V. (1990) *J Biol Chem* **265**(35), 21407-21410
 70. Kronvall, G., Grey, H. M., and Williams, R. C., Jr. (1970) *J Immunol* **105**(5), 1116-1123
 71. Kunkel, T. A. (1985) *Proc Natl Acad Sci U S A* **82**(2), 488-492
 72. Laemmli, U. K. (1970) *Nature* **227**(5259), 680-685
 73. Langman, L., Young, I. G., Frost, G. E., Rosenberg, H., and Gibson, F. (1972) *J Bacteriol* **112**(3), 1142-1149
 74. Lankford, C. L. (1973) *Crit. Rev. Microbiol.* **2**(273-331)
 75. Larsen, R. A., Letain, T. E., and Postle, K. (2003) *Mol Microbiol* **49**(1), 211-218
 76. Letain, T. E., and Postle, K. (1997) *Mol Microbiol* **24**(2), 271-283
 77. Liu, J., Rutz, J. M., Klebba, P. E., and Feix, J. B. (1994) *Biochemistry* **33**(45), 13274-13283
 78. Locher, K. P., Rees, B., Koebnik, R., Mitschler, A., Moulinier, L., Rosenbusch, J. P., and Moras, D. (1998) *Cell* **95**(6), 771-778
 79. Luckey, M., Pollack, J. R., Wayne, R., Ames, B. N., and Neilands, J. B. (1972) *J Bacteriol* **111**(3), 731-738
 80. Lundrigan, M. D., and Kadner, R. J. (1986) *J Biol Chem* **261**(23), 10797-10801
 81. Mademidis, A., Killmann, H., Kraas, W., Flechsler, I., Jung, G., and Braun, V. (1997) *Mol Microbiol* **26**(5), 1109-1123
 82. Martius, C. (1937) *Z. physiol. Chem.* **247**, 194
 83. Matzanke, B. F., Ecker, D. J., Yang, T. S., Huynh, B. H., Muller, G., and Raymond, K. N. (1986) *J Bacteriol* **167**(2), 674-680
 84. May, J. J., Wendrich, T. M., and Marahiel, M. A. (2001) *J Biol Chem* **276**(10), 7209-7217
 85. Meerman, H. J., and Georgiou, G. (1994) *Biotechnology (N Y)* **12**(11), 1107-1110
 86. Mende, J., and Braun, V. (1990) *Mol Microbiol* **4**(9), 1523-1533
 87. Mondigler, M., and Ehrmann, M. (1996) *J Bacteriol* **178**(10), 2986-2988
 88. Mortenson, L. E., Valentine, R. C., and Carnahan, J. E. (1962) *Biochem Biophys Res Commun* **7**, 448-452
 89. Murphy, C. K., Kalve, V. I., and Klebba, P. E. (1990) *J Bacteriol* **172**(5),

- 2736-2746
90. Murphy, C. K., and Klebba, P. E. (1989) *J Bacteriol* **171**(11), 5894-5900
91. Nakae, T. (1976) *Biochem Biophys Res Commun* **71**(3), 877-884
92. Neidhardt, F. C., Bloch, P. L., and Smith, D. F. (1974) *J Bacteriol* **119**(3), 736-747
93. Neilands, J. B. (1974) *Microbial Iron metabolism*.
94. Neilands, J. B. (1952) *J. Am. Chem. Soc* **74**, 4846-4847
95. Neilands, J. B., Nakamura, K. (1991) *G. Winkelmann (ed.) CRC Handbook of Microbial Iron Chelates, CRC Press, Inc., Boca Raton, Fla* 1-14
96. Neilands, J. B. (1972) *Struct. Bonding* **11**, 145-170
97. Neilands, J. B., Peterson, T., Leong, S. A (1980) *Inorganic Chemistry in Biology and Medicine (A. E. Martell, ed.) American Chemical Society* , 263-278
98. Neilands, J. B. (1981) *Annu Rev Nutr* **1**, 27-46
99. Neilands, J. B. (1981) *Annu Rev Biochem* **50**, 715-731
100. Newton, S. M., Allen, J. S., Cao, Z., Qi, Z., Jiang, X., Sprencel, C., Igo, J. D., Foster, S. B., Payne, M. A., and Klebba, P. E. (1997) *Proc Natl Acad Sci U S A* **94**(9), 4560-4565
101. Newton, S. M., Igo, J. D., Scott, D. C., and Klebba, P. E. (1999) *Mol Microbiol* **32**(6), 1153-1165
102. Nikaido, H., and Vaara, M. (1985) *Microbiol Rev* **49**(1), 1-32
103. O'Brien, I. G., Cox, G. B., and Gibson, F. (1971) *Biochim Biophys Acta* **237**(3), 537-549
104. O'Brien, I. G., and Gibson, F. (1970) *Biochim Biophys Acta* **215**(2), 393-402
105. Ogierman, M., and Braun, V. (2003) *J Bacteriol* **185**(6), 1870-1885
106. Ong, S. A., Peterson, T., and Neilands, J. B. (1979) *J Biol Chem* **254**(6), 1860-1865
107. Ozenberger, B. A., Nahlik, M. S., and McIntosh, M. A. (1987) *J Bacteriol* **169**(8), 3638-3646
108. Pappenheimer, A. M., Jr., Johnson, S. J. (1936) *Br. J. Exp. Pathol.* **17**, 335-341
109. Pappenheimer, H. (1936) *American Journal of Pathology* **12**, 627
110. Payne, M. A., Igo, J. D., Cao, Z., Foster, S. B., Newton, S. M., and Klebba, P. E. (1997) *J Biol Chem* **272**(35), 21950-21955
111. Pierce, J. R., and Earhart, C. F. (1986) *J Bacteriol* **166**(3), 930-936
112. Pierce, J. R., Pickett, C. L., and Earhart, C. F. (1983) *J Bacteriol* **155**(1), 330-336
113. Pollack, J. R., and Neilands, J. B. (1970) *Biochem Biophys Res Commun* **38**(5), 989-992
114. Porra, R. J., Langman, L., Young, I. G., and Gibson, F. (1972) *Arch Biochem Biophys* **153**(1), 74-78
115. Postle, K. (1978) *Thesis/dissertation/manuscript, University of Wisconsin, Madison*.
116. Postle, K., and Good, R. F. (1983) *Proc Natl Acad Sci U S A* **80**(17), 5235-5239
117. Postle, K., and Skare, J. T. (1988) *J Biol Chem* **263**(22), 11000-11007
118. Pugsley, A. P., and Reeves, P. (1976) *J Bacteriol* **126**(3), 1052-1062
119. Pugsley, A. P., Zimmerman, W., and Wehrli, W. (1987) *J Gen Microbiol* **133**(12), 3505-3511
120. Rabsch, W., Voigt, W., Reissbrodt, R., Tsolis, R. M., and Baumler, A. J.

- (1999) *J Bacteriol* **181**(11), 3610-3612
121. Raymond, K. N., Carrano, C. J. (1979) *Acc. Chem. Res.* **12**, 183-190
 122. Rodgers, S. J., Lee, C., Ng, C. Y., Raymond, K. N. (1987) *Inorg. Chem.* **26**, 1622-1625
 123. Rohrbach, M. R., Braun, V., and Koster, W. (1995) *J Bacteriol* **177**(24), 7186-7193
 124. Roof, S. K., Allard, J. D., Bertrand, K. P., and Postle, K. (1991) *J Bacteriol* **173**(17), 5554-5557
 125. Rutz, J. M., Liu, J., Lyons, J. A., Goranson, J., Armstrong, S. K., McIntosh, M. A., Feix, J. B., and Klebba, P. E. (1992) *Science* **258**(5081), 471-475
 126. Sawatzki, G. (1987) *Iron transport in microbes, plants and animals*. VCH press, Weinheim, Germany, 477-489
 127. Schirmer, T., Keller, T. A., Wang, Y. F., and Rosenbusch, J. P. (1995) *Science* **267**(5197), 512-514
 128. Schoffler, H., and Braun, V. (1989) *Mol Gen Genet* **217**(2-3), 378-383
 129. Schramm, E., Mende, J., Braun, V., and Kamp, R. M. (1987) *J Bacteriol* **169**(7), 3350-3357
 130. Scott, D. C., Cao, Z., Qi, Z., Bauler, M., Igo, J. D., Newton, S. M., and Klebba, P. E. (2001) *J Biol Chem* **276**(16), 13025-13033
 131. Scott, D. C., Newton, S. M., and Klebba, P. E. (2002) *J Bacteriol* **184**(17), 4906-4911
 132. Sebestyen, G., Maggipinto, G., and Andre, A. (1986) *Rev Fr Transfus Immunohematol* **29**(5), 355-376
 133. Singer, T. P., Kearney, E. B., and Zastrow, N. (1955) *Biochim Biophys Acta* **17**(1), 154-155
 134. Skare, J. T., Ahmer, B. M., Seachord, C. L., Darveau, R. P., and Postle, K. (1993) *J Biol Chem* **268**(22), 16302-16308
 135. Skare, J. T., and Postle, K. (1991) *Mol Microbiol* **5**(12), 2883-2890
 136. Smit, J., Kamio, Y., and Nikaido, H. (1975) *J Bacteriol* **124**(2), 942-958
 137. Sprencel, C., Cao, Z., Qi, Z., Scott, D. C., Montague, M. A., Ivanoff, N., Xu, J., Raymond, K. M., Newton, S. M., and Klebba, P. E. (2000) *J Bacteriol* **182**(19), 5359-5364
 138. Stephens, D. L., Choe, M. D., and Earhart, C. F. (1995) *Microbiology* **141** (Pt 7), 1647-1654
 139. Strauch, K. L., and Beckwith, J. (1988) *Proc Natl Acad Sci U S A* **85**(5), 1576-1580
 140. Szabo. (1971) *Zentralbl Bakteriol [Orig A]* **218**(3), 365-368
 141. Takeshita, S., Sato, M., Toba, M., Masahashi, W., and Hashimoto-Gotoh, T. (1987) *Gene* **61**(1), 63-74
 142. Thulasiraman, P., Newton, S. M., Xu, J., Raymond, K. N., Mai, C., Hall, A., Montague, M. A., and Klebba, P. E. (1998) *J Bacteriol* **180**(24), 6689-6696
 143. Tidmarsh, G. F., Klebba, P. E., and Rosenberg, L. T. (1983) *J Inorg Biochem* **18**(2), 161-168
 144. Trivier, D., Courcol, R.J. (1996) *FEMS Microbiol Lett* **141**(2-3), 117-127
 145. Trowitzsch-Kienast, W., Hartmann, V., Reissbrodt, R., Ambrosi, H. (1996) *Ger. Offen. (Germany)*, 14
 146. Tuckman, M., and Osburne, M. S. (1992) *J Bacteriol* **174**(1), 320-323
 147. Usher, K. C., Ozkan, E., Gardner, K. H., and Deisenhofer, J. (2001) *Proc Natl Acad Sci U S A* **98**(19), 10676-10681
 148. Vakharia, H. L., and Postle, K. (2002) *J Bacteriol* **184**(19), 5508-5512

149. van der Helm, D., Baker, J. R., Eng-Wilmot, D. L., Hossain, M. B., Loghry, R. A. (1980) *J. Am Chem. Soc.* **102**, 4224-4231
150. Venuti, M. C., Rastetter, W. H., and Neilands, J. B. (1979) *J Med Chem* **22**(2), 123-124
151. Vernon, L. P., Mangum, J. H., Beck, J. V., and Shafia, F. M. (1960) *Arch Biochem Biophys* **88**, 227-231
152. Wagegg, W., and Braun, V. (1981) *J Bacteriol* **145**(1), 156-163
153. Wang, C. C., and Newton, A. (1971) *J Biol Chem* **246**(7), 2147-2151
154. Wang, C. C., and Newton, A. (1969) *J Bacteriol* **98**(3), 1142-1150
155. Wayne, R., and Neilands, J. B. (1975) *J Bacteriol* **121**(2), 497-503
156. Yan, R. T., and Maloney, P. C. (1993) *Cell* **75**(1), 37-44
157. Yanisch-Perron, C., Vieira, J., and Messing, J. (1985) *Gene* **33**(1), 103-119
158. Yost, F. J., Jr., and Fridovich, I. (1973) *J Biol Chem* **248**(14), 4905-4908
159. Zgurskaya, H. I., and Nikaido, H. (1999) *J Mol Biol* **285**(1), 409-420